Platinum Group Metals Catalyzed Steam Methane Reforming via Micro-channel Reactor

Submitted by

Yi Zhou

In fulfilment of the requirements for the degree of

Master of Science in Engineering

University of Cape Town

January 2014

Synopsis

Steam methane reforming is a well-established industrial process used for generating hydrogen and synthesis gas. By performing this reaction in micro-channel reactors it is possible to take advantage of increased heat and mass transfer rates, allowing equipment size and residence times to be decreased by an order of magnitude which, in turn, leads to the possible utilisation of small scale steam reformers for portable fuel cell power systems.

In this study, two commercial steam reforming catalysts, namely catalysts YR and XR, and a single in-house synthesised Rh/Al_2O_3 catalyst were studied in both packed bed and micro-channel reactor configurations. All these catalysts exhibited stable activity in the packed bed reactor experiments.

Catalyst YR, wash-coated onto the micro-channel reactor plates by the commercial partner, was evaluated at conditions of 700 °C, 1 bar_g, steam to carbon ratios of 2, 3 and 5, and a range of *space velocities*. Catalyst activity was found to be stable for experiments for up to 100 hours on-stream. It was confirmed experimentally that micro-channel reactor exhibited catalyst performance as high as 10-fold that of packed bed reactors when considering activity per total mass of catalyst charged. Moreover, it was demonstrated that performance suitable for downstream low temperature fuel cell integration could be achieved at temperature as low as 700 °C yet still at high specific space velocities exceeding 100 000 standard $ml/g_{cat}h$.

An in-house catalyst coating technique based on that described by Zapf et al. (2006) was evaluated for all three catalyst. And, in all cases, such coated micro-channel reactors exhibited an immediate and continuous decline in activity with time-on-stream. Although the reason for this deactivation was not determined, it was shown experimentally that neither high temperature nor steam induced sintering, nor carbon deposition are the cause of the rapid activity loss. Likewise, the coating process was shown not to inherently affect catalyst activity and neither alumina addition to the catalyst coating nor reduction in catalyst particle size effected any improvement in reforming stability. These latter observations, together with visual inspection of deactivated micro-channel reactors, do not point to catalyst erosion but catalyst loss during use should be further investigated. In

addition, it is recommended that alternative coating binders and two-step coating/metallization approaches be evaluated in future studies.

Acknowledgements

At this point I am glad to take the opportunity to express my gratitude to everyone who contributed directly or indirectly to the successful completion of this work. Foremost, I wish to thank my supervisor Prof. Jack Fletcher for letting me work in his lab and supporting me in many ways during the last three years. I would also like to thank Mr Stephen Roberts for the fruitful discussions, and for acting as the co-supervisor in my project.

I am also grateful to Mr Walter Böhringer and Mr Niels Lüchters for their help and support, interesting discussions, and for providing a pleasant working atmosphere. In particular, I would like to mention my colleagues Mr Kubefu Maduna, Mr David Tsui and Mr Peter Malatji for helping me wherever they could.

Without the support of the administrative and technical staff at the Centre for Catalysis Research, it would not have been possible to complete this research. I would like to express my respect for their excellent support: Ms Debbie De Jager, Ms Eloise Williams, Mr Marc Wüst, Mr Gideon Kaufmann, Mr Waldo Koorts and Mr Dirk Reyskens.

In addition, I am grateful to HySA/Catalysis for funding this study.

Most importantly, I am obliged to thank my caring parents Menglin and Jianmei for their constant love and invaluable support during the last three years and all my life before.

Last but not least, I wish to thank all family and friends for their support and encouragement, contributing in many ways to make this part of my life a memorable experience.

Declaration

I know the meaning of plagiarism and declare that all the work in the document, save for that which is properly acknowledged, is my own

……. *Date …….*

Yi Zhou

Table of contents

List of Figures

List of Tables

Nomenclature

Symbol	Description
SMR	Steam methane reforming
USGS	United States Geological Survey
PGM	Platinum group metals
PEM	Proton exchange membrane
MCFC	Molten carbonate fuel cell
SOFC	Solid oxide fuel cell
S/C	Molar steam to carbon ratio
nm	Nanometre
µm	Micrometre
h	Hour
ppm	Parts per million
PVA	Polyvinyl alcohol
Tylose	Methylhydroxyethyl cellulose
PEG	Polyethylene glycol
BET	Brunauer-Emmett_Teller
TEM	Transmission electron microscopy
rpm	Revolutions per minute
MFC	Mass flow controller
BPR	Back-pressure regulator
SGHSV	Gas-hourly space velocity (h^{-1}) at standard conditions of 0 °C and atmospheric pressure
SSV	Specific space velocity at 0 °C and atmospheric pressure ($ml/g_{cat}h$)
MS5	Molsieve 5A
PPQ	Pora Plot Q
sccm	Standard cubic centimetre per minute

1 Introduction

The past few years have seen great interest in the development of fuel cell technology. This is largely due to the low greenhouse gas emissions and a potentially superior efficiency of fuel cells compared to combustion engines.

At the centre of this development, hydrogen fuelled fuel cells containing platinum group metal (PGM) catalysts are the most important types of such fuel cell systems. PGM occur as rare minerals, with noticeable reserves in only 5 countries as shown in Table 1-1 (USGS, 2011). 95% of the world's PGM reserves make South Africa a global player in the world of hydrogen economy.

Table 1-1: PGM world reserves by country (USGS, 2011)

Country/region	PGM (metric tones)	Share %
South Africa	92,000	95.3
Russia	1,100	1.7
USA	900	1.4
Canada	310	0.5
Others	800	1.2

Fuel cells require hydrogen for their operation, thus fuel processing (production of hydrogen) becomes a vital part of this technology. In recent years, research and development has focused increasingly on small applications and portable fuel cell systems, e.g. for household energy supply or automobiles. This has put a lot of pressure on reducing the size of the fuel cell and fuel processing systems, such that novel micro-channel reactors with wash-coated catalysts are of interest in fuel processors. Since the catalysts may occasionally be exposed to air, they should not be pyrophoric and not re-oxidise, requirement which cannot be met by the traditional base-metal catalytic systems used in industry but only by noble, PGM catalysts.

This project focuses on the fuel processing system, more specifically, the steam reforming step. Since the major markets for small fuel cell systems are potentially overseas, especially

in Europe and Northern America, methane has been chosen as the fuel to the steam reforming process for reason of its ready availability in these markets.

This project evaluated two commercial and one experimental (prepared in-house) PGM steam reforming catalysts which were wash-coated onto the micro-channel reactors.

2 Background and literature review

Globally, both developed and developing countries are demanding more and more new energy sources and consume more and more oil. However, the world is also concerned with climate change which is generally ascribed to the large amount of greenhouse gases, particularly carbon dioxide (CO_2), generated through fossil fuel combustion. The developed nations have committed to reduce their greenhouse gas and other hazardous chemical emissions. Therefore, tremendous work has been done on the development of cleaner energy production technologies, production of cleaner fuels, as well as energy-efficient and hazardous free/less processes in the chemical industry.

One of the technologies that still needs to prove its capability to contribute to the energy market is related to hydrogen and fuel cells (Neef, 2009). Fuel cell technology (use of hydrogen as fuel) is attracting increasing attention because it offers potential for lower emissions, owing to a potentially superior efficiency compared with combustion engines.

Fuel cell technology is expected to develop gradually in the commercial markets until 2015, where after its adoption will likely increase rapidly (Anttila et al. 2006). This potential was recognized by South Africa with the establishment of its national hydrogen and fuel cell technologies programme under the name Hydrogen South Africa (HySA).

In the transport sector, vehicles with a fuel cell, an electric drive train and a hydrogen tank are being developed today. The benefit over vehicles run on diesel or petrol combustion engines, includes higher efficiencies and zero-emissions (Neef, 2009). Fuel cells in the stationary sector (for residential energy and industrial application) may employ different fuel, i.e. hydrocarbons, which are converted into hydrogen *in situ* via a process called fuel processing (Neef, 2009).

2.1 Fuel cells

A fuel cell is an electrochemical cell that converts a source of fuel into an electrical current (Wikipedia.org, 2013). Inside the cell, the fuel, typically H_2, reacts with an oxidant, typically oxygen (O_2) from air, to generate electricity, with the two half-cells separated by the

selective electrolyte. The fuel cell has no moving parts – making it a quiet and reliable source of power.

The electrolyte that separates the anode and cathode is an ion-conducting material. At the anode, hydrogen is stripped of its electrons so that the hydrogen ions (protons) pass through the electrolyte layer while the electrons pass through an external electrical circuit as a direct current that can power an external load. At the cathode, the protons are recombined with the electrons and oxygen to form water (Figure 2-1) (Wikipedia.org, 2013).

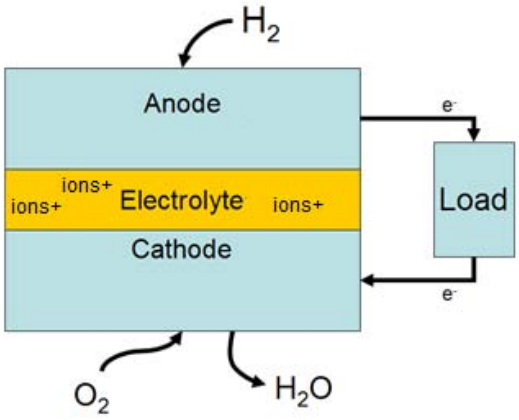

Figure 2-1: Schematic diagram of a fuel cell (Wikipedia.org, 2013)

The chemical reactions which occur are shown below.

Anode Reaction:	$2H_2 \leftrightarrow 4H^+ + 4e^-$	**reaction 1**
Cathode Reaction:	$O_2 + 4H^+ + 4e^- \leftrightarrow 2H_2O$	**reaction 2**
Overall Cell Reaction:	$2H_2 + O_2 \leftrightarrow 2H_2O$	**reaction 3**

The most commonly used fuel cell, proton exchange membrane (PEM) fuel cell, makes use of a polymer membrane which is able to transport protons. The PEM fuel cells use noble-metal catalysts notably platinum, on a conducting material that serves as the electrode, anode and cathode, positioned on either side of the membrane, respectively. Nafion® membranes (a sulphonated fluorocarbon polymer developed by DuPont) are the most commonly used membrane materials (Kolb, 2008). The H_2 is fed to one side of the membrane electrode assembly (anode) and O_2 or air to the other (cathode). PEM fuel cells

deliver high power density, offering the advantage of low weight and volume, when compared with other fuel cells (Kolb, 2008). Moreover, they operate at relatively low temperatures, around 80 °C, which allows for short start-up periods resulting in less wear on system components and, consequently, in higher durability.

A typical PEM fuel cell produces a voltage of 0.6 V to 0.7 V at full load (Wikipedia.org, 2013). To be able to deliver the desired energy capacity, individual cells are combined in series and parallel, where series connections yield higher voltage and parallel arrangement allows for a higher current. For practical PEM fuel cell systems running on reformate, 80% hydrogen utilisation is typical (Kolb, 2008). However, hydrogen utilisation in the fuel cell may drop to lower levels when decreasing the electric power withdrawal from the fuel cell while keeping the reformate flow constant (Kolb, 2008).

Carbon monoxide (CO) poisons the platinum catalysts which are used in conventional low temperature PEM fuel cells. This is due to CO being preferentially adsorbed on the platinum (Pt) catalyst particles' surface, such that the desired hydrogen splitting reaction can no longer take place (Kolb, 2008). However, this poisoning can be suppressed or at least be reduced for certain metal-platinum alloys, typically alloys with ruthenium (Ru), iron (Fe), cobalt (Co) and tungsten (W). For such alloys, Pt adsorbs CO preferentially while water is adsorbed on the second metal, promoting the in-situ oxidation of CO to CO_2. The long term CO tolerance of PEM fuel cells may be increased from a few ppm to values between 50 and 100 ppm via such alloy systems (Schmidt et al., 1994). The poisoning effect of any unconverted CH_4 is very small for conventional PEM fuel cells and up to 5 vol% methane is known to have no detrimental effect on the performance (Narusawa et al., 2003).

Other fuel cells exist which operate at much higher temperature, e.g. the molten carbonate fuel cell (MCFC) that operates at ca. 650 °C and the solid oxide fuel cell (SOFC) that operates at between 800 – 1000 °C but which makes them unsuitable for transportation and small portable applications due to the slow start-up time (Carrette et al., 2001) . The high operating temperature also places stringent durability requirements on the materials used (Kolb, 2008).

2.2 Fuel processing

Hydrogen production technologies, in general, can be divided into two main categories: fuel processing and non-reforming technologies, e.g. water electrolysis, the latter being beyond the scope of this study. Fuel processing is the process of converting hydrocarbons, alcohols or other energy carriers into H_2 or a hydrogen-rich gas mixture (reformate). The reaction normally takes place in the gas phase and is heterogeneously catalyzed.

A typical fuel processor for the production of a feed appropriate PEM fuel cells comprises reforming of the original fuel to produce syngas, water gas shift (WGS) conversion of most of the resulting CO to CO_2 and H_2, and a final purification stage involving either preferential oxidation (PrOx) or selective methanation of the remaining CO. Additionally, a furnace to heat the initial steam reforming reactor, fuel and/or water evaporators as well as heat exchangers are required, the latter to stepwise reduce the feed temperature of the individual downstream reactors and to improve the overall system efficiency (Kolb, 2008) as shown in Figure 2-2.

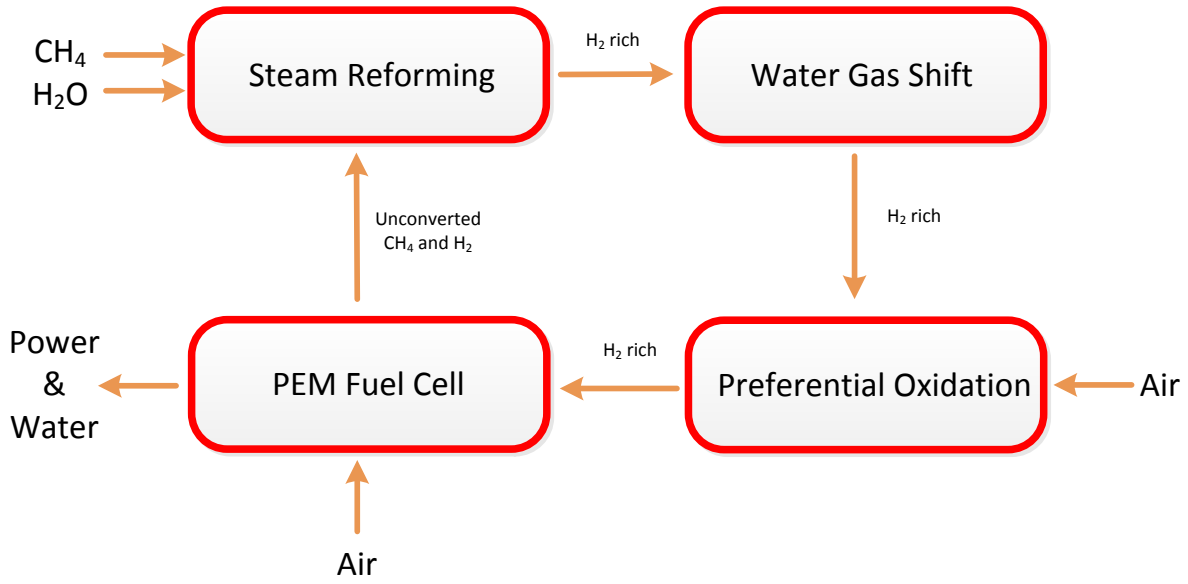

Figure 2-2: Block flow diagram of a typical fuel processing system

2.2.1 Reforming

There are three primary techniques for the initial step in producing hydrogen from hydrocarbon fuels, namely steam reforming, partial oxidation (POX) and autothermal reforming (ATR).

2.2.1.1 Steam reforming

The first steam reforming of coal to produce H_2 for the classic Haber-Bosch ammonia process was commercialized in 1917. This process reacts coal with steam to produce H_2 in an endothermic reaction (4) followed by the moderately exothermic water gas shift reaction (5). Since that time, carbon, in one form or another, has been used to extract hydrogen from water relying on these reactions (Twigg, 1989).

$$C + H_2O \rightarrow CO + H_2 \qquad \textbf{reaction (4)}$$

$$CO + H_2O \leftrightarrow CO_2 + H_2 \qquad \textbf{reaction (5)}$$

Generally speaking, steam reforming is the gas phase reactions in which energy carriers, such as hydrocarbons ($C_xH_yO_z$), react with steam to produce a H_2 and CO gas mixture, according to reaction (6) (Kolb, 2008). The product mixture of the endothermic reaction is called reformate.

$$C_xH_yO_z + (x - z)H_2O \leftrightarrow xCO + \left(x - z + \frac{y}{2}\right)H_2 \qquad \textbf{reaction (6)}$$

A typical fuel used in steam reforming is methane (CH_4). Other fuels typically used are liquid petroleum gas (LPG), methanol, ethanol, etc.

Steam reforming does not require O_2 and has a lower operating temperature than POX and ATR. It produces reformate with a high H_2/CO ratio which is beneficial for H_2 production (Holladay et al., 2009), such that steam reforming is the preferred process for H_2 production in industry.

2.2.1.2 Partial oxidation

Partial oxidation (POX) is the conversion of fuels with O_2 or air, according to reaction (7) (with air) (Kolb, 2008).

$$C_xH_yO_z + \frac{(x-z)}{2}(O_2 + 3.76N_2) \rightarrow xCO + \frac{y}{2}H_2 + 3.76\frac{(x-z)}{2}N_2$$ **reaction (7)**

The POX reaction is much faster than steam reforming but the disadvantage is that it forms (i) significantly higher amounts of CO compared with steam reforming, thus putting additional load onto the subsequent CO transformation stages and (ii) when carried out with air, it introduces a diluent (N_2) (Giroux et al., 2005).

2.2.1.3 Autothermal reforming

Autothermal reforming (ATR) is the reaction of steam reforming with an additional amount of air and is illustrated in reaction (8) (Kolb, 2008).

$$C_xH_yO_z + n(O_2 + 3.76N_2) + (x - 2n - z)H_2O \rightarrow xCO + \left(x - 2n - z + \frac{y}{2}\right)H_2 + 3.76nN_2$$ **reaction (8)**

In the case of O_2 is increased to a level where the energy generated by the oxidation reaction balances the energy consumption via steam reforming, the overall reaction becomes theoretically self-sustaining or autothermal (Kolb, 2008). However, in practical systems, heat loss need to be compensated and normally is via additional oxygen co-feed. ATR also requires either an expensive and complex O_2 separation system to feed pure O_2 to the reactor or the product gas is diluted with N_2 from air (Kolb, 2008).

2.2.2 CO clean up

For PEM fuel cells operating on reformate, the CO concentration needs to be minimised, preferably to levels below 5 ppm, via a combination of water-gas shift conversion and either preferential oxidation (PrOx) or selective methanation.

2.2.2.1 Water-gas shift

Water-gas shift (WGS) is the CO conversion process that follows the reformer. The purpose is to convert most of the CO in the reformate to CO_2.

$$CO + H_2O \leftrightarrow CO_2 + H_2$$ **reaction (5)**

The reaction is slightly exothermic and equilibrium limited. Industrially, the reaction is usually divided into two consecutive steps, namely a high temperature shift stage to convert most of the CO and low temperature shift to achieve high overall equilibrium conversion. If a single step WGS reaction was utilised, a considerably larger reactor bed would be required due to the depressed kinetics associated with low temperature operation only. Depending on the feed composition, the CO concentration in the high temperature water-gas shift product ranges between 2 and 3 vol%, whereas in the low temperature water-gas shift product it ranges between 0.05 - 1 vol% (Joensen and Rostrup-Nielsen, 2002).

2.2.2.2 Preferential oxidation

Preferential oxidation (PrOx) is one of the two reaction options to remove the remaining CO after WGS reaction.

$$CO + \frac{1}{2}O_2 \rightarrow CO_2$$ **reaction (9)**

However, the reaction is accompanied by the undesired side reaction, as per reaction (10).

$$H_2 + \frac{1}{2}O_2 \rightarrow H_2O$$ **reaction (10)**

PrOx usually requires excess air with a minimum O/CO ratio of between 1.5 and 2.0. Assuming full conversion of CO, for every mole of CO converted, between 0.5 and 1.0 mole of H_2 is lost. Most catalysts applied for the PrOx of CO have some activity for WGS and also its reverse reaction (11) (Kolb, 2008). Consequently, depending on conditions, notably higher temperatures, the ultimate CO levels from PrOx may be limited.

$$H_2 + CO_2 \leftrightarrow H_2O + CO$$ **reaction (11)**

2.2.2.3 Selective Methanation

Selective Methanation is the conversion of the remaining CO to CH_4 using some of the H_2 produced.

$$3H_2 + CO \leftrightarrow H_2O + CH_4$$ **reaction (12)**

The main advantage of methantion over PrOx is that no air addition is required. However, methantion consumes three moles of H_2 per mole of CO converted, which is larger than the losses by PrOx (Kolb, 2008). Additionally, the methantion catalyst must be selective to CO, versus the comparatively large amounts of CO_2 present, since CO_2 methantion would consume vast amounts of hydrogen.

2.3 Steam Methane reforming

The steam methane reforming (SMR) process consists of two reversible reactions, a strongly endothermic reforming reaction (13) and the moderately exothermic WGS reaction (5).

$CH_4 + H_2O \leftrightarrow CO + 3H_2$ ΔH°298 = + 206 kJ/mol **reaction (13)**

$CO + H_2O \leftrightarrow CO_2 + H_2$ ΔH°298 = − 41 kJ/mol **reaction (5)**

The reforming reaction (13) is strongly endothermic, so the forward reaction is favoured by high temperature and low pressure (Figure 2-3). The WGS reaction (5) is exothermic, equimolar, and is promoted by low temperature but normally unaffected by changes in pressure. PEM fuel cells in small scale operation are typically operating at slightly elevated pressure, which benefits the upstream steam reforming process.

The stoichiometric requirement for steam to carbon molar ratio (S/C) is 1.0 in SMR reaction. However, this is not practicable in steam reforming environment since all catalysts so far developed tend to promote carbon deposition reactions. These reactions, however, can only be suppressed by using an excess of steam, with the minimum S/C is typically around 1.7. Furthermore, the reforming reaction itself is also promoted by an excess of steam (Figure 2-3) and in practise ratios between 3.0 and 3.5 are commonly used (Twigg, 1989).

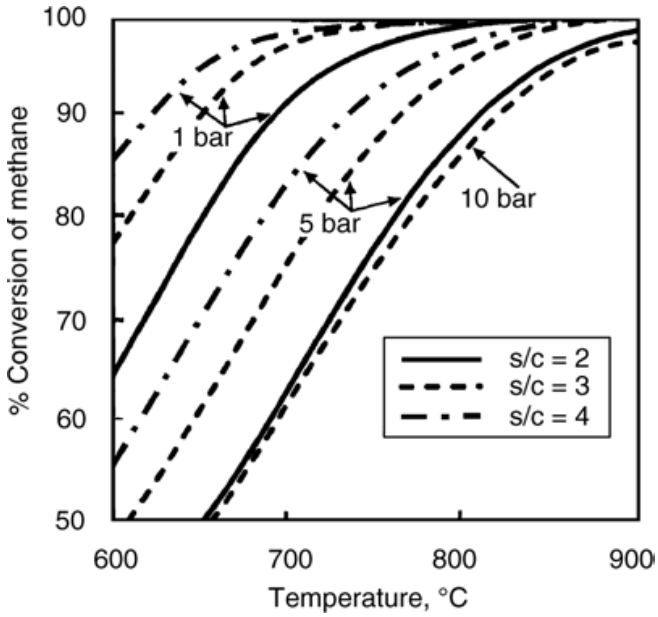

Figure 2-3: Equilibrium conversion of SMR versus reaction temperature for various S/C ratios and operating pressures (Joensen and Rostrup-Nielsen, 2002)

The SMR reaction mechanism is dependent on the catalyst, primarily on the active metal and the nature of the support. One of the earliest proposed rate expressions were provided by Xu and Froment, (1989). They studied kinetic and mechanistic details on a Ni/$MgAl_2O_4$ catalyst and concluded the following mechanistic scheme:

$s1$: $CH_4 + S \leftrightarrow CH_4 \cdot S$

$s2$: $H_2O + S \leftrightarrow O \cdot S + H_2$

$s3$: $CO \cdot S \leftrightarrow CO + S$

$s4$: $CO_2 \cdot S \leftrightarrow CO_2 + S$

$s5$: $H \cdot S + H \cdot S \leftrightarrow H_2S + S$

$s6$: $H_2S \leftrightarrow H_2 + S$

$s7$: $CH_4 \cdot S + S \leftrightarrow CH_3 \cdot S + H \cdot S$

$s8$: $CH_3 \cdot S + S \leftrightarrow CH_2 \cdot S + H \cdot S$

$s9$: $CH_2 \cdot S + O \cdot S \leftrightarrow CH_2O \cdot S + S$

$s10$: $CH_2O \cdot S + S \leftrightarrow CHO \cdot S + H \cdot S$

$s11$: $CHO \cdot S + S \leftrightarrow CO \cdot S + H \cdot S$ (rate determining step)

$s12$: $CHO \cdot S + O \cdot S \leftrightarrow CO_2 \cdot S + H \cdot S$ (rate determining step)

$s13$: $CO \cdot S + O \cdot S \leftrightarrow CO_2 \cdot S + S$ (rate determining step)

* S represents the catalyst surface site

The rate equations that were obtained based on the rate determining steps are:

For $CH_4 + H_2O \leftrightarrow CO + 3H_2$,

$$r_1 = \frac{k_1}{P_{H_2}^{2.5}}(P_{CH_4}P_{H_2O} - \frac{P_{H_2}^3 P_{CO}}{K_1})/(DEN)^2 \quad \textbf{eqn 1}$$

For $CO + H_2O \leftrightarrow CO_2 + H_2$,

$$r_2 = \frac{k_2}{P_{H_2}}(P_{CO}P_{H_2O} - \frac{P_{H_2}P_{CO_2}}{K_2})/(DEN)^2 \quad \textbf{eqn 2}$$

Where $DEN = 1 + K_{CO}P_{CO} + K_{H_2}P_{H_2} + K_{CH_4}P_{CH_4} + K_{H_2O}P_{H_2O}/P_{H_2}$

There are many other groups have continued the work of Xu and Froment and presented their own mechanisms. Rostrup-Nielsen et al. (2002) proposed a model which is presented below:

$s1$: $CH_4 + 2 \cdot S \leftrightarrow CH_3 \cdot S + H \cdot S$

$s2$: $CH_3 \cdot S + S \leftrightarrow CH_2 \cdot S + H \cdot S$

$s3$: $CH_2 \cdot S + S \leftrightarrow CH \cdot S + H \cdot S$

$s4$: $H_2 + 2 \cdot S \leftrightarrow CO_2 + 2H \cdot S$

Another mechanism had been proposed by Wei and Iglesia (2004). In their study, the reactions of CH_4 with CO_2 and H_2O on Rh clusters were investigated and it was concluded that the reaction rates were proportional to CH_4 partial pressure, however, it is independent of CO_2 and H_2O partial pressures, which led them to the conclusion that the C-H bond activation steps were those of principal kinetic relevance. The activation of C-H bonds has also been shown to be irreversible and that recombinative desorption steps of H atoms with OH groups form H_2 or H_2O.

$s1$: $CH_4 + 2 \cdot S \rightarrow CH_3 \cdot S + H \cdot S$ (rate determining step)

$s2$: $CH_3 \cdot S + S \rightarrow CH_2 \cdot S + H \cdot S$

$s3$: $CH_2 \cdot S + S \rightarrow CH \cdot S + H \cdot S$

$s4$: $CH \cdot S + S \rightarrow C \cdot S + H \cdot S$

$s5$: $CO_2 + 2 \cdot S \leftrightarrow CO \cdot S + O \cdot S$

$s6$: $C \cdot S + O \cdot S \leftrightarrow CO \cdot S + O \cdot S$

$s7$: $CO \cdot S \leftrightarrow CO + S$

$s8$: $H \cdot S + H \cdot S \leftrightarrow H_2 \cdot S + S$

$s9$: $H \cdot S + O \cdot S \leftrightarrow OH \cdot S + S$

$s10$: $OH \cdot S + H \cdot S \leftrightarrow H_2O \cdot S + S$

$s11$: $H_2O \cdot S \leftrightarrow H_2O + S$

Comparing the Wei and Lglesia mechanism with the Xu and Froment mechanism, it can be seen that the former mechanism indicates that reactions of carbon intermediates with oxygen are the rate determining step, which means that oxygen plays bigger role in the reaction kinetics in the case of Rh. In the other hand, the mechanism of Xu and Froment indicates that the reactivity of the metal towards C-H bond breaking governs the overall reaction kinetics in the case of Ni.

2.3.1 Reforming catalyst

Traditional SMR catalysts for the industrial production of H_2 and syngas are based on Ni or Co applied as shell catalysts. These catalysts are usually synthesised by precipitating Ni or Co as an insoluble compound, from a soluble salt, in the presence of refractory supports including mixture of aluminium oxide, magnesium oxide, calcium oxide and calcium aluminate cement. These supports usually are sufficiently porous to allow gas to gain access to the Ni surface. Normally between 7 and 80 wt% Ni is used. Alternatively, the Ni can be incorporated by impregnating a preformed catalyst support, e.g. alumina or aluminate, with a solution of a nickel salt which is subsequently decomposed by heating to the oxide (Twigg, 1989). SMR catalysts are often promoted with alkali or alkaline-earth compounds to accelerate carbon removal (Rostrup-Nielsen, 1993).

The calcination and reduction procedures and the metal precursor used to impregnate the support strongly affect the catalytic properties of the prepared catalyst. Wang and Lu (1998a) studied the effect of the nickel precursor on the Ni/ɣ-Al_2O_3 activity under methane reforming condition. They found that inorganic precursors (e.g. nickel nitrate) derived catalysts are more active and stable than organic-derived ones. Wang and Lu (1998b) also

found that Ni/MgO reduced at 500 °C is not as active as when reduced at 700 °C. This is further confirmed by Matsumura and Nakamori (2004) in their study on the reforming of CH_4 over Ni/ɣ-Al_2O_3 catalysts.

Ni catalysts need to be reduced to achieve full activity. Ni loses activity in contact with air through oxidation, an event which requires subsequent reactivation. Additionally, the heat generated by oxidation of the metallic Ni may cause degradation of the catalysts through sintering (Farrauto et al., 2003). Ni catalysts in their active form are pyrophoric, which means that they spontaneous ignite when exposed to air (Farrauto et al., 2003). This leads to problems in the actual operation of small scale fuel processors that are not operated continuously but in start/stop mode, especially when the feed container needs to be changed or replaced.

Christensen (1996) calculated that the effectiveness factor of Ni steam reforming catalysts in industrial processes was approximately 20%. An excess of catalyst and the low cost of the Ni catalyst normally counterbalanced this low catalyst utilisation. However, the situation is rather different for smaller scale fuel processor applications where the mass of the catalyst and the size of the reactor are critical issues. Thus formulations of catalysts with higher activity such as PGMs show great advantages. Furthermore, the high cost may further be counterbalanced by a better utilisation of the catalyst, e.g. as achieved by washcoating thin catalyst layers onto the walls of micro-channel reactor (Section 2.4.1).

Trimm and Önsan (2011) also pointed out that none of the aforementioned difficulties with Ni catalyst occurs with PGM based catalysts. PGM based catalysts are catalysts containing metals such as rhodium (Rh), ruthenium (Ru), platinum (Pt), palladium (Pd) and rhenium (Re) or mixtures thereof. Alumina, magnesia or rare earth oxides such as ceria and zirconia or mixtures thereof serve as the carrier material (Trimm and Önsan, 2011). The same group of researchers have also studied the turn-over numbers for SMR over alumina-supported catalysts and found that Rh is the best catalyst for this reaction (Turn over numbers: Rh (13) > Ru (9.6) > Pd (1.0) ~ Ni (1.0) > Pt (0.9)). Rh catalysts become more attractive due to the metal's decreased price compared to platinum. Regardless, Rh metal content utilised in the catalysts has to be minimised (Trimm and Önsan, 2011).

Wang et al. (2004) prepared Rh catalysts on an alumina carrier for SMR reaction in micro-channel reactors. Catalysts were prepared with 1, 5 and 10 wt% Rh content and achieved stable catalyst activities over a range of S/C ratios. The Rh crystallite sizes ranged from 6.3 nm in 1 wt% Rh catalyst to 15.3 nm in 10 wt% Rh catalyst. The catalysts containing 5 wt% Rh showed the highest activity (Figure 2-4) and, experimental results confirmed that the Rh/MgO-Al_2O_3 catalysts were very active for methane steam reforming as well as showed excellent resistance to coke formation at stoichiometric S/C ratio of 1 for over 14 hours on stream with no sign of deactivation (Wang et al., 2004).

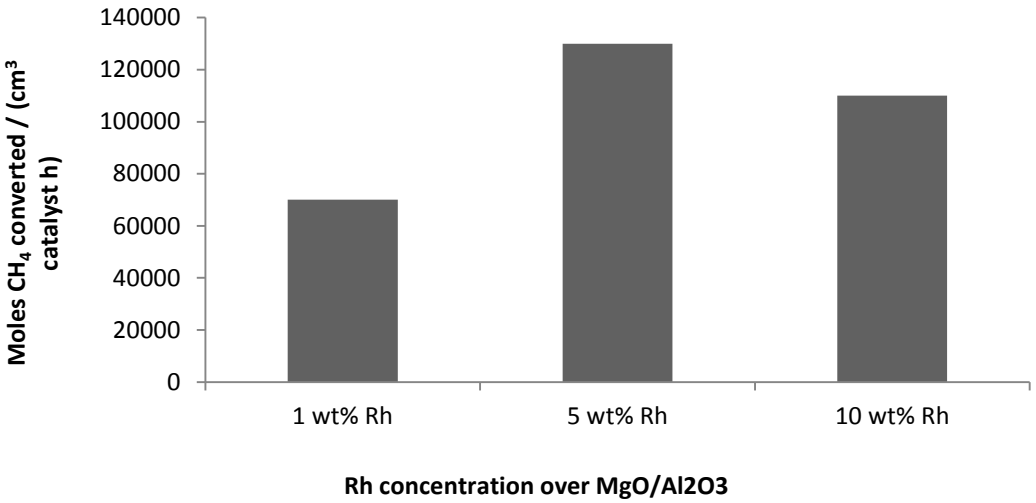

Figure 2-4: Effect of Rh loading on steam methane reforming activity of Rh/MgO–Al_2O_3 catalysts (830 °C, 12 atm, S/C ratio = 2, contact time = 1.9 ms) (Wang et al., 2004)

Johnson et al. (2007) reported stable performance of Rh catalysts, prepared from α-alumina shims by impregnation with rhodium. A sample with 3.7 wt% Rh showed stable performance during a 100 h test at 900 °C (Johnson et al., 2007).

2.3.2 Conventional steam methane reforming

Steam methane reformers have been built over a wide range of sizes. A scheme for a conventional steam methane reformer is shown in Figure 2-5. For large scale chemical processes such as an oil refinery, steam reforming produces 0.7 to 2.8 million standard cubic meters of H_2 per day (Rostrup-Nielsen, 1993). In order to supply the heat for the overall endothermic steam-reforming reaction, the catalyst is packed into several high temperature

resistant alloy tubes (typically 7.5 – 12.0 meters long) placed inside a furnace equipped with burners (usually using CH_4 gas as fuel) as indicted in Figure 2-5 (Rostrup-Nielsen, 1993). Typical inlet temperatures are 450 – 650 °C, and the products gas leaves the reformer at 700-950 °C depending on the applications (Rostrup-Nielsen, 1993).

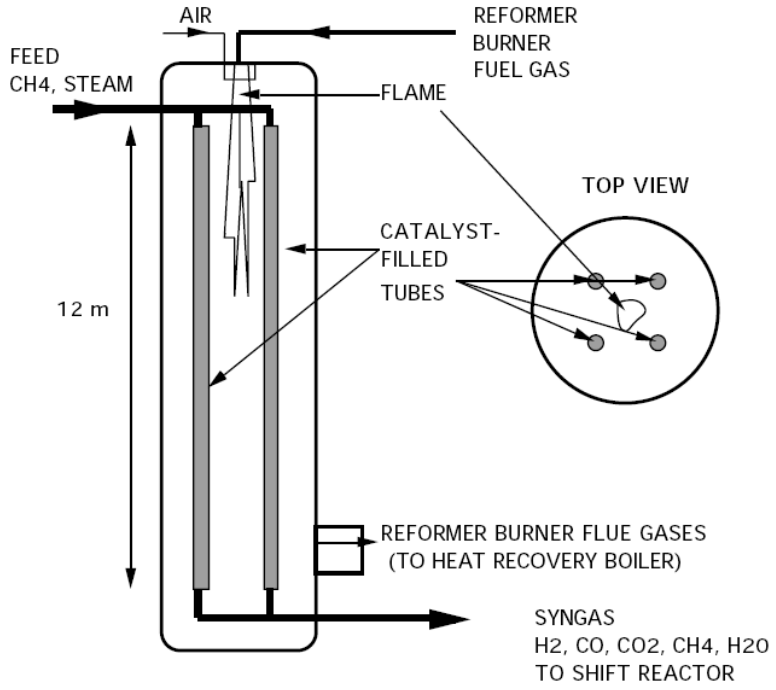

Figure 2-5: Conventional steam methane reformer (Rostrup-Nielsen, 1993)

These long tube reactors, however, suffer from a number of inherent problems. Pronounced axial and radial temperature gradients can exist because of the limited heat transfer rate in the packed bed (Kim and Kwon, 2006). In addition, because of the limitations in the heat transfer rate, this type of reactor typically requires a long time to reach working temperature from cold start-up. Furthermore, the packed bed reactors suffer from large gas pressure drop in the catalyst tube due to the catalyst packings. For these reasons, it is generally believed in hydrogen and fuel cell research, that a more compact, lower cost reformer would be needed for standalone H_2 production.

2.3.3 Integrated fuel processing

On an industrial scale, the heat source for the reforming process is supplied by heating tubular steam reforming reactors externally via homogeneous combustion as shown in

Figure 2-5. For stationary fuel cell systems on the scale of larger power plants this technology is still applicable (Kolb, 2008). However, the smaller the energy supply system becomes, the less viable this solution is due to the fact that the heat loss, integration and space demands become more stringent. As discussed in Section 2.1, fuel cell systems operating on reformate do not consume H_2 completely and a significant amount, typically 20%, leaves the fuel cell anode unconverted. This unconverted H_2 may be fed back to the fuel processing chain to provide heat for reactions (Mathiak et al., 2004). Integrated heat exchange/reactor configurations open the door to such integrated fuel processor embodiment.

A methane or natural gas fuel processor with a thermal energy rating of 2.5 kW coupled with a 1 kW_{el} PEM fuel cell, as shown in Figure 2-6, was described by Mathiak et al. (2004). The reformer utilized a Ni catalyst and was operated between 750 and 800 °C. The PrOx reactor was operated at an O/CO ratio of 3.5 and at steady state operation a CO content between 20 and 50 ppm could be achieved. 500 W of energy was supplied to the steam reformer by burning the recirculated anode off-gas in the burner (Mathiak et al., 2004).

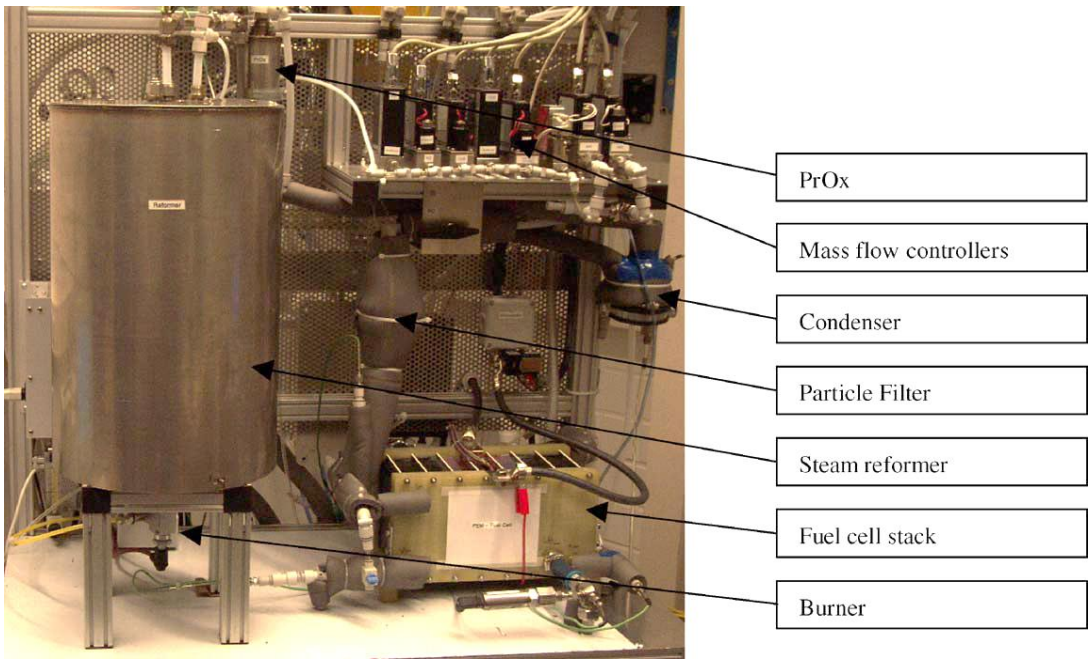

Figure 2-6: Coupled fuel processor/fuel cell stack. (Mathiak et al., 2004)

Seris et al. (2005) presented a prototype CH_4 fuel processor designed to supply a 15 kW fuel cell and the system is shown in Figure 2-7. It comprises steam reforming coupled with anode

off-gas combustion as well as high and low temperature WGS in multiple adiabatic packed bed reactors. The prototype fuel processor is shown in Figure 2-8 − in the foreground the pre-reformer and the high temperature WGS reactors are visible. However, the reformer/combustion block with steam generation and flue gas heat recovery are not visible and were incorporated inside the larger metal block (Seris et al., 2005).

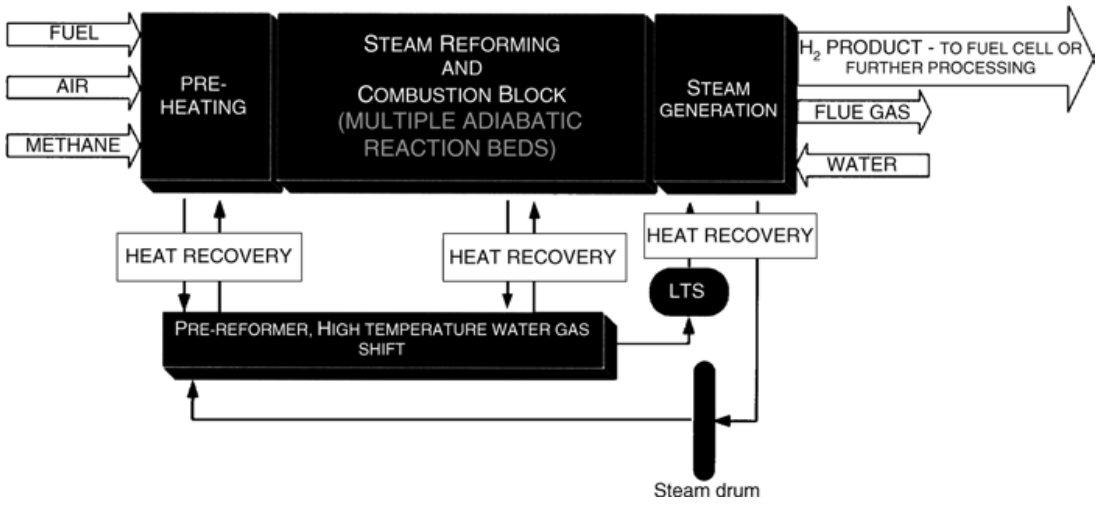

Figure 2-7: Schematic diagram of the 15-KW prototype methane fuel processor (Seris et al., 2005)

As discussed above, when the exothermic combustion reaction and the endothermic reforming reaction are taking place on opposite sides of the same wall, the heat produced by combustion could be readily transferred to and consumed by the reforming reaction. In so doing, the heat exchange is significantly intensified and the bulk stream temperature difference (ΔT_{bulk}) between the two sides is greatly reduced (Reuse et al., 2004). As the reactor dimension reduces to the micro-scale (20 – 600 µm), even in the situation of $\Delta T_{bulk} <$ 50 K, the heat transfer efficiency (defined as the ratio of the heat utilized by the steam reforming to the heat released by the combustion reaction) could exceed 0.8, while in a conventional heat exchanger a maximum of only 0.6 is attainable (Reuse et al., 2004). Consequently, the development of integrated fuel processor systems at the micro scale is indicated.

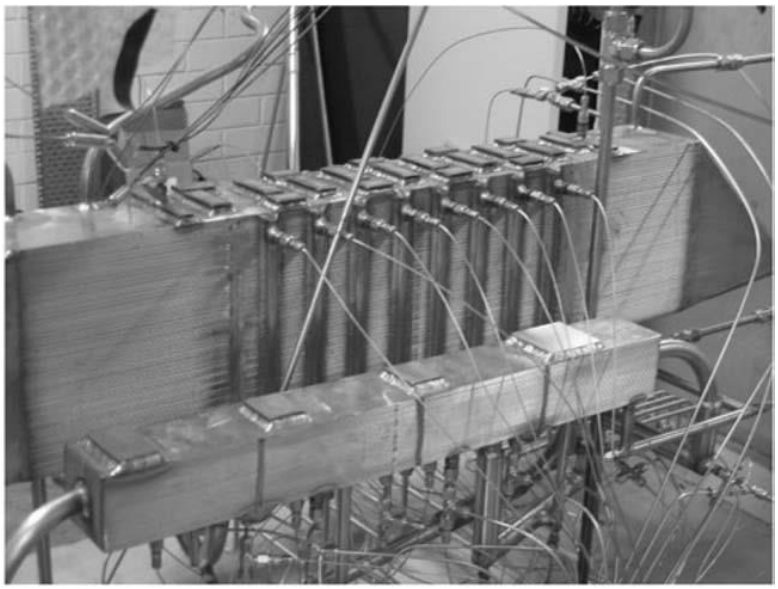

Figure 2-8: 15-kW prototype methane fuel processor developed by Seris et al. (2005)

2.4 Micro-structured reforming

Mostly, micro-structured reactors have multiple parallel channels with diameters between 10 and several hundred micrometres.

The small parallel flow path reduces the distance between the heat source and the heat sink, such that the corresponding heat transfer by radiation and convection is greatly enhanced. In addition, since the catalyst is incorporated into the system as a thin layer covering a metallic or ceramic surface, the reactors exhibit a very low pressure drop when compared to conventional packed bed reactors (Kiwi-Minsker and Renken, 2005).

The main feature of micro-structured reactors is their high surface-to-volume ratio, which is in the range of 500 -50 000 m^2/m^3 compared to more traditional chemical reactors such as packed bed reactors, and which provides a strong “driving force” to speed up thermodynamic processes (Ehwald et al., 2000). The surface-to-volume ratios in conventional laboratory and production vessels are normally around 100 m^2/m^3 and seldom exceed 1 000 m^2/m^3. Normally, micro-structured reactors are operated under laminar flow. The heat transfer coefficient is inversely proportional to the channel diameter and their values are typically about 10 kW/m^2 K, roughly one order of magnitude higher than in conventional equipment (Ehrfeld et al., 1999). This high heat transfer property permits

utilization of the full potential of catalysts during highly endothermic or exothermic reactions and avoids hotspots or coldspots (Kolb and Hessel, 2004). The small diameters of the reactor channels ensure a short radial diffusion time leading to a narrow residence time distribution. Avoiding heat- and mass-transfer limitations are the main objectives for micro-structured reactor development in comparison to more conventional apparatus. In addition, the small reactant and product inventories lead to inherent safety during the reactor operation. It has been reported that micro-structured reactors run safely even under extreme conditions, including within the explosion regime (Veser et al., 1999). Moreover, small reactor dimensions facilitate the use of distributed production units at the place of consumption, avoiding transport and storage of dangerous materials, and scale-up, by multiplying the number of micro-structured reactors in parallel or series without change of the channel geometry, is a straightforward process.

In summary, micro-structured reactors are suitable for fast, highly exothermic or endothermic reactions because they offer process intensification, inherent reactor safety, broader reaction conditions including operation within the explosion regime, distributed production and faster process development (Kolb and Hessel, 2004). Consequently, micro-structured fuel processors may be small, efficient, modular, lightweight and potentially inexpensive.

2.4.1 Micro-channel steam reforming

Micro-channel reactors are defined as a casing for performing reactions which results in micro-flow phenomena whereby characteristic flow guidance and unique processing properties occur (O'Connell et al., 2009). Typically, a micro-channel plate or element consists of multiple micrometer-sized channels which are connected to reservoirs containing reactants and products (Truter, 2011).

Cao et al. (2005) presented micro-structured catalysts used for SMR in micro-channel reactors. Two types of engineered catalysts were evaluated in micro-channel reactors with different configurations. One catalyst, designated DF, consists of two single felts with identical dimensions (0.25 mm X 9 mm X 51 mm) and another catalyst, designated C, is in a corrugated shape known as a "ruffle", as shown in Figure 2-9. Performance eveluating

showed that catalyst DF is more active than catalyst C. However, the stability result of these catalysts was not disclosed.

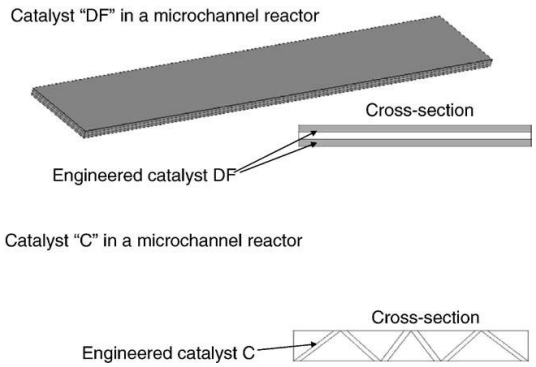

Figure 2-9: Mirostructured catalysts in micro-channel reactors (Cao et al., 2005).

Ni catalyst coated on Fecralloy® micro-channel foils were tested for SMR by De Miguel et al. (2010). Three Ni catalysts on different support (MgO, Al_2O_3 and CeO_2/Al_2O_3) were described. The catalysts were applied to the micro-channel foils (Figure 2-10) using a pipette and the excess slurry was removed with adsorbent paper. Each micro-channel reactor tested in the study consisted a stack of 21 foils clamped together inside a test reactor. MgO and Al_2O_3 supported catalysts showed excellent methane steam reforming activity. However, the Ni-CeO_2/Al_2O_3 catalyst activity was not stable, and a deactivation (decline in conversion) slope of 11 %/h was observed (de Miguel et al., 2010).

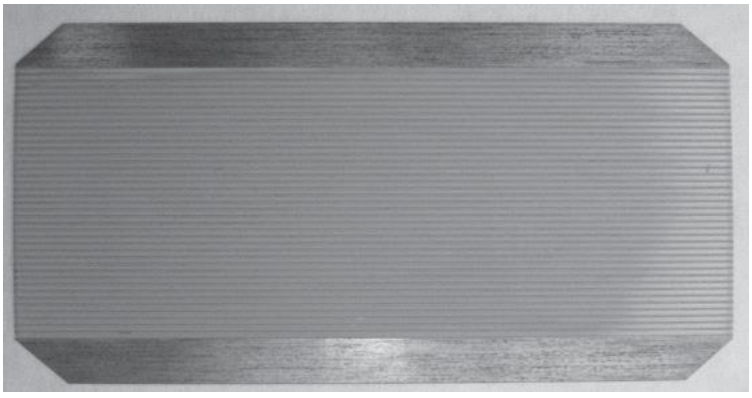

Figure 2-10: Picture of a catalyst coated micro-channel foil (de Miguel et al., 2010)

Kolb et al., (2004) presented a propane steam reformer based on micro-channel technology. Wash-coated alumina catalyst coatings were introduced onto micro-channels plates as

shown in Figure 2-11, subsequently welded face-to-face to form a micro-channel reactor. In-house prepared Rh, Pt and Pd catalysts were tested in a standard screening protocol at a S/C ratio of 1.4, temperatures of 450, 550 and 650 °C and an 8 millisecond residence time. The Rh catalyst was found to be stable over 6 hours of catalytic testing. However, the Pt and Pd catalysts deactivated significantly within 1 hour at 650 °C, which was attributed to coke formation (Kolb et al., 2004).

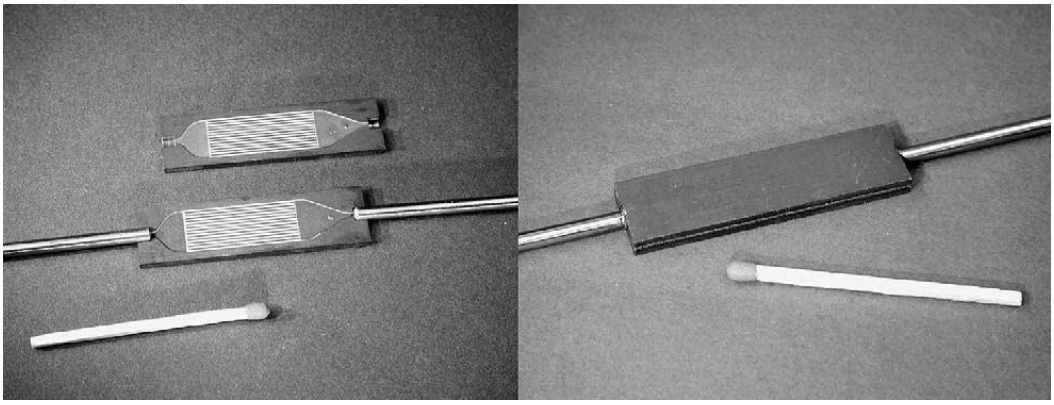

Figure 2-11: Reactor applied for propane steam reforming; left: coated plates with tubing; right: welded plates (Kolb et al., 2004)

2.4.2 Advantages and disadvantages of micro-channel reactors

As discussed previously, one of the main aspects giving micro-reactors superior performance when compared to conventional reactors is the increased surface-to-volume ratio (inverse of the hydraulic diameter) between 500 - 50 000 m^2/m^3(Ehwald et al., 2000). The advantages which stem from the high surface-to-volume ratios include superior mass and heat transfer properties.

Internal mass transfer limitations are determined by pore diffusion in the catalyst for both packed bed and micro-channel reactors. For packed bed reactors, the reactants must diffuse through the catalyst pellets. Similarly, in the micro-channel reactors, the reactants on the external surface of the catalyst layer must diffuse through the catalyst coating, however, the catalyst coating is generally much thinner in comparison to the pellet radius which reduces the prevalence of internal mass transfer limitations (Walter et al., 2005).

Heat transfer coefficients in micro-channel reactors typically exceed 10 kW/m^{2}K which is as much as an order of magnitude greater than the conventional heat exchangers which have overall heat transfer coefficients below 2 kW/m^{2}K (Ehwald et al., 2000). In several reactions the micro-channel reactor achieved a better performance for the same temperature in comparison to the conventional reactor (Navascuès et al., 2010; Sebastian et al., 2009; Yueng et al., 2009).

The disadvantages of micro-channel reactors in production stem from the scaling law whereby the processing equipment becomes more cost-effective with increasing size (Peters, 2003). The significant challenge encountered when numbering up from an individual micro-channel reactor to a multiple stack of micro-channel reactors, is the ability to uniformly distribute the inlet flow to the parallel arrangement of micro-channel reactors (Quiram et al., 2007).

In micro-channel reactors, laminar flow prevails which makes external mass transfer dependant only on molecular diffusion driven by concentration gradients (Walter et al., 2005). The extent of the concentration gradient in the micro-channels will mainly govern external mass transfer limitations in the micro-channel reactor since there are no mixing effects as is the case in fixed-bed reactors.

Fouling and the need for cleaning of the equipment are other disadvantages to be overcome in order for the micro-channel reactors to be commercialized (Wörz et al., 2001).

2.4.3 Fabrication of micro-channel reactors

Material of construction

The choice of material for construction takes into account corrosion and thermal properties. Various materials such as glass, silicon, stainless steel, aluminium and copper have been used to make micro-channel reactor plates.

Iron-chromium-aluminium alloys (FeCralloy) are a particularly advantageous material due to the formation of a surface oxide layer, during thermal pre-treatment, which improves adherence of the catalyst coating. However, the high price of this material is delaying

commercial uptake of the micro-channel reactors. Materials like FeCralloy also present an extreme challenge in regard to the techniques used for joining the parts (Zhao et al., 2003).

Zapf et al., (2006) showed that by applying a combination of suitable pre-treatment and coating technique it was possible to achieve coatings with very good adhesion on stainless steel micro-channels. They showed that the most important issue for the good adhesion is the thermal pre-treatment of the stainless steel, which generates a thin oxide layer that better matches the chemical nature of the washcoat, similar to FeCralloy, but with more flexibility in the choice of fabrication materials. The techniques for joining stainless steel parts are well established, while FeCralloy substrates still present an extreme challenge.

Micro-structuring

There are several different methods available to form the micro-channels in the plate, including micro-milling, electro-discharge machining, wet chemical etching, punching, embossing, laser micro-machining and sintering (Hessel et al., 2005).

The micro-structuring of stainless steel plates was applied by wet chemical etching in this study. In wet chemical etching, a photo-resist is used for masking the plates and usually an iron chloride solution is used for etching. This technology is suitable for mass production and channel depths can vary from in the range of 100 - 600 μm, which is the channel size usually applied in micro-structured fuel processing applications (Kolb, 2008).

Catalyst coating

There are various coating techniques available which are dependent on the material of the micro-channel reactor and the catalyst. These techniques includes wash-coating, chemical vapour deposition, cathodic sputtering, sol-gel deposition, electrophoretic deposition, etc. (Meille, 2006). However, the most prominent coating technique for catalysts is wash-coating which allows both the coating of a catalyst carrier and the coating of already made catalyst onto the substrate (Kolb, 2008). A more extensive description of wash-coating technology is provided in Section 2.5.

Micro-channel plate sealing

After catalysts are coated onto the micro-channel plates, two coated plates are sealed together face-to-face to form a micro-channel reactor. Laser welding technology is generally applied because of the amount of energy used to join the micro-channel plates is low and limited to only the plate edges. This is particularly beneficial as the catalyst cannot tolerate the high temperatures associated with conventional welding technology. Other bonding techniques which can be applied include electron beam welding, diffusion bonding, brazing, and sintering (Hessel et al, 2005).

2.5 Catalyst wash-coating

In terms of micro-channel reactors, the wash-coating technique described by Zapf et al. (2006) has frequently been employed to apply various metal oxide supported catalysts onto the micro channel plates.

In this method, the coating suspension comprises a ɣ-alumina supported catalyst (average particle size 3 µm), deionised water, polyvinyl alcohol (PVA) binder and acetic acid. The stainless steel (German grade 1.4571) micro-channel plates are cleaned and thermally treated at 800 °C so that a thin oxide layer forms. The channels are filled completely with coating suspension and any surplus is removed. Catalyst coated reactors were tested (100 hours) for steam reforming of propane and stable and high activity was observed (Zapf et al., 2006).

Venkataraman et al. (2003) studied steam reforming of methane in a catalytic wall reactor. The FeCralloy plates were first oxidized in air at 900 °C to form a layer of alumina on the surface of the metal substrate. ɣ-alumina was used as the support for the active metals and was wash-coated onto the metal substrate. The ɣ-alumina was partially converted to α-alumina when the alumina-coated metal substrate was subsequently fired to ~ 1 000 °C, after which it was impregnated with a solution of H_2PtCl_6. The resulting catalyst coated wall reactor was tested for SMR reaction and a high conversion and stable operation was reported (Venkataraman et al., 2003).

Zhai et al. (2011) studied SMR over a Ni catalyst in a micro-channel reactor. In their study, alumina was thermally sprayed onto the FeCralloy substrate at a temperature of 1 200 °C, to produce the metal-ceramic complex substrate. The binding force between the two substances was greatly enhanced due to the ceramic particles embedding within the metal surface oxide layer. The metal-ceramic substrate was subsquently impregnated with a solution of $Ni(NO_3)_2$ or $RhCl_3$. Such catalyst coated plates showed excellent catalytic performance in the SMR reaction and long-term stability was observed (Zhai et al., 2011).

2.5.1 Properties of the wash-coating suspension

Key issues relating to the wash-coating suspension include catalyst concentration, catalyst particle size, the solvent used and the binder applied.

2.5.1.1 Catalyst concentration

Catalyst concentration in the suspension has direct effect on the viscosity of the suspension which is closely related to the suspension stability, reproducibility and uniformity of the final coating layer. An increase in solids concentration results in a lower inter-particular distance and lower fluidity which causes the viscosity to increase. Mitra and Kunzra (2008) found the viscosity of zeolite suspensions to increase exponentially with zeolite concentration as long as the zeolite concentration in the coating suspension does not exceed 50 %.

2.5.1.2 Particle size

Catalyst (or support) particle size is an important variable in obtaining a stable suspension.

Agrafiotis and Tsetsekou (2000a) studied the effect of particle size on suspension properties for the wash-coating of ɣ-alumina onto cordierite monoliths. It was found that a washcoat prepared from 2 µm particles produced a more adherent coating in comparison to washcoats from larger, 17 and 52 µm, particle sizes.

Nijhuis et al. (2001) reported that slurry-coating particles of approximately 5 µm will produce suitably porous catalyst layer. Coating with smaller particles is not recommended, because for smaller particles a denser layer with smaller pores will be formed in which diffusion resistances can occur. Coating with particles larger than 5 µm will cause an

irregular final catalyst layer. The result of this irregular coating is usually a system with a bimodal pore distribution, with small pores originating from the pores of the coated particles and larger pores, typically 2 µm, originating from the inter-particle voids.

2.5.1.3 Solvent

Water is commonly used as the solvent in most wash-coating suspensions. Properties of the suspension can be modified using different solvents since the viscosity and surface tension of the solvent will affect the final coating layer. However, this has seldom been researched.

2.5.1.4 Binder

A binder is always included in coating suspensions. The binder not only improves the stability of the suspension, but also the adhesion and loading of the coating layer (Mitra and Kunzra, 2008). Typically, a binder consists of particles of much smaller size than those of the catalyst in use, enabling small binder particles to pack between the spaces of the larger catalyst particles. Normally, two types of binders are considered inorganic and organic. Organic binders improve the surface contact between the larger catalyst particles during the drying process, but are ultimately removed during the calcination step. During the process of drying and calcination, the smaller binder particles are moved to the point of contact between the larger catalyst particles by capillary forces, hence increasing the surface contact between the larger particles which, in turn, aids in the anchorage of the catalyst particles (Agrafiotis and Tsetsekou, 2000b).

Poly vinyl alcohol (PVA) is a frequently used as an organic binder. The addition of PVA to a zeolite ZSM-5 suspension improved the adherence of the wash-coating onto FeCralloy monoliths (Eleta et al., 2009). In the paper presented by Zapf et al. (2006) for coating ɣ-Al_2O_3 onto micro-channels, 5 wt% PVA was added to the wash-coating suspension. However, it has also been reported for alumina coating, that the addition of 1.5 wt% PVA resulted in a slower water evaporation rate during drying, with the prevention of subsequent shrinking and cracking of the alumina layer (Hwang et al., 2007).

Other frequently used organic binders are methylhydroxyethyl cellulose (Tylose), and polyethylene glycol (PEG). The binders' molecular weight and chemical structure influences the thickening effect so that, for the same amount of binder, a trend of increasing viscosity

was observed as: PEG < PVA < Tylose (Germani et al., 2007). Moreover, a higher bulk density coating resulted, leading to cracking and thus poor adhesion. Tylose was found to provide the best compromise between layer density and shrinkage (Germani et al., 2007).

Previously, the addition of Al_2O_3 has been used as a inorganic binder to improve the strength of the zeolite extrudates (Kasture et al., 2007). The wash-coating of ɣ-Al_2O_3 has also resulted in coatings with good adherence (Zapf et al., 2006). Truter (2011) also claimed that an increase in ɣ-Al_2O_3 composition improves the adherence of the washcoat on the micro-channel plates. This improvement in adherence may be attributed to the ɣ-Al_2O_3 binder having a smaller particle size and hence reducing the average particle size, as well as decreasing the suspension viscosity (Truter, 2011).

2.5.2 Properties of the catalyst coating layer

2.5.2.1 Uniformity and reproducibility

The uniformity (a measure of the homogeneity of a suspension's composition or character) and reproducibility (degree of agreement in coating between different batches of suspensions) of the catalyst coating layer are critical for the properties of the catalyst. High uniformity and reproducibility needs to be achieved since large variations will have negative impact on the adhesion, catalyst loading, layer porosity and resulting catalyst activity.

Both Mitra and Kunzra (2008) and Agrafiotis and Tsetsekou (2000a) have concluded that a low solids concentration (approximately 20 wt%) should be used to enhance coating reproducibility. It was found that the viscosity of the suspension influences the uniformity and reproducibility of the catalyst coating layer and low solids concentration translates to a low viscosity suspension which improves both the uniformity and reproducibility of the catalyst coating.

Moreover, in a paper presented by Germani et al. (2007), it was concluded that high viscosity suspensions produce thicker coatings on the micro-channel side walls and lower viscosity suspensions producing thicker coating in the bottom of the micro-channel.

2.5.2.2 Adhesion tests

Various tests have been developed to quantify the adhesion stability of a washcoat. In one method developed by Yasaki et al. (1993), the coating layer was exposed to ultrasonic treatment for 1 hour in petroleum ether and subsequent drying at 110 °C for 2 hours, after which the weight loss was determined.

Another method has been presented by Zapf et al. (2006) in which a drop test was developed. In this test, the coated plate was dropped from a fixed height and the weight loss was recorded. A detailed description of this method is given in experimental Section 4.2.2.4.

3 Objectives of study

The aims of this study are to investigate the stability and activity of commercial PGM catalysts and to determine operating conditions suitable for the optimum performance of selected catalysts with respect to SMR in micro-channel reactors. More specifically, the following objectives have been identified:

- To test whether or not commercial PGM steam reforming catalysts are still applicable when transferred as a coating onto micro-channel reactors
- To test and compare such commercial catalysts for the steam reforming of methane in micro-channel reactors
- To determine optimum operating conditions by varying temperature, pressure, S/C ratio and space velocity of the selected catalysts
- To determine whether the catalysts and coating procedures employed yield stable SMR performance at the conditions of interest

4 Experimental

The experimental part of this project involves testing commercial and self-prepared catalysts, in both packed bed and micro-channel reactor configurations.

4.1 Catalysts and physical-chemical characterization

4.1.1 Commercial catalysts

The steam reforming catalysts XR and YR were supplied by two different commercial partners. These catalysts are specified for SMR duty; however, due to confidentiality agreements, no further details about the catalysts can be disclosed in this publication other than that catalyst XR is a ZrO_2-CeO_2 supported platinum catalyst. Catalyst XR was supplied in powder form and was wash-coated in-house onto the micro-channel reactors. Catalyst YR was wash-coated onto the same micro-channel reactor by the second commercial partner and also supplied in egg-shell form as for packed bed testing.

4.1.2 Catalyst synthesis

Additionally, an alumina supported Rh catalyst was prepared by incipient wetness impregnation. 6 g of alumina powder was pre-calcined at 800 °C for 2 hours. 0.18 g rhodium nitrate (36 wt% Rh) salt was mixed with 2.4 ml of deionised water and the metal solution was added to the alumina support at room temperature. Thereafter, the mixture was exposed to ultrasonic treatment under vacuum for 15 minutes. The resulting catalyst was subsequently dried in air and calcined at 450 °C for 2 hours.

4.1.3 Micronizing

For some of the experiments conducted, the catalyst was micronized into smaller particle sizes using a McCrone micronizing mill with water as the ‘solvent’. Approximately 4 ml of catalyst was milled each time. After micronizing, a wide particle size distribution was found (Appendix B) and, in general, 40 -50 vol% of the catalyst particles were larger than 10 µm. It was also found that micronizing for longer times did not further reduce the particle sizes.

4.1.4 Catalyst characterisation techniques and procedures

4.1.4.1 Brunauer–Emmett–Teller surface area and H_2 chemisorption

Brunauer–Emmett–Teller (BET) surface area analysis was performed using the standard N_2 adsorption method in a Micromeritics apparatus (ASAP 2000) equipped with two Edwards vacuum pumps (E2M-0.7).

CO Chemisorption was undertaken in the same apparatus according to the following procedure. The powdered sample was heated to 100 °C in flowing N_2 to remove adsorbed water. N_2 was then replaced with H_2 and the temperature increased to 450 °C at 10 °C/min. The temperature was maintained at 450 °C for one hour, after which the H_2 flow was stopped and the sample chamber evacuated to a pressure of 1 µm Hg for two hours. The temperature was subsequently lowered to 35 °C at which chemisorption was performed.

4.1.4.2 Transmission electron microscopy

A Nano-TEM (TECNAI-20) instrument was used with an 80 kV to 200 kV electron beam. The catalyst sample was supported on copper grids for TEM analysis and the images obtained allowed for calculation of particle sizes directly from the size on the photographic print.

4.1.4.3 Determination of the catalyst Rh content

A Varian 730 ICP-OES (inductively coupled plasma - optical emission spectrometer) instrument was used to determine the Rh content of fresh catalysts. The sample was digested with a mixture of hydrochloric, hydrofluoric and nitric acids in a MARS-5 microwave digester, followed by neutralization with boric acid prior to analysis.

4.2 Micro-channel reactor

4.2.1 Micro-channel plates

Micro-channel plates used in this work are made from stainless steel (German grade 1.4571) and the micro-channels were acid-etched by Ätzetechnik Herz GmbH in Germany. Table 4-1 provides the elemental analysis of the micro-channel reactor plate. A schematic view of the

micro-channel plate is presented in Figure 4-1, showing relevant physical dimensions. There are two 1/8" holes drilled at the inlet and the outlet of the micro-channel plate to incorporate 1/8" stainless steel tubes for feed delivery and product removal, respectively, and each plate comprised of 15 hemi-circular channels, each roughly 300 µm deep and 500 µm wide. The micro-channel plates were thermally pre-treated, wash-coated, calcined and welded together face-to-face to form a micro-channel reactor (Section 4.2.2.4).

Table 4-1: Stainless steel micro-channel plate composition

Element	**wt%**
Carbon	≤ 0.08
Silicon	≤ 1.0
Manganese	≤ 2.0
Phosphorus	≤ 0.045
Sulphur	≤ 0.015
Chromium	16.5 – 18.5
Molybdenum	2.0 – 2.5
Nickel	10.5 – 13.5
Titanium	5 × C ≤ 0.7

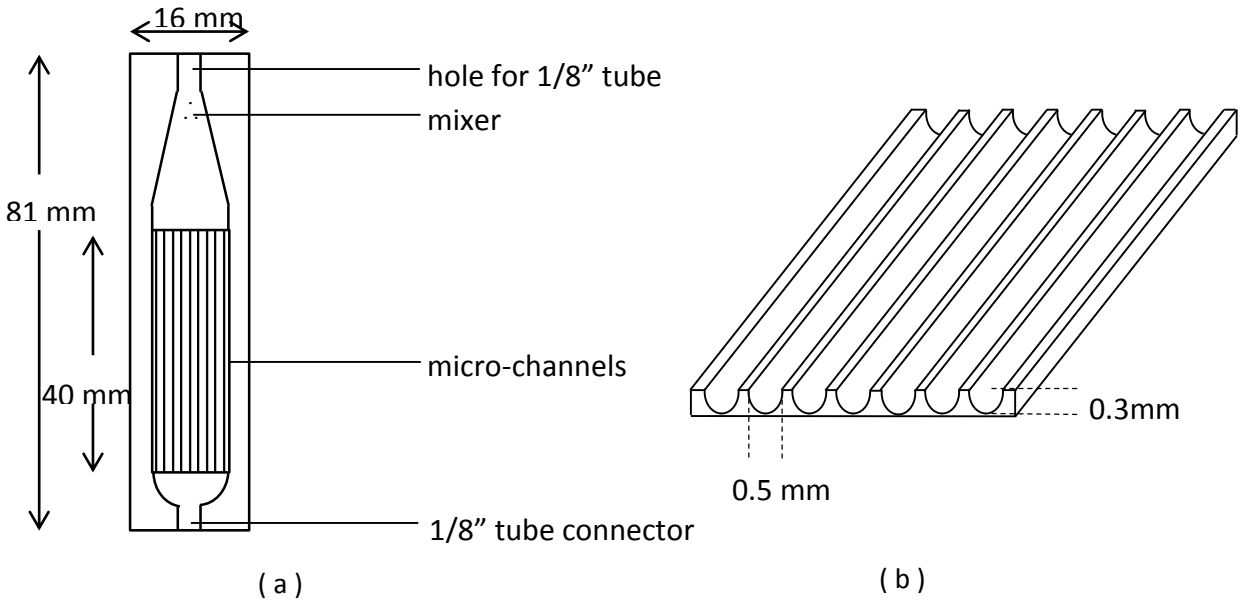

Figure 4-1: A typical micro-channel plate (a) top view and (b) channel cross-sectional view

4.2.2 Wash-coating methodology

Catalysts were wash-coated onto the micro-channel plate based on the method described by Zapf et al. (2006) which involves pre-treatment of the micro-channel plates, preparation of a catalyst coating suspension, wash-coating of the suspension onto the micro-channel plates and a post-coating processes.

4.2.2.1 Pre-treatment of the micro-channel plate

The plates were first cleaned in an ultrasonic bath with isopropanol for 15 minutes to remove residual chlorine from the acid etching process, followed by drying at ambient conditions for 30 minutes.

The plates were further calcined in air at 800˚C for 2 hours according to the temperature programme presented below:

- Heat to 120 ˚C at 1 ˚C/min and hold for 2 hours
- Heat to 800˚C at 1 ˚C/min and hold for 2 hours
- Cool to room temperature

During calcination a thin metal oxide layer formed on the surface of the stainless steel plate for purposes of improving adhesion between the micro-channel plate and the catalyst support during the subsequent washcoating process. After thermal treatment, the plates are darker in colour compared to their initial shiny metallic colour, and due to the formation of the oxide layer.

The thermally treated micro-channel plates are handled with gloves to eliminate possible alteration of the weight of the plates due to operating by bare hands and weighed prior to catalyst coating. Gloves should be worn at all times after thermal treatment.

4.2.2.2 Preparation of the catalyst washcoating suspension

To prepare the catalyst suspension, 5 g of polyvinyl alcohol (PVA) and 75 ml deionised water were mixed in a container and placed into a waterbath with a magnetic stirrer and was stirred at 160 rpm at 65˚C for 3 hours to dissolve the PVA, after which the solution was left overnight without stirring at room temperature to release the air from the solution.

Thereafter, 20 g of catalyst powder was added to the PVA solution followed by 1 g of acetic acid. The mixture was stirred at 160 rpm at 65˚C for 2 hours, followed by 3 days stirring at room temperature to form a homogeneous suspension.

A simple test was used to check whether the suspension was homogeneous. It involved checking the sharpness of the suspension edges on the container wall when swirling the suspension container. The suspension was considered to be homogenous and ready for coating if the suspension edges are 'smooth'. If the suspension edges appeared rough or jiggered, it was left stirring at room temperature until such time as it passed the visual inspection test.

4.2.2.3 Suspension coating process

The area outside the channels on the micro-channel plates was masked with polymer tape before applying the coating suspension (Figure 4-2). The masking tape was applied as close to the channels as possible but not overlapping them.

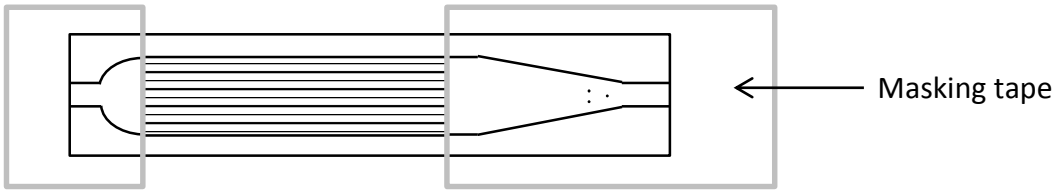

Figure 4-2: Masking of a micro-channel reactor

A few drops of the suspension was placed in the middle of the channels as shown in Figure 4-3; the amount of suspension being sufficient for the process since subsequent suspension addition adversely affects the quality of the final catalyst coating (Truter, 2011). A scraper with a sharp edge was used to scrape the suspension from the middle to one end of the micro-channel (step 1 in Figure 4-3) and repeated from the middle to the other side (step 2 in Figure 4-3). Finally the suspension was scraped over the complete length of the channels (step 3 in Figure 4-3). Caution was taken to ensure that the suspension completely filled the ends of all channels (Truter, 2011).

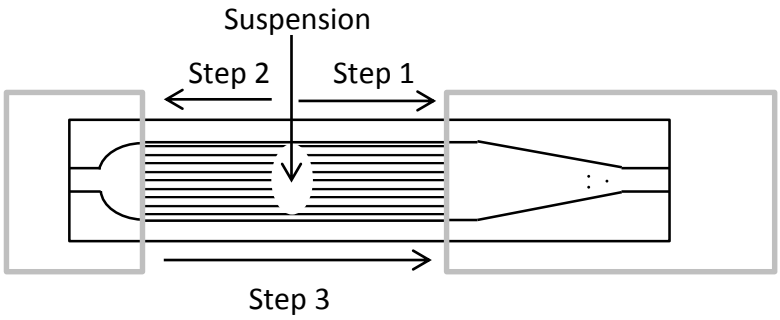

Figure 4-3: Suspension scraping sequence

4.2.2.4 Post-coating treatment

After the wash-coating process, the plates were dried at ambient conditions. Once dried, the masking tapes were removed and the plates were further dried and calcined, according to the processes below, to remove the binder (PVA), acetic acid and residual water – A process which was shown to be effective for this purpose by Thermogravimetric analysis (Appendix F). The calcination temperature is largely dependent on the type of catalyst used. For alumina supported catalysts, the following temperature programme was used:

- Heat to 120˚C at 1 ˚C/min and hold for 2 hours
- Heat to 600˚C at 1 ˚C/min and hold for 2 hours
- Cool to room temperature

Alternatively, for ceria supported catalyst, the following temperature programme was used:

- Heat to 120˚C at 1 ˚C/min and hold for 2 hours
- Heat to 450˚C at 1 ˚C/min and hold for 6 hours
- Cool to room temperature

After calcination, any excess catalyst outside the micro-channels was removed. Thereafter, the micro-channel plates were weighted and the amount of the catalyst was determined take into account their pre-coating dry weight as determined in Section 4.2.2.1.

A drop test was performed to test catalyst adhesion. As shown schematically in Figure 4-4, the micro-channel plate was attached to the metal block with the catalyst coating layer facing sideways and dropped along a metal rod onto the base. The process was repeated 5

times and the plate was subsequently weighed. The weight loss resulting from this drop test was used to assess the quality of catalyst adhesion.

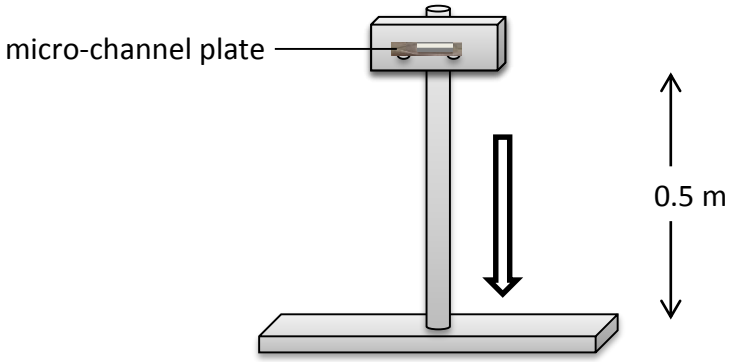

Figure 4-4: Drop test experimental apparatus

After completion of the drop test, the micro-channel plates were laser welded together, face-to-face, with the corresponding 1/8 inch tubing to form a reactor (refer to Figure 4-5). Pulsco-laser welding technology was utilised in the welding process due to the high accuracy and concentrated heat source, therefore eliminating potential thermal damage to the catalyst coating.

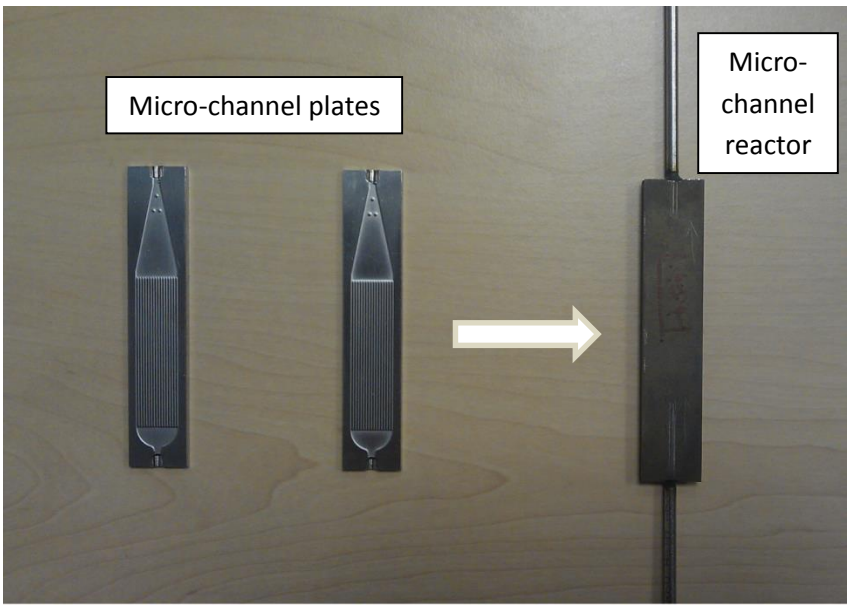

Figure 4-5: Individual micro-channel plates and welded micro-channel reactor

4.3 Steam methane reforming test unit

A piping & instrumentation diagram (P&ID) of the steam reforming test unit used in this study is presented in Figure 4-6. The equipment consists of a feed delivery section for gases and steam, a down-flow vapouriser and packed bed reactor (PBR)/micro-channel reactor assembly, followed by a water knock-out system downstream and prior to a product analysis section (online gas chromatography).

4.3.1 Feed delivery

All the dry gases used in this work are supplied from cylinders (supplied by Air liquid SA or Air Products SA). Gas flow rates are regulated by mass flow controllers (MFCs, Brooks Instruments, T97692 series), calibrated for standard temperature and pressure (STP, 0 °C and 1 atmosphere pressure).

All the dry gases were mixed in a blending pot and were introduced into the reactor via a further reactor MFC. An intentional excess dry gas entering the blending pot and left via the by-pass stream (via spring-loaded back pressure regulator BPR-1) representing the mixed dry gas composition for chromatographic analysis.

Water was introduced by an HPLC pump (Lab Alliance series 1500) via a 50 cm length of capillary column (50 µm internal diameter) to the inlet of the vapouriser section of the vapouriser-reactor assembly. The purpose of the capillary column was achieving a stable liquid flow by creating a pressure difference between the pump head and the vapouriser. Depending on the reactor type used, packed bed or micro-channel configuration, the vapouriser section was introduced differently.

4.3.2 Vapouriser

As indicated in Section 4.3.1, liquid water was introduced into the top of the vapouriser via an intermediate length of capillary tubing with the end of the capillary in physical contact with the vapouriser packing so as to ensure ‘smooth’ vaporization of the water flow and the avoidance of dropwise flash vaporization.

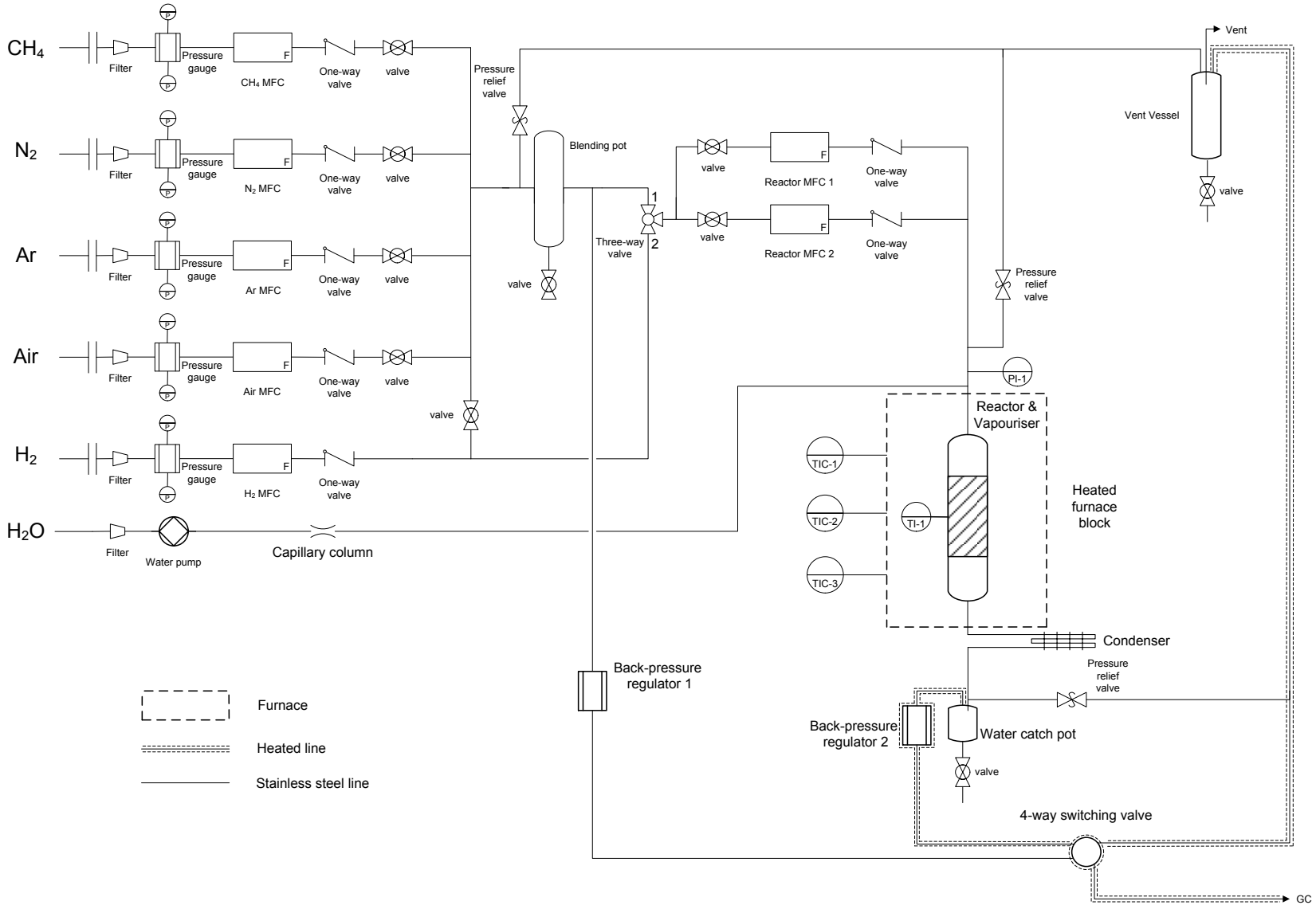

Figure 4-6: Schematic of experimental steam methane reforming apparatus

For the packed bed reactor configuration, as indicated in Figure 4-8, the top part of the reactor tube serves as a vapouriser which is packed with clean silicon carbide (1 mm granulate) to enhance heat transfer inside the vapouriser.

For the micro-channel reactor configuration, the vapouriser-reactor assembly used is shown in Figure 4-10. Clean silicon carbide (1 mm granulate) was used as the packing material and a layer of quartz wool was placed at the bottom of the vapouriser to prevent any silicon carbide passing into the micro-channel reactor.

4.3.3 Reactor assembly

Two different types of reactor configurations were used in this study. The packed bed reactor was made from German grade 1.4401 stainless steel. The micro-channel reactors were made from German grade 1.4571 stainless steel. Both reactor systems were inserted into cylindrical cores within a furnace comprising three heating bands. All the three heating bands were controlled individually to maintain the temperature of the catalysts bed as close to isothermal as possible - sample temperature profiles being illustrated in Figure 4-7.

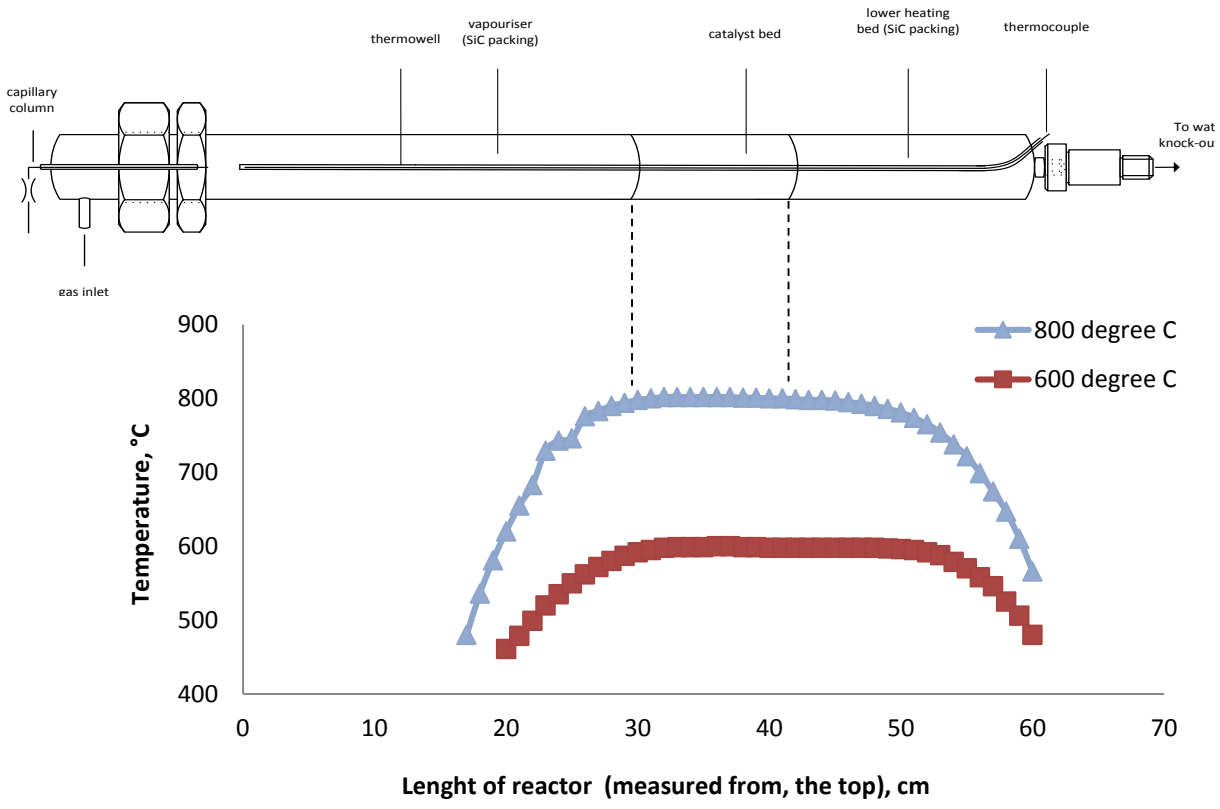

Figure 4-7: Temperature profiles with the packed bed reactor configuration

4.3.3.1 Packed bed reactor

The packed bed reactor, illustrated in Figure 4-8, consists of an approximately 70 cm long stainless steel tube of 16 mm internal diameter and comprises a vapouriser zone, catalyst zone and a lower heating zone. A thermowell of 3 mm diameter is incorporated axially in the reactor to accommodate a K-type thermocouple.

The reactor was mounted in vertically in a bench vice and the lower heating zone packing (1 mm silicon carbide granulate) was loaded first. The packing was compacted by gently tapping the external reactor wall. Thereafter, 0.3 g of catalyst was diluted with fine silicon carbide (300 µm particle size) to a total volume of 2 ml and loaded into the reactor, taking up an effective bed length of approximately 20 mm. Finally, the remaining reactor volume (vapouriser zone) was completely filled with 1 mm silicon carbide granulate such that, upon mating the reactor body with the gas and liquid delivery head, the liquid water capillary entered to approximately 10 mm below the surface of the vapouriser packing. The position of the catalyst bed was determined by the location and length of the furnace isothermal zone and the amount of silicon carbide granulate packed into the lower heating zone.

4.3.3.2 Micro-channel reactor

The welded micro-channel reactor was fitted into metal sleeves as shown in Figure 4-9 before attachment to the vapouriser body and head assembly, and insertion into the furnace. The purpose of the metal sleeves is to provide better heat conductivity and also to ensure an isothermal temperature profile in the micro-channel reactor configuration. These metal sleeves were made of Inconel® alloy. Sleeves S1 and S4 (Figure 4-9a) have a circular key-hole to accommodate the 1/8 inch stainless steel inlet/outlet tubes, whereas sleeves S2 and S3 (Figure 4-9b) have a rectangular key-hole to accommodate the micro-channel reactor body. All sleeves include a thermowell to accommodate the reactor measurement thermocouple.

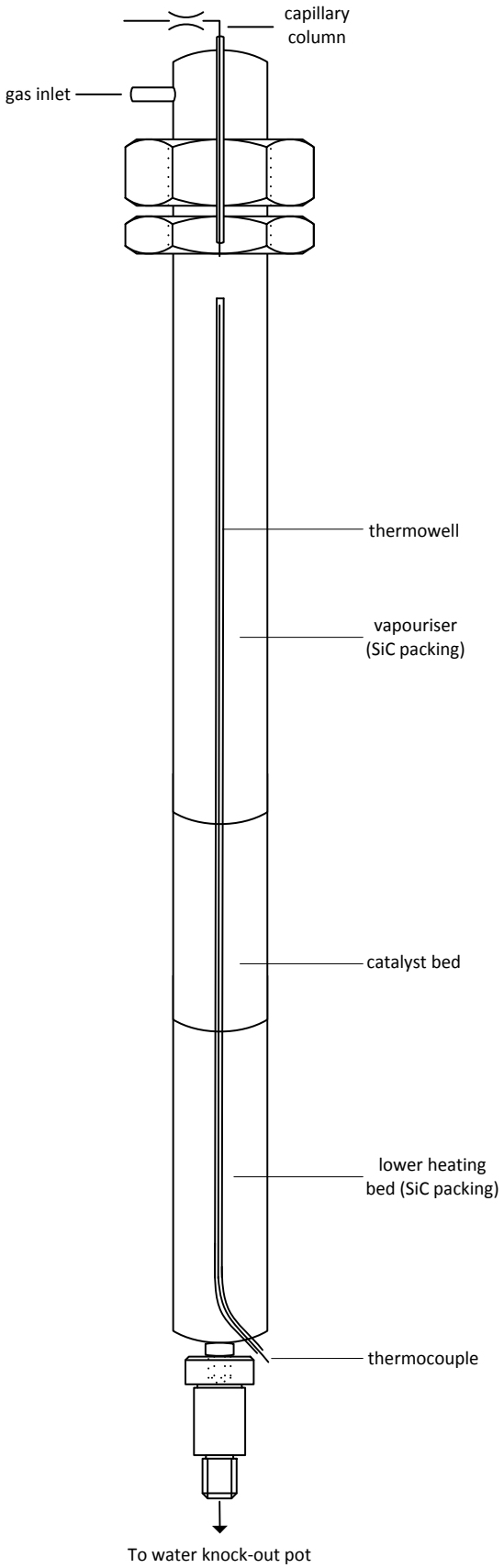

Figure 4-8: Packed bed reactor configuration

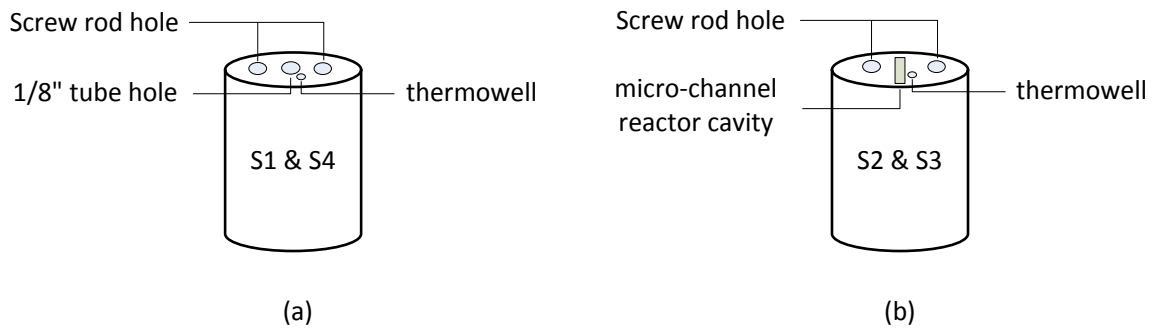

Figure 4-9: Micro-channel reactor sleeves

The micro-channel reactor was placed into the sleeves and secured with the screw rods. Figure 4-10 illustrates the completed micro-channel reactor assembly.

4.3.4 Water knock-out section

Unconverted steam was condensed after the reactor by a water knock-out section and only dry gas products were analysed by the on-line GC. The water knock-out section consists of a coil condenser and a water catch pot. The condenser consists of a jacketed 1/8 inch stainless steel coil through which the reactor effluent gas flows and a mixture of ethylene glycol and water was used as coolant (2 °C) in a counter current flow arrangement. The condensed water was collected in the catch pot. The water knock-out section was designed for a residence time of between 1 and 2 minutes, depending on the effluent gas flow rate.

4.4 Operating conditions

Catalysts were investigated for SMR performance across a range of operating conditions, most notably temperature, steam to carbon ratio and specific mass flow rate.

Dry gas composition

The dry gas feed comprised of 98 vol% CH_4 and 2 vol% Argon (Ar), the letter as an internal standard for online GC analysis.

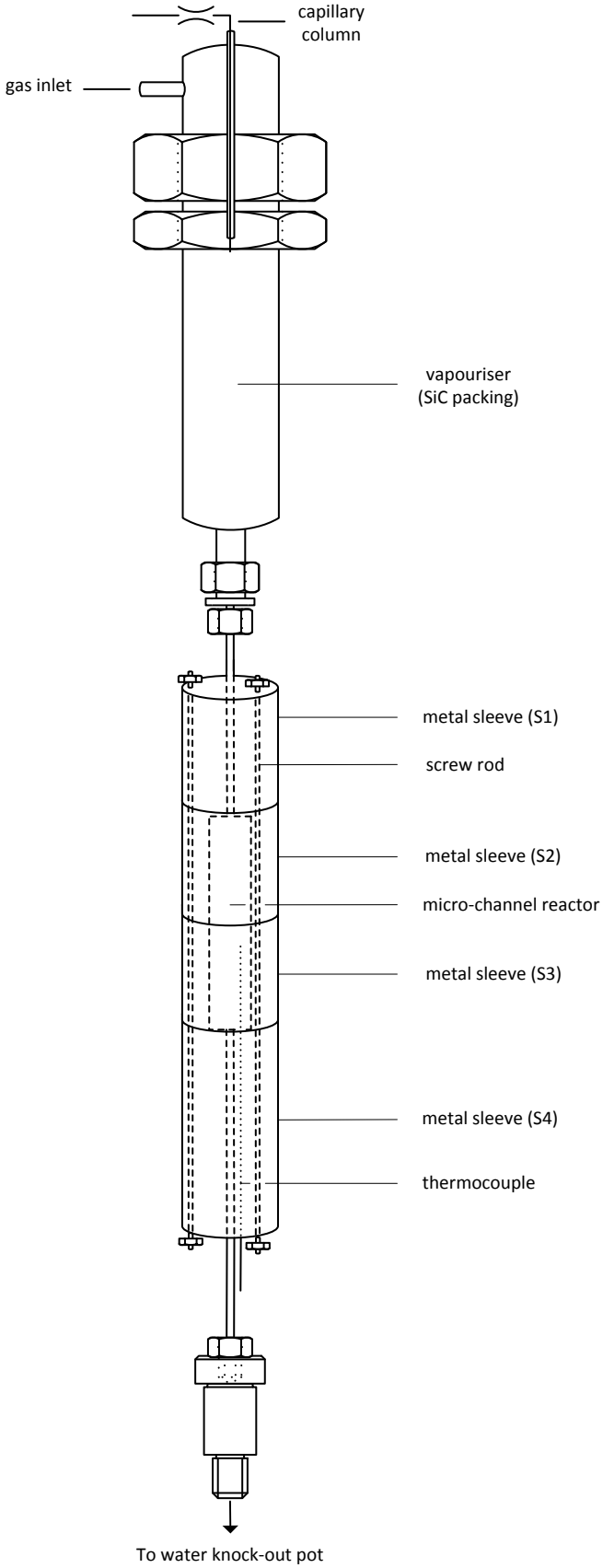

Figure 4-10: Micro-channel reactor configuration

Temperature

The catalyst performance evaluations were conducted in a temperature range between 700 °C and 900 °C.

Pressure

Reaction pressure was controlled by means of a spring-loaded back-pressure regulator (Tescom 44-4700 series) which was placed downstream of the water knock-out section. All experiments were carried out at a pressure of 1 bar_g.

Steam to carbon ratio (molar)

Steam to carbon (S/C) ratios were calculated based on the operational requirements of a hypothetical downstream PEM fuel cell. To avoid membrane dehydration and cathode flooding inside the fuel cell, lower and higher humidification ranges of 50% relative humidity at 70 °C and 80% relative humidity at 100 °C, respectively, were considered – corresponding to molar steam to carbon ratios between 2 and 5 for the reformer feed (Appendix C). Therefore, molar steam to carbon ratios of 2, 3 and 5 were evaluated.

Minimum CH_4 conversion targets

From literature (Section 2.1), the CH_4 content in the fuel cell feed must be less than 5 vol% to avoid any detrimental effect on the performance of the fuel cell. Consequently, at S/C ratios of 2, 3 and 5, minimum CH_4 conversion targets are 80%, 77% and 70%, respectively (Appendix C).

Space velocity

Standard gas-hourly space velocity (SGHSV) is the simplest definition (eqn 3) to relate flow rate to the catalyst mass and is frequently used in commercial systems employing packed bed reactors. The definition becomes less usefull when the catalyst is coated onto a monolith or plate because of it is not clear of which volume to use.

$$SGHSV, h^{-1} = \frac{\dot{V}_{feed,dry}}{V_{catalyst}} \qquad \textbf{eqn 3}$$

In this study, *specific space velocity* (*SSV*) is used, which is defined as the ratio of the volume flow of the dry feed (at standard conditions; 0 °C and 1 atm) to the weight of the catalyst:

$$SSV, ml(h \cdot g_{catalyst})^{-1} = \frac{\dot{V}_{feed,dry}}{M_{catalyst}} \qquad \textbf{eqn 4}$$

This value is independent of the way in which the catalyst is introduced into the system (Kolb, 2008).

4.5 Steam methane reforming test procedures

4.5.1 Reactor assembly and leak test

The packed bed (Figure 4-8) or welded micro-channel reactor (Figure 4-10) assembly is inserted into the heating furnace, followed by connection of the feed and effluent lines, and insertion of the thermocouples into the reactor thermowell. A leak test is performed at 5 bar_g for approximately 5 hours prior to an experiment with a typical pressure loss of less than 0.1 bar over the 5 hours duration of the test.

4.5.2 Catalyst reduction

After satisfactory completion of the leak test, the catalyst is reduced in H_2 at a flow rate of 20 sccm. The temperature of the reactor was ramped up to 750 °C at a rate of 1 °C per minute from ambient temperature and hold at 750 °C for 2 hours before changing to reaction temperature.

4.5.3 Reactor operation

4.5.3.1 Start-up procedure

It should be noted that all heated lines indicated in Figure 4-6 were maintained at 60 °C.

- The dry gas feed mixture was introduced into the blending pot via appropriate setting on the CH_4 and Ar mass flow controllers. The excess dry gas was released through the by-pass stream via a back-pressure regulator
- Water pump was started at the desired setpoint

- After about 30 minutes the H_2 was switched off and the dry gas feed was introduced into the reactor
- Pressure was increased to reach the operating pressure of 1 bar_g

4.5.3.2 On-line procedures

Specific procedures were followed when a reaction condition was changed; whereafter a time interval of approximately 6 hours was allowed for re-establishing steady state conditions.

When temperature is increased, a heating rate of 1 °C per minute is applied. When decreasing temperature, the new set point is set and the reactor allowed to cool naturally.

When adjusting *SSV*, both the dry gas and steam feed are adjusted accordingly to maintain the same steam to carbon ratio and avoid coke formation during the adjustment. When increasing *SSV*, the steam flow rate is adjusted and stabilised first, followed by the dry gas feed adjustment. When decreasing *SSV*, the dry gas feed is adjusted first followed by steam adjustment.

4.5.3.3 Shut-down procedure

- When shutting down the experiment, methane and argon gas flow are terminated by switching off the CH_4 and Ar mass flow controllers. Immediately afterwards, nitrogen flow is established to flush the system and ensure the complete removal of reactants from the reactor
- Heating to the reactor (furnace) is switched off. It took approximately 6 hours to cool down from reaction temperature to room temperature
- Typically 30 minutes are required before switching off the steam flow.

4.5.3.4 Sampling procedure

Both feed and product gas streams were sampled by means of a 4-way switching valve downstream of the water knock-out pot, as shown in Figure 4-6. During product gas sampling, the water-free gas is passed to the online GC via the 4-way switching valve whilst the dry feed gas stream is directed to the vent via the vent vessel, and vice-versa in the case of dry feed gas sampling and analysis.

4.6 Steam methane reforming product analysis

4.6.1 Gas chromatography

Feed and product gas were analysed online using a Varian CP-4900 micro GC fitted with 3 columns; a 10 m Molsieve 5A column (MS5-10m), a 20 m Molsieve 5A column (MS5-20m) and a 10 m Pora Plot Q column (PPQ). The column oven temperatures and carrier gases were independently controlled with conditions as shown in Table 4-2. The total analysis time was 7 minutes. The retention times of the individual gaseous components are listed in and a typical dry gas chromatogram is shown in Table 4-3. H_2 peak areas in MS5-10m column, Ar peak areas in MS5-20m column and CO_2 peak areas in PPQ column were used in the data-work-up. It should be pointed out that CH_4 and CO were detected both in MS5-10m and MS5-20m columns but, because the H_2 carrier gas yields bigger peak areas, CH_4 and CO peak areas in MS5-20m column were used for the data work-up.

Table 4-2: Gas chromatography operating conditions

	MS5-10m Column	MS5-20m Column	PPQ Column
Injector temperature (°C)	40	43	42
Oven temperature (°C)	50	50	50
Pressure (Static, kPa)	150	150	80
Carrier gas	Ar	H_2	H_2

Table 4-3: Component retention times

Component	Column	Retention time (min)
Hydrogen	MS5-10m	0.6
Argon	MS5-20m	1.0
Methane	MS5-20m	2.1
Carbon monoxide	MS5-20m	3.3
Carbon dioxide	PPQ	0.4

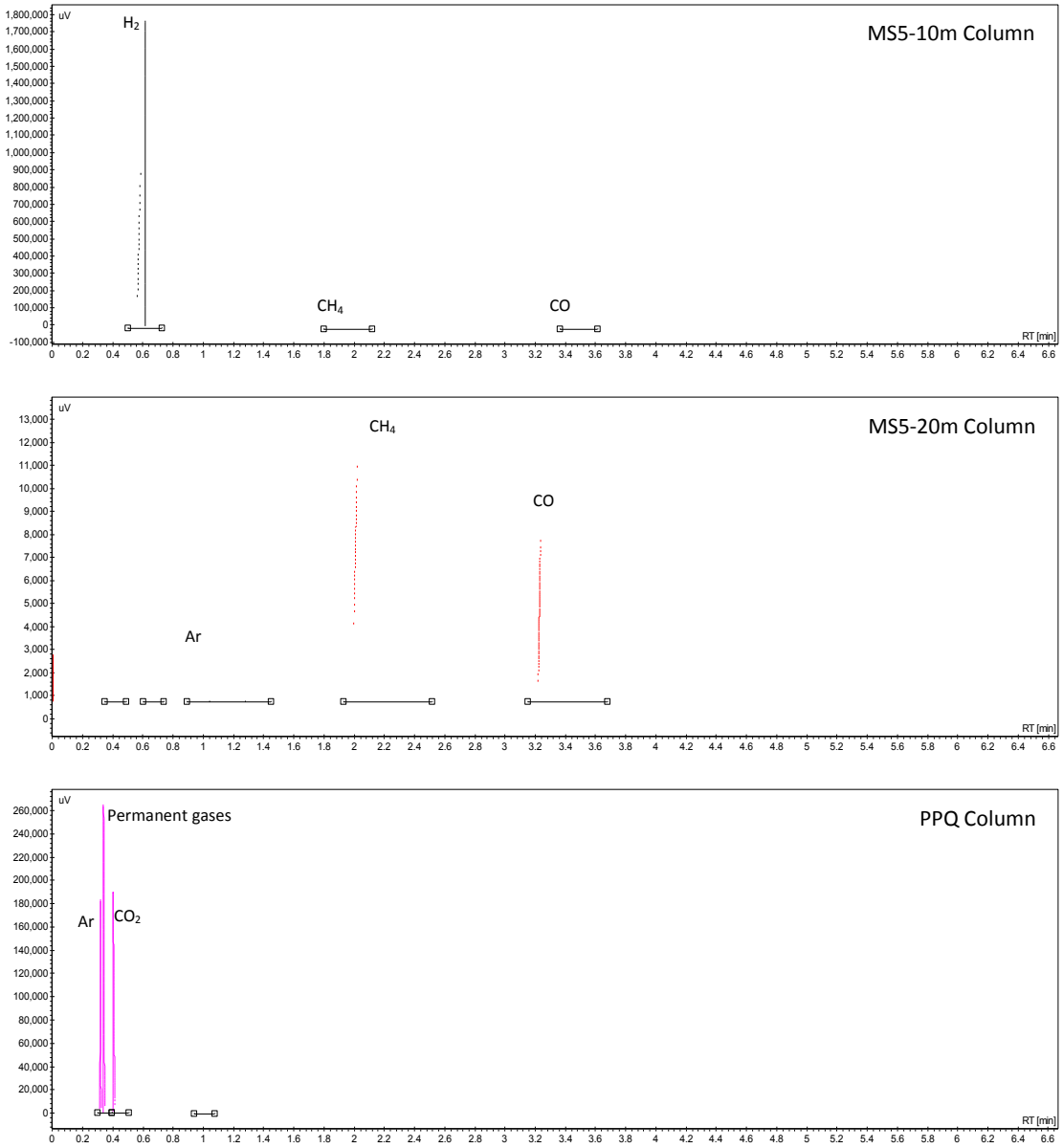

Figure 4-11: Typical chromatograms of the dry gas analysis

4.6.2 Chromatographic data workup

GC chromatogram peak areas were related to volumetric flow rate of individual gases by the relative response factors (RRF), and making uses an internal standard gas (Ar) of known volumetric flow rate. Determination of the response factors can be found in Appendix G.

Once the RRF was determined, the molar flow rates of reactant and product were calculated using eqn 5.

$$RRF_{species} = \frac{(\frac{Moles_{species}}{Moles_{Ar}})}{(\frac{Area_{species}}{Area_{Ar}})}$$ **eqn 5**

The conversion of CH_4 was calculated using eqn 6.

$$Conversion_{CH_4}, \% = \frac{F_{CH_4,feed} - F_{CH_4,product}}{F_{CH_4,feed}} \times 100\%$$ **eqn 6**

Carbon balance was calculated using eqn 7.

$$Carbon\ balance, \% = \frac{Carbon_{in}(CH_4\ from\ by-pass)}{Carbon_{out}(CH_4, CO\ and\ CO_2\ from\ product\ stream)} \times 100$$ **eqn 7**

The conversion of CO in the water gas shift reaction was calculated using eqn 8.

$$Conversion_{CO}, \% = \frac{F_{CO_2,product}}{F_{CO,product} + F_{CO_2,product}} \times 100\%$$ **eqn 8**

5 Results and discussion

Three catalyst formulations were evaluated in this study.

Commercial catalyst YR was supplied both as an egg shell (2 mm diameter pellets) and tested in packed bed reactor as well as in the form of a wash coating on the standard micro-channel plates used in this study (Section 4.2.1). The wash coating was applied by the commercial partner according to their proprietary procedure but the thermal pretreatment of the micro-channel plate prior to wash coating was conducted according to the standard method of this study (Section 4.2.2.1).

Catalyst XR was supplied by a different commercial partner, in powder form, and tested both in packed bed and micro-channel reactor (in-house coated) configurations.

In addition, an alumina supported Rh catalyst was prepared in-house and tested both in packed bed and micro-channel reactor (in-house coated) configurations.

For ease of referral, catalysts (Table A-1) and experiments (Table A-2) are tabulated on a fold-out reference page in Appendix A.

5.1 Preliminary findings

5.1.1 Micro-channel reactor drop test results

Drop tests were performed on every coated micro-channel plate, whether coated in-house or by commercial partner (i.e. catalyst YR). Catalyst weight loss from the drop test was determined and proved to be negligible. As a consequence, adhesion between the catalyst and the micro-channel plate was considered good under ambient condition.

5.1.2 Performance evaluation methodology

Due to the limited supply of the commercial catalyst, especially in case of commercially coated micro-channel reactors, the different reaction conditions were tested within the same experimental run, i.e. on the same catalyst sample. A specific reaction condition was always tested at the beginning of the experiment and re-checked at various intervals during

the experiment, as illustrated in Figure 5-1. As an example, reaction condition A was checked at the beginning of the experimental run, thereafter, the experiment went through a series of condition changes, e.g. *SSV*, S/C ratio or temperature, with the catalyst performance at condition A being re-evaluated at various junctures between major sets of experimental conditions so as to determine the stability of the catalyst to the various conditions evaluated.

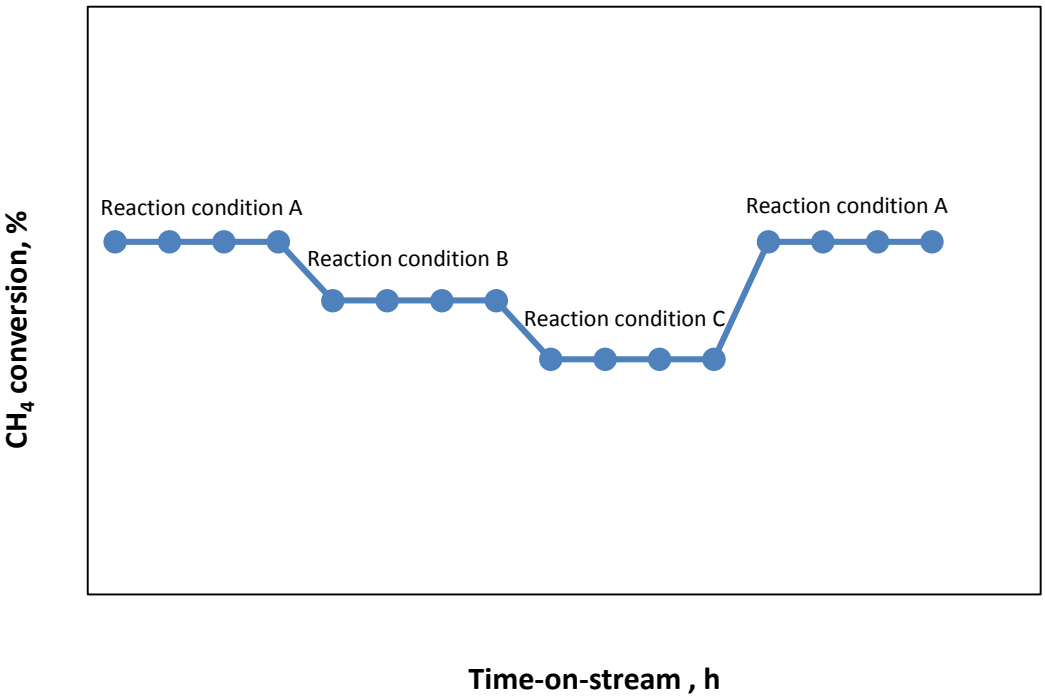

Figure 5-1: Conceptual condition testing for stability monitoring

5.1.3 Inertness of the micro-channel reactor

An uncoated micro-channel reactor (blank) was tested for SMR activity at 700 °C and 1 bar_g (Experiment 1). The flow rates of CH_4 and water used were the same as for the equivalent catalysed experiment, Experiment 3. The results, shown in Figure 5-2, indicate no detectable CH_4 conversion and it can be concluded that the metals of the micro-channel plates are not active for the SMR reaction at these conditions. The absolute fluctuations in CH_4 conversion data, as shown in Figure 5-2, are small and are considered due to experimental error associated with variations in gas and liquid flow rates, reactor temperature and chromatographic analysis.

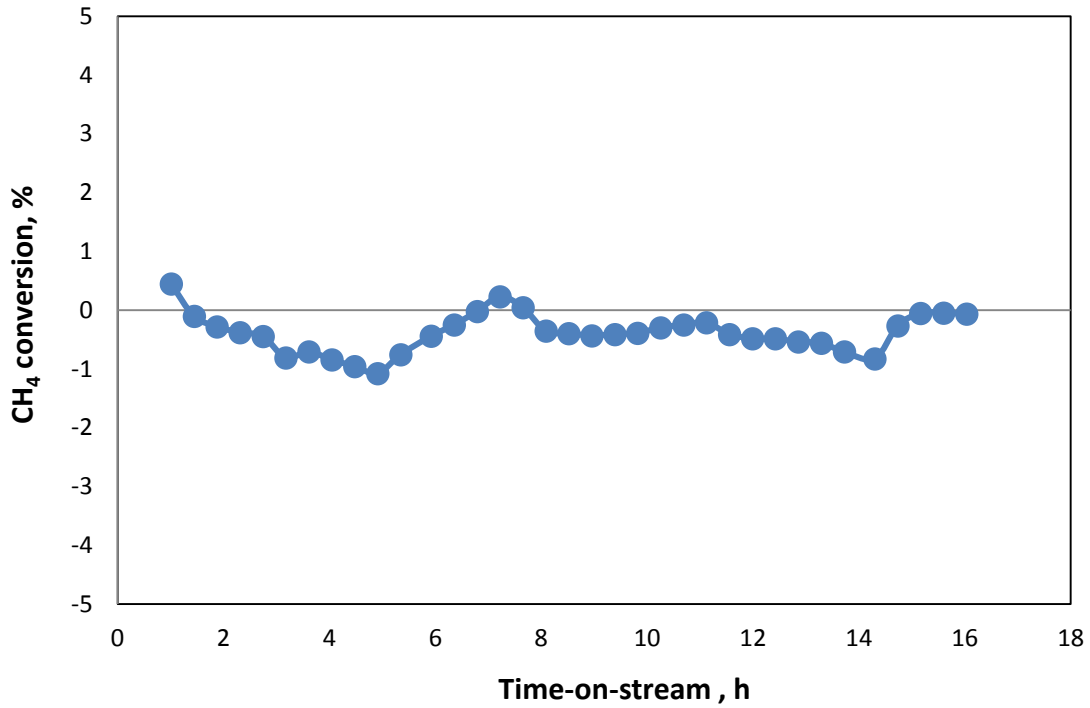

Figure 5-2: Blank micro-channel reactor experiment at 700 °C and 1 bar_g (Experiment 1)

5.1.4 Reproducibility of results

Figure 5-3 shows methane conversion versus *SSV* data for two different experiments (Experiments 3 and 4) based on catalyst YR coated micro-channel reactors under conditions of 700 °C, 1 bar_g and S/C of 3.

Good reproducibility is observed; both experiments have similar CH_4 conversion activity with the corresponding *SSV* under identical operating conditions.

5.1.5 Carbon balance

The carbon balance (eqn 7, Section 4.6.2) was found to be accurate within 100 % ± 2 throughout the conversion ranges conducted for all experiments of this study – as may be seen from the tabulated experimental data in Appendix A.

As such, the product analyses and conversion data of this study are considered to be robust.

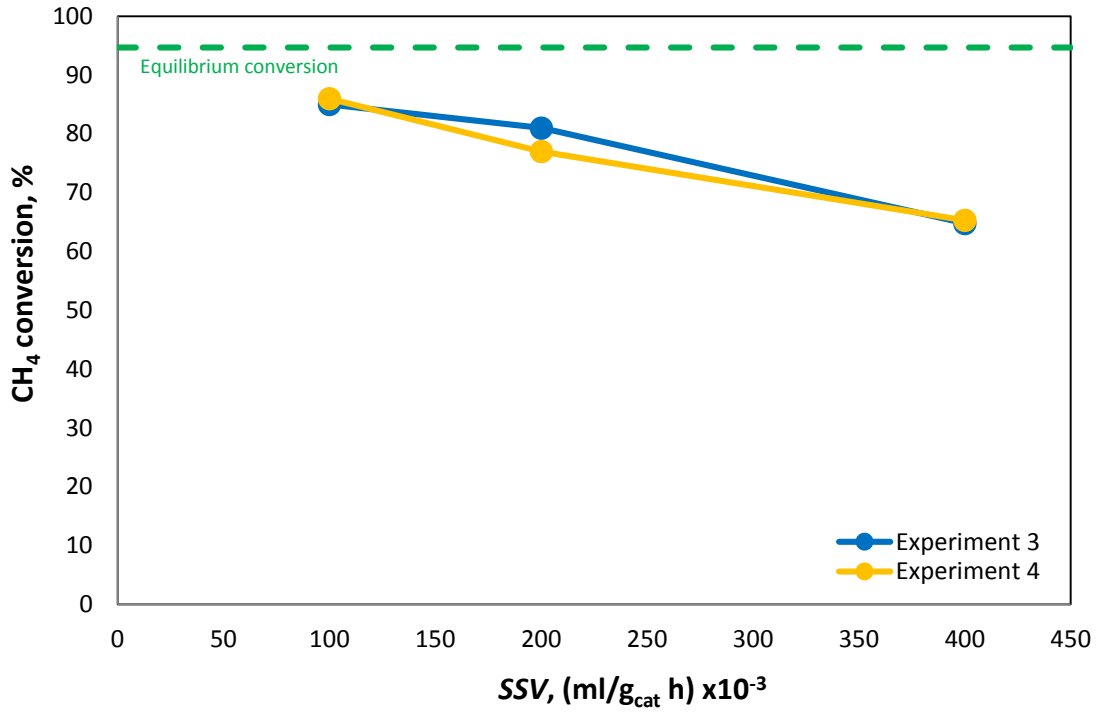

Figure 5-3: Reproducibility for catalyst YR in micro-channel reactor at 700 °C, 1 bar_g, S/C of 3 and various *SSV* (Experiments 3 and 4)

5.2 Commercial catalyst YR

5.2.1 Packed bed catalyst stability test

An experimental run (Experiment 2) was performed using the commercial catalyst YR (egg shell form) in packed bed reactor to evaluate the stability of the catalyst. Figure 5-4 presents CH_4 conversion versus time-on-stream data for this experiment at 700 °C, 1 bar_g, S/C of 3 and *SSV* of 10 000 ml/(g_{cat}h).

Nonetheless, the commercial catalyst YR may be considered to be stable at the conditions of this test, reaching a steady-state CH_4 conversion of 85% for 90 hours.

Although it can be seen from Figure 5-4 that the catalyst reaches and maintains a steady-state stable performance over the 90 hours on-stream time of the test, it is noticeable that the catalyst activity increases steadily over the first two days on stream before levelling off.

It is not clear why the activity increases over the first two days on stream. However, an initial "settling in" of catalytic activity over hours or days is not uncommon.

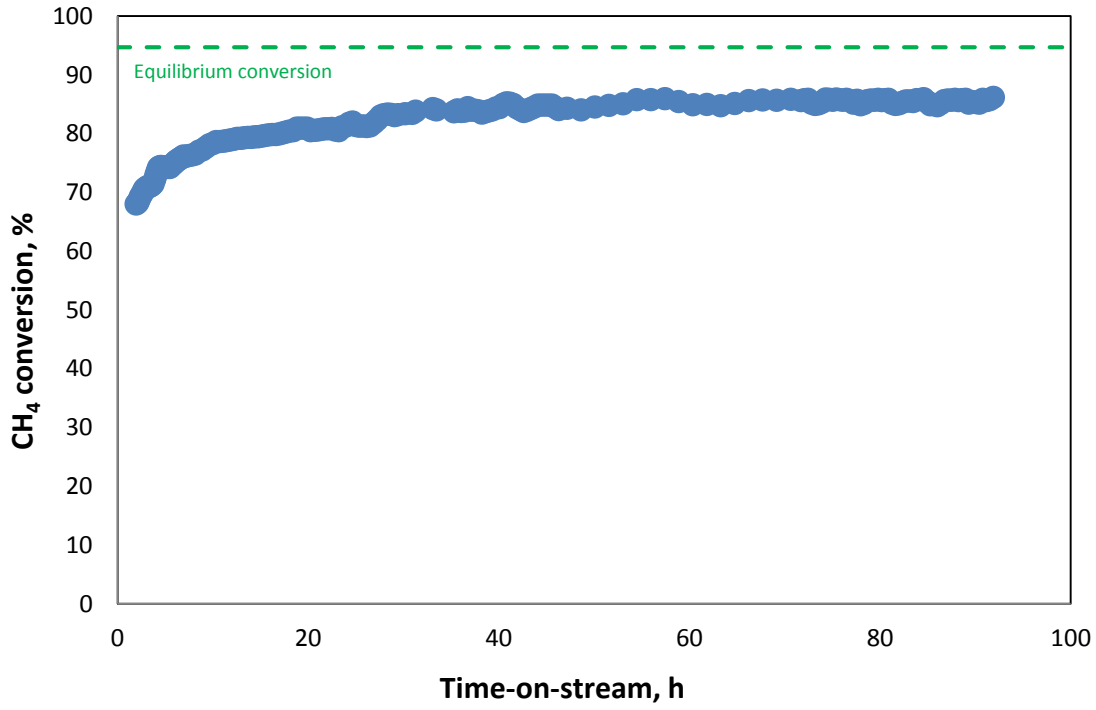

Figure 5-4: Stability performance of the commercial catalyst YR in a packed bed reactor at temperature of 700 °C, 1 bar_g, S/C of 3 and a *SSV* of 10 000 ml/(g_{cat}h) (Experiment 2)

5.2.2 Commercially coated micro-channel reactor

5.2.2.1 Catalyst stability

Figure 5-5 shows CH_4 conversion versus time-on-stream for catalyst YR in a micro-channel reactor configuration at two different times in Experiment 3. A similar "settling in" period was also observed (refer to results for Experiment 2, Figure 5-4) over the first day on-stream but not shown in Figure 5-5. Test conditions were 700 °C, 1 bar_g, S/C of 3 and *SSV* of 200 000 ml/(g_{cat}·h) and a CH_4 conversion of 82% at 20 hours versus 81% at 140 hours on stream were recorded. These results confirm that the catalyst was stable under the above mentioned conditions, at least for the period of 140 hours (6 days) on stream.

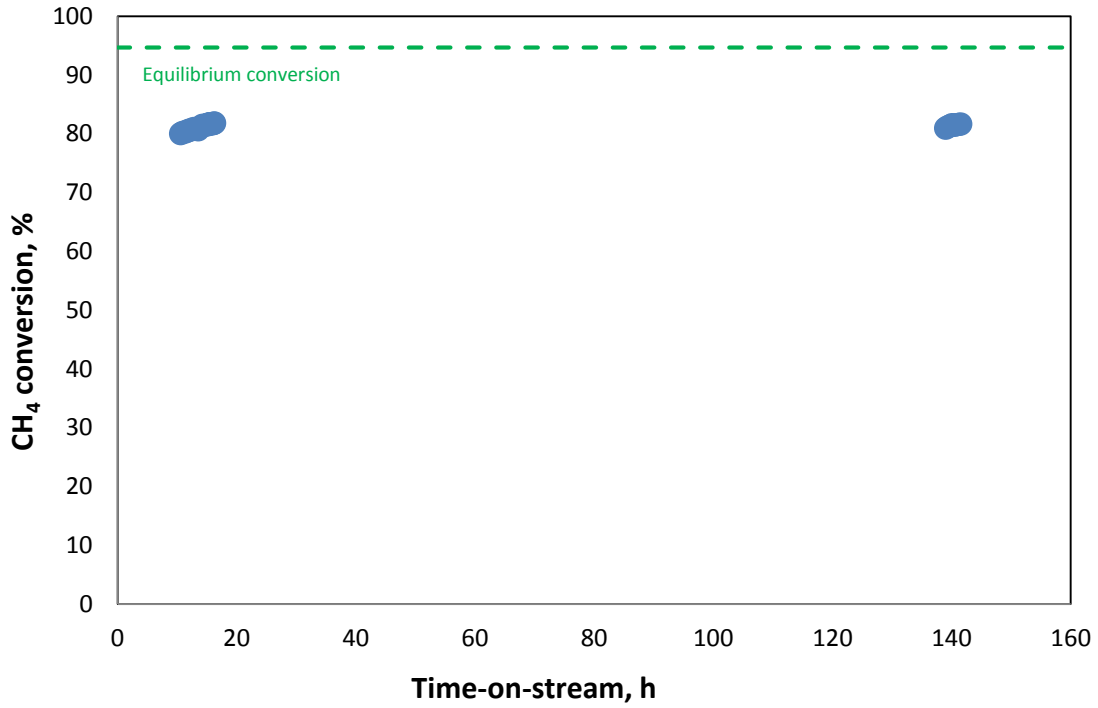

Figure 5-5: Stability performance of commercial catalyst YR in micro-channel reactor configuration at 700 °C, 1 bar_g, S/C of 3 and *SSV* of 200 000 ml/(g_{cat}·h) (Experiment 3)

5.2.2.2 Effect of S/C ratio and *SSV*

SSV-conversion data was generated for the commercial catalyst YR on micro-channel reactors at 700 °C and 1 bar_g. Three different S/C ratios, namely 2, 3 and 5, were tested. Figure 5-6 shows the results of the activity tests performed on this commercial catalyst compared to the maximum conversion attainable at equilibrium. At S/C ratio of 2 (blue data points in Figure 5-6), the steady state CH_4 conversion was 46% at *SSV* of 500,000 ml/(g_{cat}h), which begins to approach the equilibrium conversion at *SSV* of 50,000 sml/(g_{cat}h). Similar trends were observed for the other two S/C ratios, although, as expected, at higher conversion levels but in all S/C cases approaching the associated equilibrium conversion at *SSV* of 50 000 ml/(g_{cat}h) and below.

The seemingly lower than expected conversion levels at *SSV* above 200 000 ml/(g_{cat}h) for S/C of 5 (Figure 5-6) may possibly be due to incomplete vaporization of the water feed at these high water flow rates (high *SSV* and high S/C) with a consequence less in effective S/C ratio and possibly liquid water reaching the micro-channel reactor catalyst layers. However,

no experimental evidence (e.g. depressed reactor temperature) for this conjecture was observed/recorded. Even so, the data of Figure 5-6 was reproducible at these conditions.

The Higher CH_4 conversion with increasing the S/C ratio (as indicated in Figure 5-6) is in agreement with the literature that the reforming reaction itself is promoted by an excess of steam (Twigg, 1989).

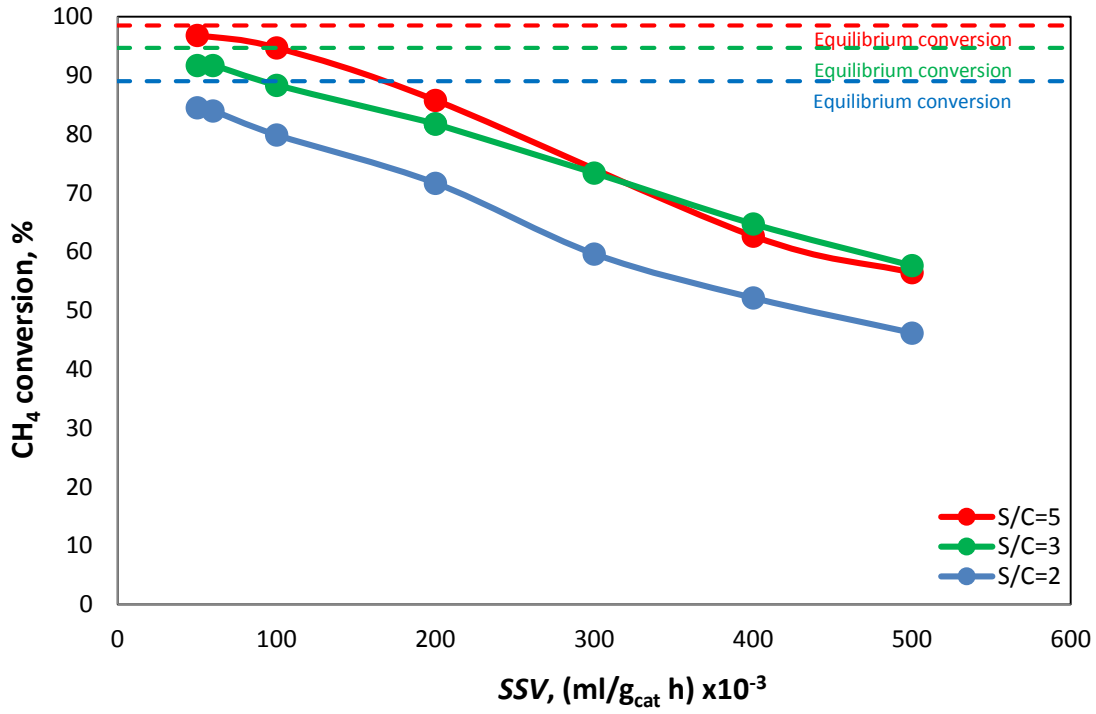

Figure 5-6: Catalyst YR performance in micro-channel configuration as a function of *SSV* and S/C ratio [700 °C and 1 bar_g (Experiments 3 and 4)]

5.2.2.3 WGS activity

The water-gas-shift (WGS) reaction may be considered as a subsequent reaction to the main SMR reaction, which converts the CO into CO_2. Assuming the SMR reaction, directly, to produce only CO and H_2, Figure 5-7 presents the results of CO conversion in the subsequent WGS reaction versus CH_4 conversion in the SMR reaction at the corresponding *SSV* and S/C ratios, and at 700 °C and 1 bar_g. The calculations in respect of the equilibrium CO conversion can be found in Appendix E.

As indicated in Figure 5-7, as CH_4 conversion increases, CO conversions approach their corresponding equilibrium values. For purposes of the minimum CO product concentration from SMR, CO conversion peaks at 57 % for a S/C ratio of 3 (likewise at 59% for S/C of 2). However, at this specified reaction condition, the CH_4 conversion is also only 57 % and too low to meet the CH_4 conversion target of 77 %. Therefore, high CO product concentrations from SMR must be compensated by the subsequent CO clean up processes.

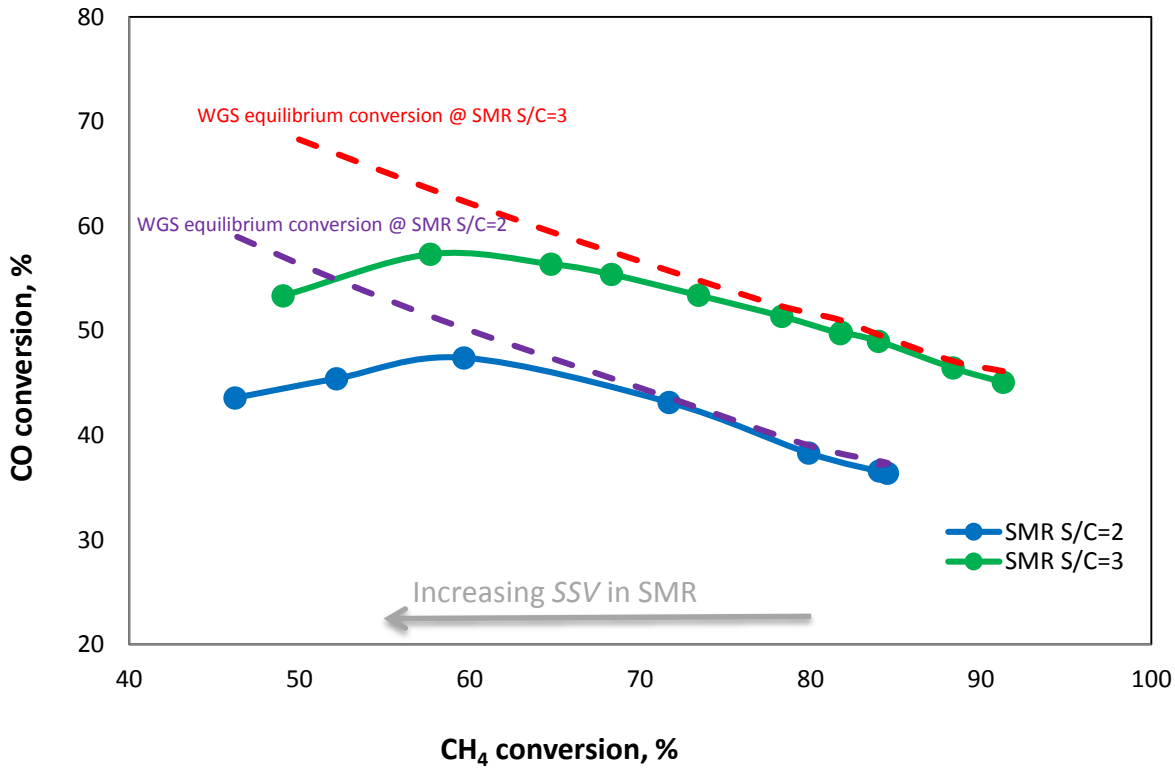

Figure 5-7: Catalyst YR WGS activity versus methane conversion in micro-channel configuration (Experiments 3 and 4)

5.2.3 In-house YR-coated micro-channel reactor test

In an attempt to evaluate, separately, the in-house coating technique, the catalyst layer on the commercially supplied egg-shell YR catalyst was scraped off, micronized and wash-coated onto the micro-channel reactor according to the method described by Zapf et al., (2006) – Section 4.2.2.

The in-house coated micro-channel reactor was tested at 700 °C, 1 bar_g, *SSV* of 80 000 ml/(g_{cat}h) and S/C of 3 (Experiment 5). The results are shown in Figure 5-8 and it can be seen

that the CH_4 conversion reached a peak of 66% after 8 hours and starts to decline with almost all of the catalyst activity was lost by the end of the experiment, after 4 days on-stream. The reason for the catalyst deactivation is not known.

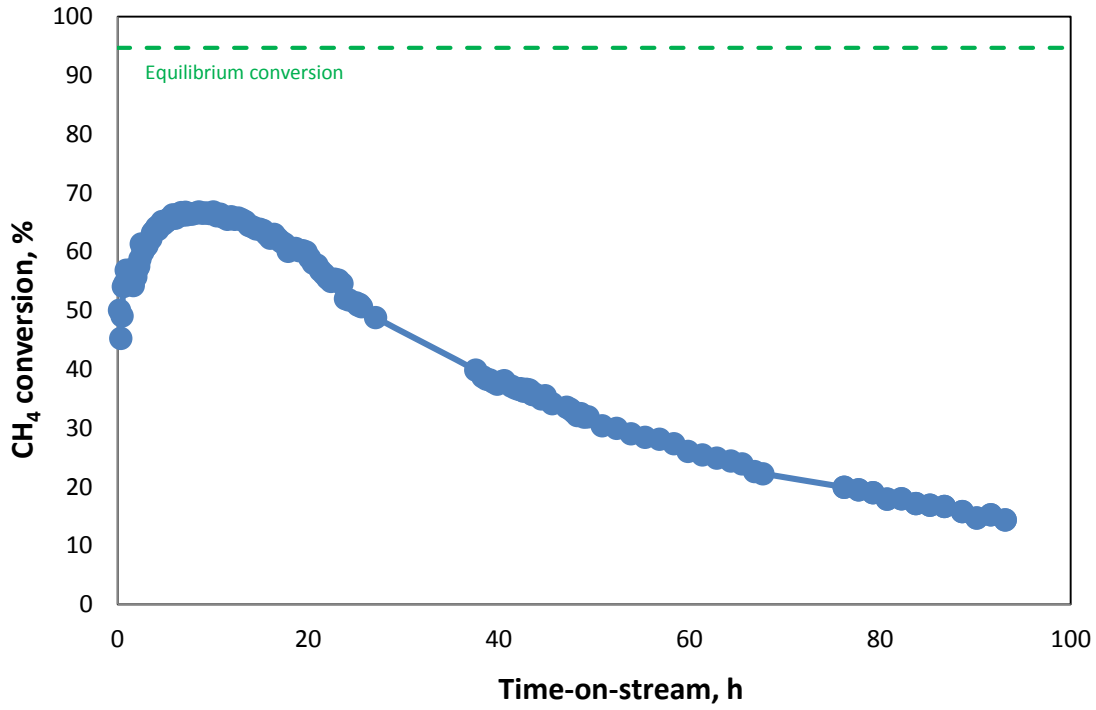

Figure 5-8: Stability of the in-house coated commercial catalyst YR in micro-channel configuration at 700 °C, 1 bar_g, S/C of 3 and *SSV* of 80 000 ml/(g_{cat}h) (Experiment 5)

5.3 Commercial catalyst XR

5.3.1 Packed bed catalyst stability test

Experiment 6 was performed using the commercial catalyst XR in a packed bed reactor to evaluate the stability of the catalyst at 700 °C, 1 bar_g, S/C of 3 and *SSV* of 7 500 ml/(g_{cat}h). Figure 5-9 presents the CH_4 conversion versus time-on-stream data for this experiment.

After 40 hours -on-stream, CH_4 conversion over catalyst XR was 76%, whereas after 90 hours the CH_4 conversion was 73%. From these data, it can be concluded that the catalyst was stable under the reaction conditions applied and over the period of roughly 4 days.

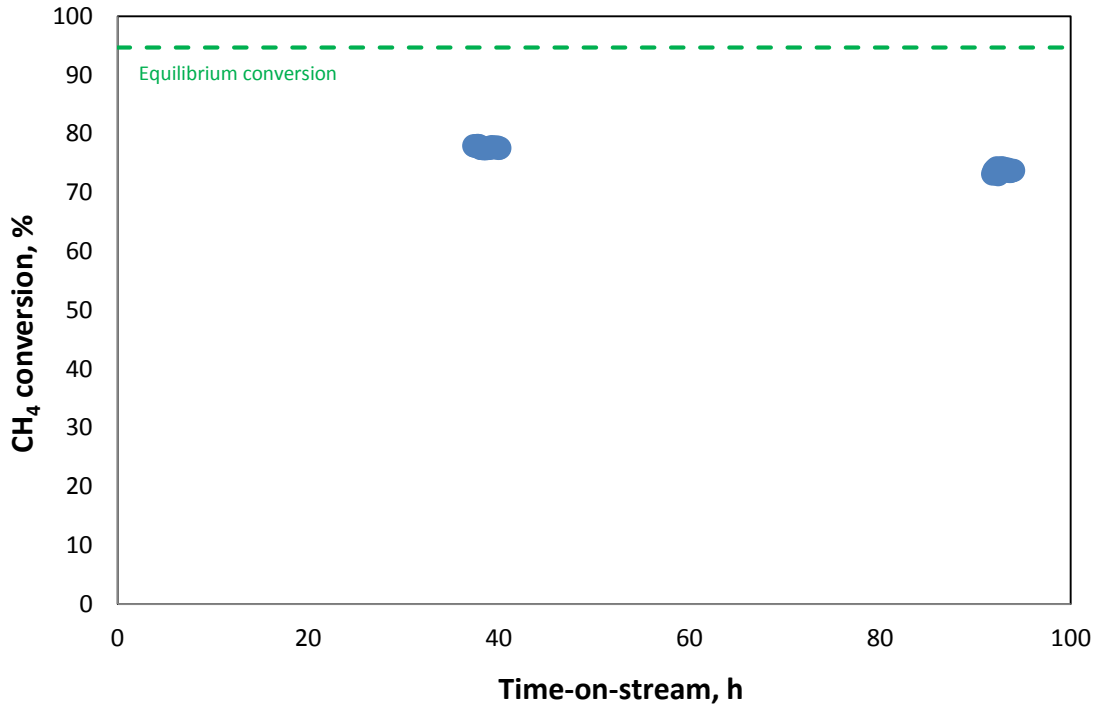

Figure 5-9: Stability of the commercial catalyst XR in a packed bed reactor at 700 °C, 1 bar_g, S/C of 3 and *SSV* of 7 500 ml/(g_{cat}h) (Experiment 6)

5.3.2 In-house coated micro-channel reactor tests

Commercial catalyst XR was wash-coated in-house onto the micro-channel reactor according to the method described by Zapf et al. (2006) – see section 4.2.2.

5.3.2.1 Temperature effects on stability

Experimental runs were performed to evaluate the stability of catalyst XR in micro-channel reactors at various reaction temperatures while the S/C ratio, *SSV* and pressure were kept constant. Experiment 7 was performed at a reaction temperature of 700 °C and Experiments 8 and 9 were performed at reaction temperatures of 800 °C and 900 °C, respectively. The results are presented in Figure 5-10. It is clear from Figure 5-10 that catalyst XR deactivates immediately from the beginning of each experimental run, in stark contrast to the findings for the powdered XR catalyst in packed bed configuration (Figure 5-9). It is also noticeable that the rate of deactivation increases with increasing temperature between 700 °C and 900 °C.

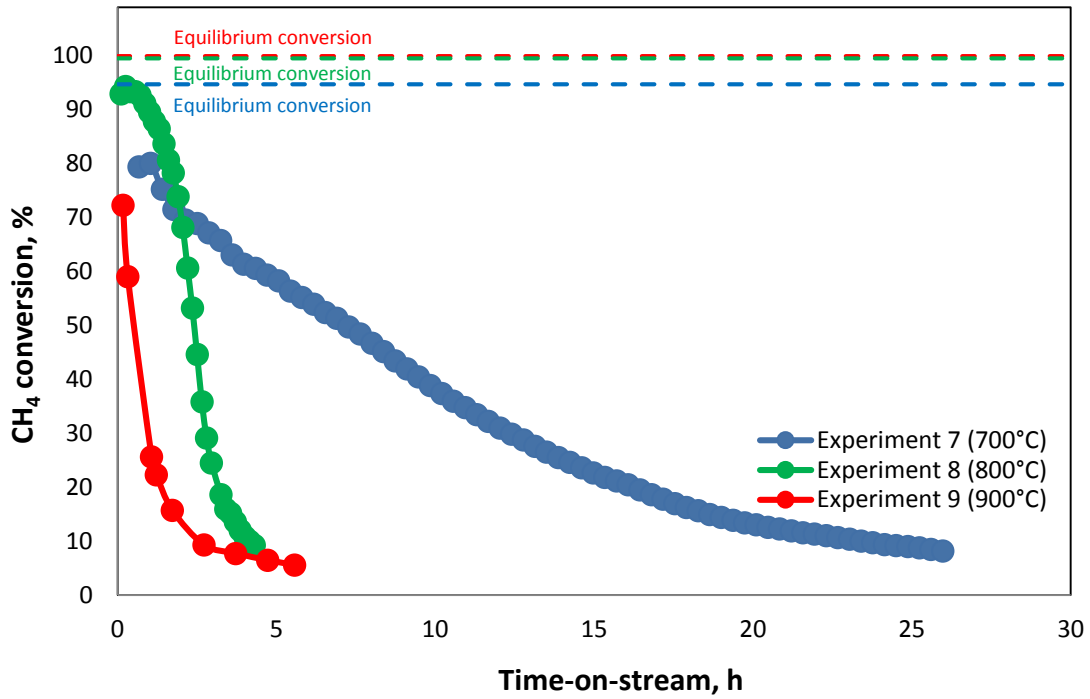

Figure 5-10: Stability of commercial catalyst XR in micro-channel configuration at 700 °C (Experiment 7), 800 °C (Experiment 8) and 900 °C (Experiment 9), 1 bar_g, S/C of 3 and *SSV* of 30 000 ml/(g_{cat}h)

To explore possible reasons for this rapid deactivation, in the micro-channel configuration, a series of experiments were conducted on catalyst XR coated micro-channel reactors, including thermal & hydro-thermal effects (Experiments 10 and 11), wash-coating procedures (Experiment 12) and the potential stabilizing effect of alumina addition to the coating suspension (Experiment 13).

5.3.2.2 Thermal and hydro-thermal effects on catalyst

Experiment 10 was performed to check the effect of high temperature on the catalyst performance and the results are shown in Figure 5-11. After reduction (Section 4.5.2), a fresh catalyst XR coated micro-channel reactor was 'aged' at 700 °C, 1 bar_g and *SSV* of 30 000 ml/(g_{cat}h) in N_2 flow for about 14 hours as opposed to the typical pre-reaction period of 30 minutes at this temperature. Thereafter, CH_4 and steam was introduced to replace N_2 and the initial conversion of CH_4 was found to be 80%, a similar level to that observed in

Experiment 7 (Figure 5-10) which indicates that the high temperature itself does not alter the catalyst activity.

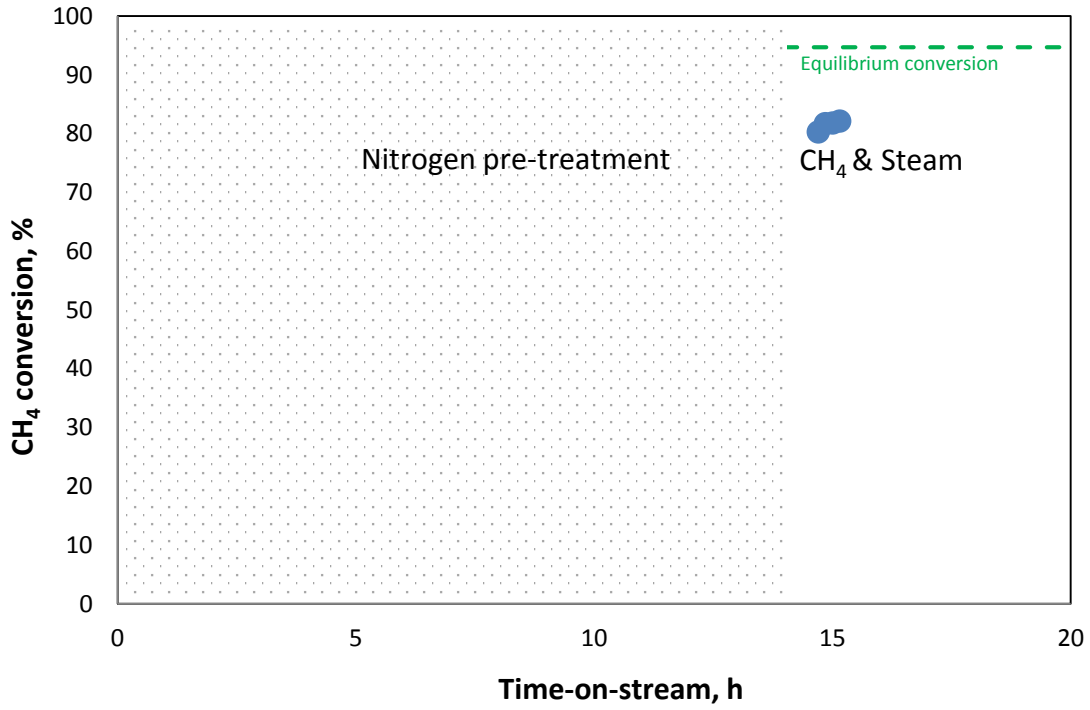

Figure 5-11: Effect of high temperature pre-treatment on catalyst XR coated micro-channel reactor activity at 700 °C, 1 bar_g, S/C of 3 and *SSV* of 30 000 ml/(g_{cat}h) (Experiment 10)

An additional test (Experiment 11) was performed to evaluate the hydro-thermal stability of catalyst XR in the micro-channel reactor. After reduction, a fresh catalyst XR coated micro-channel reactor was treated at 700 °C, 1 bar_g and *SSV* of 30 000 ml/(g_{cat}h) with both steam and N_2 (3 to 1 molar ratio). After 14 hours CH_4 was introduced to replace N_2. The results shown in Figure 5-12 indicate that the initial CH_4 conversion was 81% which is in agreement with the initial CH_4 conversion achieved in Experiments 7 (Figure 5-10) and 10 (Figure 5-11). Therefore, it may be concluded that steam induced sintering is also not the cause of the rapid catalyst deactivation.

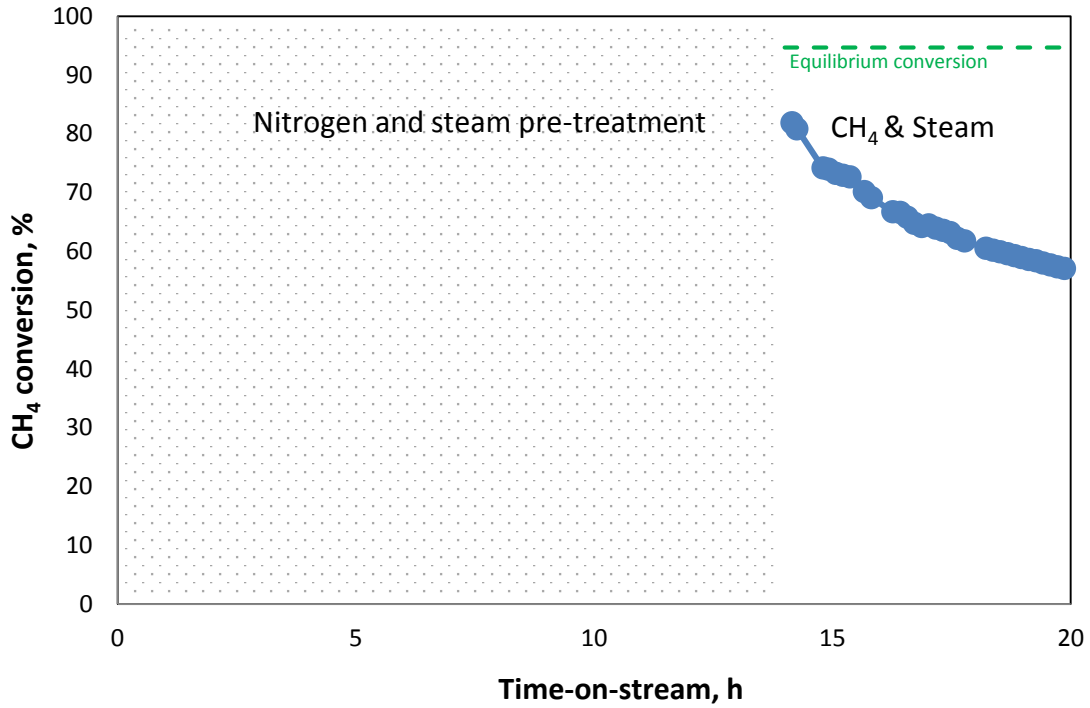

Figure 5-12: Effect of high temperature and steam on XR catalyst in micro-channel reactors at 700 °C, 1 bar_g, S/C of 3 and *SSV* of 30 000 ml/(g_{cat}h) (Experiment 11)

5.3.2.3 Effect of wash-coating process

Experiment 12 was performed to determine any effect of the wash-coating process, in particular the intimate catalyst-metal (substrate) adhesion and thermal treatment, on the catalyst performance in the micro-channel reactor configuration.

Catalyst XR was coated on the backside of the micro-channel plates (smooth surfaces), followed by processing according to the same treatment process as described in section 4.2.2 which includes cleaning and thermal treatment of micro-channel plates, catalyst suspension preparation and wash-coating catalyst onto the backside of micro-channel plates and, subsequent calcination. The thus coated and treated catalyst was scraped off the plates and granulated into particles of normally 250 µm. The resulting catalyst performance was evaluated in the packed bed reactor at 700 °C, 1 bar_g, S/C of 3 and *SSV* of 7 500 ml/(g_{cat}h) and the results are presented in Figure 5-13.

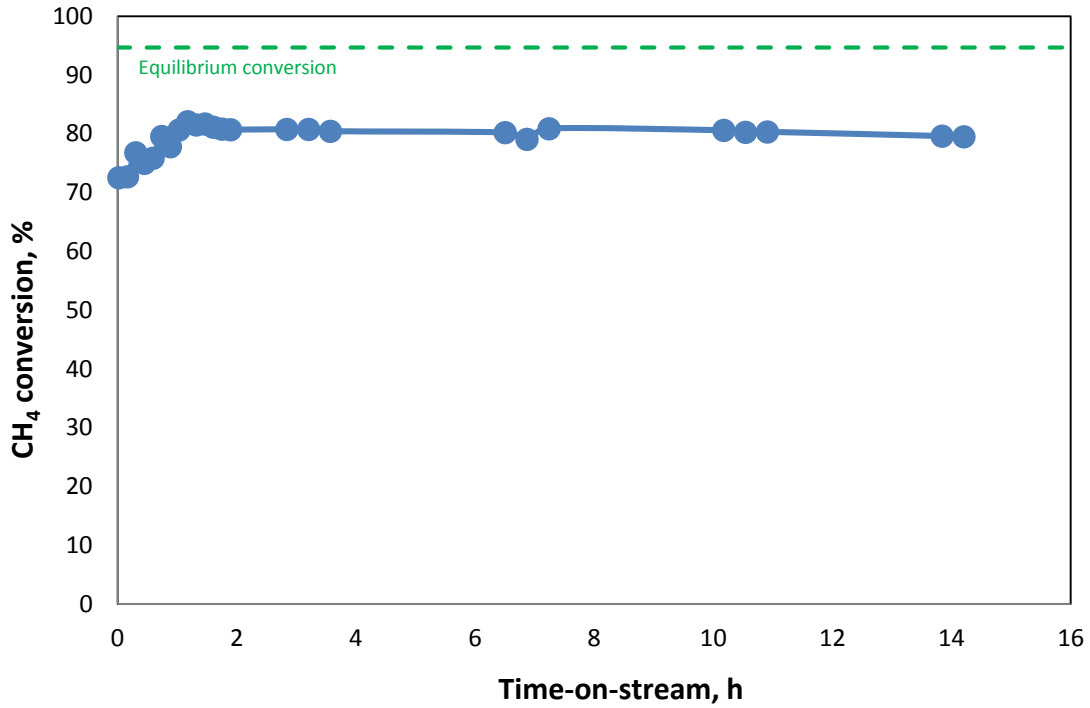

Figure 5-13: Performance of granulated wash-coat catalyst XR in packed bed configuration at 700 °C, 1 bar_g, S/C of 3 and *SSV* of 7,500 ml/(g_{cat}h) (Experiment 12)

After a short "settling in" period (quite possibly an experimental artefact), CH_4 conversion was steady at 80% for 14 hours on stream, which is in excellent agreement with the packed bed performance of fresh catalyst (CH_4 conversion of 78%) in Experiment 6 (Figure 5-9) as well as the initial performance of the fresh wash-coated catalyst – 80% CH_4 conversion (Experiment 7, Figure 5-10). This agreement suggests that the wash-coating process, itself, leads to no observable changes in the catalytic properties of catalyst XR.

5.3.2.4 Effect of alumina addition to washcoat

Literature reported that alumina promotes improved adhesion between catalyst and metal substrate (Truter, 2011), an additional 25 wt% fine alumina powder (3 nm particle size) was added to the coating suspension of catalyst XR and wash-coated onto micro-channel plates according to the standard method (Section 4.2.2). The resulting catalyst performance (Experiment 13) at 700 °C, 1 bar_g, S/C of 3 and *SSV* of 30 000 ml/(g_{cat}h) is presented in Figure 5-14.

After the initial "settling in" period, CH_4 conversion peaks at 52% and immediately declines such that almost all activity is lost within 16 hours. The lower peak CH_4 conversion (52%) than that of 80% observed for washcoating in the absence of alumina addition (Experiment 7, Figure 5-10) is expected since the additional alumina in the washcoat effectively lowers the active metal loading in the catalyst coating.

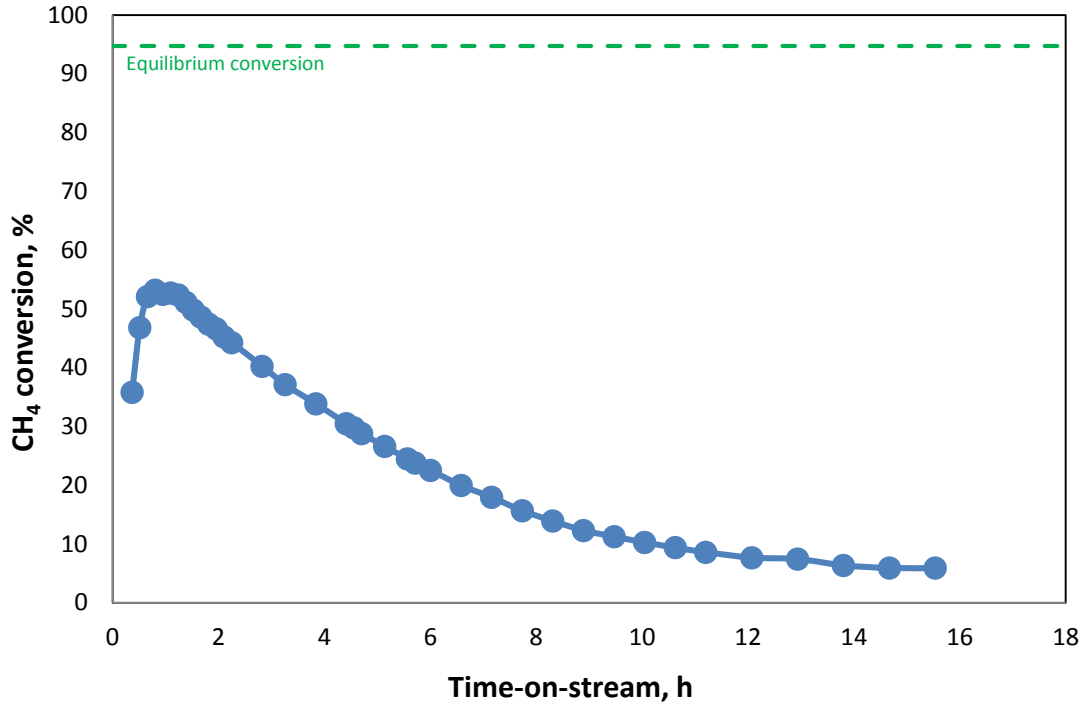

Figure 5-14: Effect of additional washcoat alumina on catalyst XR in micro-channel configuration at 700 °C, 1 bar_g, S/C of 3 and *SSV* of 30 000 ml/(g_{cat}h) (Experiment 13)

5.3.2.5 Effect of catalyst particle size reduction

Agrafiotis and Tsetsekou (2000a,b) reported that a washcoat from 2 µm particles resulted in improved coating adhesion in comparison to washcoats formed from larger (17 and 52 µm) particles. Therefore, catalyst XR was washcoated with a reduced particle size distribution (Appendix B) and evaluated at 700 °C, 1 bar_g, S/C of 3 and *SSV* of 30 000 ml/(g_{cat}h) (Experiment 14), the results of which are shown in Figure 5-15. A maximum CH_4 conversion of 30 % was observed, followed by a rapid loss in activity within 4 hours.

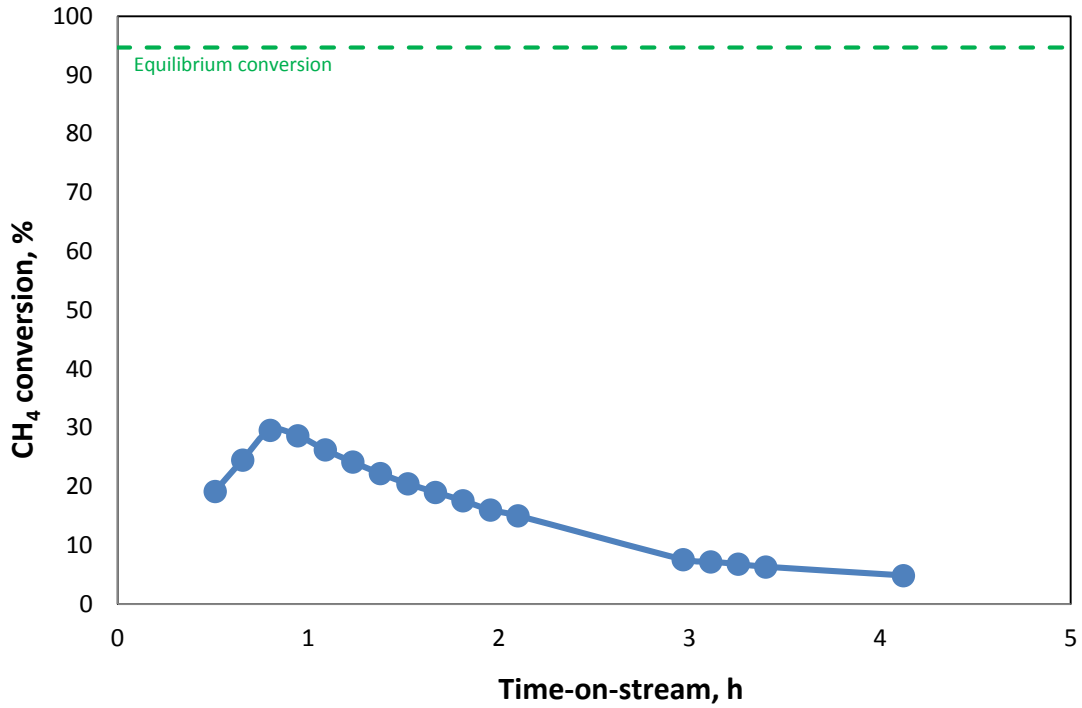

Figure 5-15: Effect of reduced particle size in catalyst XR washcoat performance at 700 °C, 1 bar_g, S/C of 3 and *SSV* of 30 000 ml/(g_{cat}h) (Experiment 14)

5.4 Rh/Al_2O_3 catalyst

Findings in respected of the Rh/Al_2O_3 catalyst prepared in-house are presented below.

5.4.1 Physico-chemical Characterisation

The results from characterization studies of the fresh Rh catalyst are presented in Table 5-1. The metal loading was confirmed by ICP to be 0.9 wt% which is close to the target value of 1 wt%. Metal crystallite size determinations from both TEM and H_2 chemisorption analysis are in good agreement (given the pre- and post-reduction conditions, respectively) with an average crystallite size of approximately 1 nm. A typical TEM image is presented in Figure 5-16 where the highlighted circles (as examples) indicate the Rh particles.

Table 5-1: Rh catalyst chemisorption analysis results

Properties	Value	Units
Rh loading[a]	0.9	wt %
BET surface area[b]	161	m^2/g sample
Metal surface area[c]	4.2	m^2/g sample
Dispersion[c]	95	%
Average Rh particle size[c]	1.16	nm
Average Rh particle size[d]	0.94	nm

a Determined by ICP – catalyst un-reduced
b Determined by N_2 adsorption – catalyst un-reduced
c Calculation from H_2 chemisorption results on a pre-reduced catalyst
d Determined by TEM – catalyst un-reduced

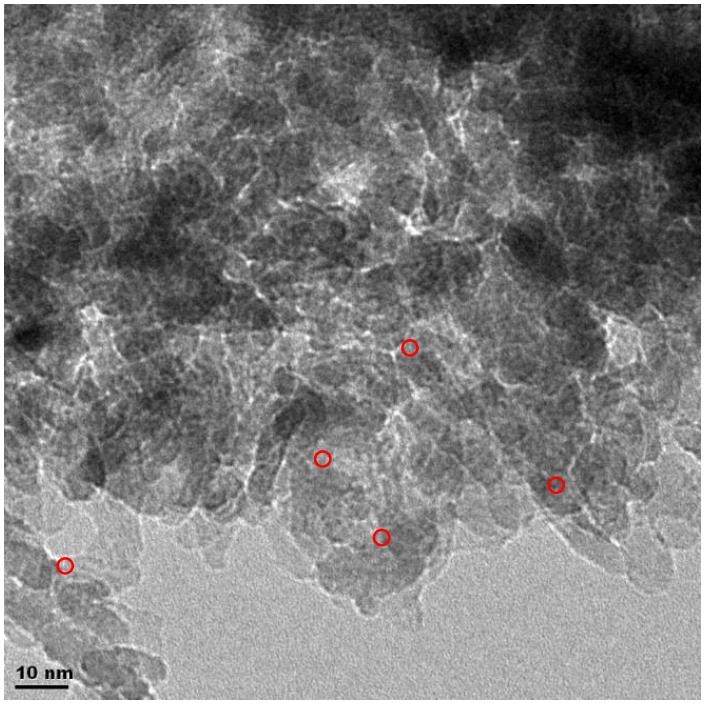

Figure 5-16: A typical TEM image for the Rh catalyst (un-reduced)

5.4.2 Packed bed catalyst performance

The Rh catalyst was evaluated for SMR as a granulate in a packed bed reactor at 700 °C, 1 bar_g, S/C of 3 and *SSV* of 40 000 ml/(g_{cat}h) (Experiment 15). CH_4 conversions versus time-on-stream data are presented in Figure 5-17.

After an initial "settling in" period of approximately 40 hours, stable activity was observed, at least for the 110 hours of the experiment with an eventual steady-state conversion of approximately 84%.

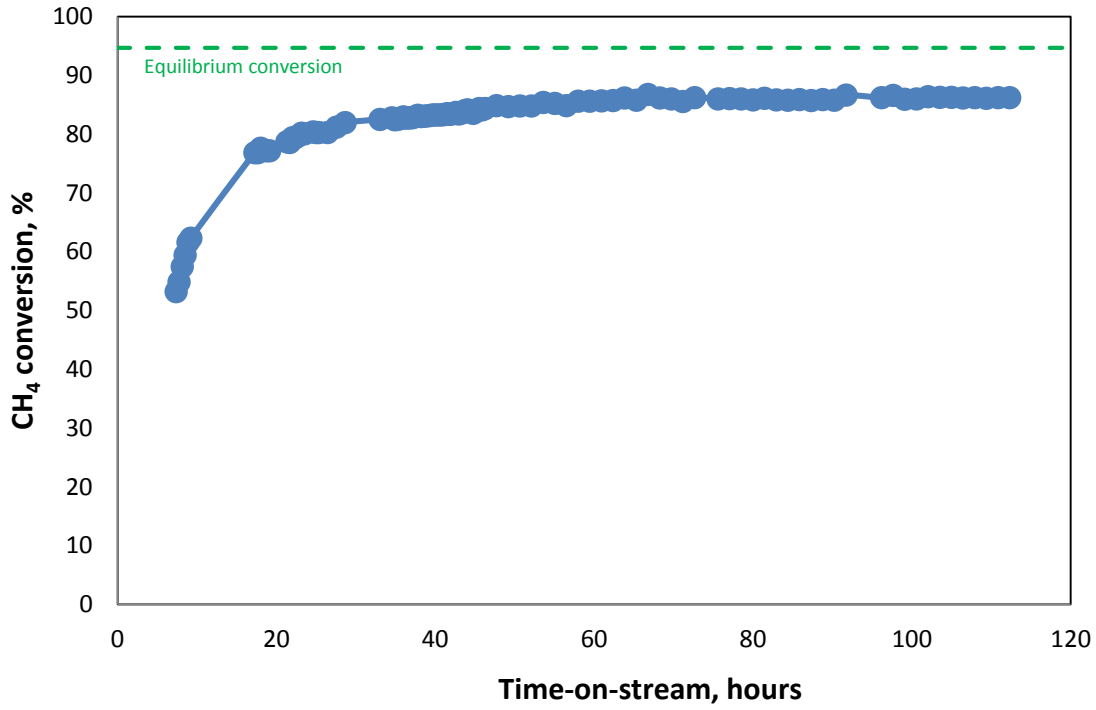

Figure 5-17: Performance of Rh/Al_2O_3 in packed bed configuration at 700 °C, 1 bar_g, S/C of 3 and *SSV* of 40 000 ml/(g_{cat}h) (Experiment 15)

5.4.3 Micro-channel reactor performance

The performance of the Rh/Al_2O_3 catalyst was evaluated in a micro-channel reactor in Experiment 16 under the same reaction conditions as applied in the packed bed reactor test (Experiment 15) and the results are presented in Figure 5-18. After initial "settling in" time of approximately 10 hours, the activity of the Rh catalyst starts declining and is completely lost the catalytic activity after 80 hours at the conditions of the experiment. The maximum conversion observed was also substantially lower than the steady-state catalyst performance shown in the packed bed reactor at the same reaction conditions.

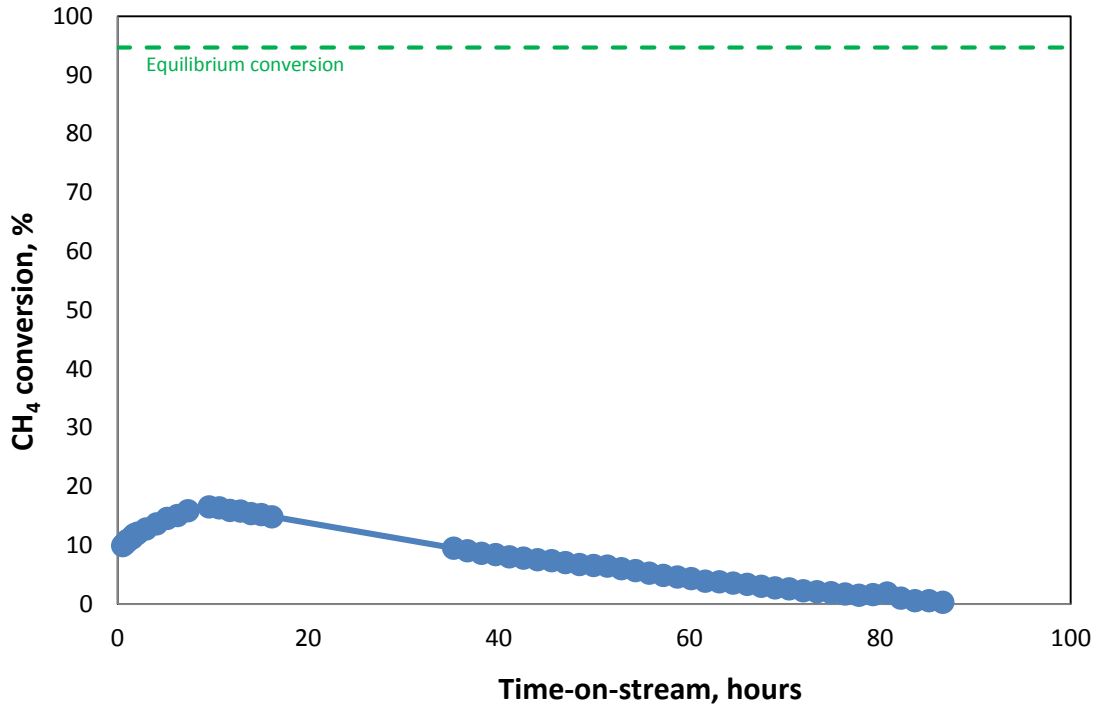

Figure 5-18: Performance of Rh/Al_2O_3 in micro-channel configuration at 700 °C, 1 bar_g, S/C of 3 and *SSV* of 40 000 ml/(g_{cat}h) (Experiment 16)

6 Conclusions and recommendations

The catalytic performance of three catalysts, namely catalyst XR, catalyst YR and Rh/Al_2O_3, were evaluated in this study for steam methane reforming, both in packed bed and micro-channel configurations.

Commercial catalyst YR performs adequately for fuel processor application when considering the demands of a low-temperature PEM fuel cell in a combined power generator. Catalyst performance, also, is stable over the typically 100 hour experimental durations investigated, both in packed bed and micro-channel configurations. However, the coating method applied by the commercial partner for micro-channel reactors remains unknown.

It is to be noted, that the productivity of the commercial catalyst YR in the micro-channel configuration is significantly higher than the case for the packed bed reactor. For equal CH_4 conversions of 85%, micro-channel *SSV* of 150 000 ml/(g_{cat}h) are applicable (Experiment 3), in contrast to that of only 10 000 ml/(g_{cat}h) in the packed bed arrangement (Experiment 2). Although this is likely to mostly arise from the substantially underutilized configuration of the egg-shell catalysts applied for packed bed evaluation, it also demonstrates the extended mass and heat transfer range of the micro-channel geometry. Moreover, these findings lead support to the potential of the micro-channel configuration for overall process intensification (and size reduction) in the case of fuel processor reforming stages.

Indeed, taking into account the minimum CH_4 conversion target of 77 % at a S/C ratio of 3 and a total pressure of 1 bar_g (Section 4.4), this performance can be achieved at a temperature as low as 700 °C and a specific space velocity as high as 250 000 ml/(g_{cat}h)! Even at the very low S/C ratio of 2, the required minimum CH_4 conversion (80%) can be achieved at a specific space velocity of 100 000 ml/(g_{cat}h). The aforementioned conditions are indicated by literature (Twigg, 1989; Wang et al., 2004) to be outside of any carbon formation regime, consistent with the stable catalyst activity observed in this study (at least for the 100 – 150 hours on-stream periods considered).

To evaluate the in-house coating technique, catalyst YR (scraped off the commercially supplied egg-shell pellets, Experiment 5), catalyst XR (Experiments 7, 8 and 9) and Rh/Al_2O_3

(Experiment 16) were wash-coated onto micro-channel plates according to the method described by Zapf et al. (2006). Although all these catalysts exhibited stable time-on-stream activity in the packed bed reactor, once coated onto micro-channels, a steady decrease in activity was observed with time-on-stream.

From the stable activities observed in the packed bed reactor, it may be concluded that thermal degradation of these catalysts is unlikely under the conditions of this study. Severe hydro-thermal conditioning of the freshly coated catalysts in the micro-channel reactor, prior to commencing of SMR, showed no change in the initial activity and leads further support to the deduction that high temperature or steam induced sintering of the active metals or the catalyst support is unlikely (Experiments 10 and 11). Unfortunately, physical evidence to support this claim in respect of sintering could not be obtained for reason of the prevailing non-analysis agreements.

Twigg (1989) suggested that a minimum of S/C of 1.7 is sufficient to suppress the carbon formation. Wang et al. (2004) concluded that for alumina supported Rh catalyst showed strong resistance to coke formation even at a S/C ratio as low as 1. Moreover, all the catalyst tests in the packed bed reactor configuration showed no sign of deactivation. It is to be concluded, therefore, that due to the S/C ratios applied in this study, coking is not the cause of the rapid catalyst deactivation observed in all micro-channel reactor experiments coated according to the method of Section 4.2.2.

To establish whether the wash-coating method itself is detrimental, catalyst XR was coated onto flat plates of the same metal grade as the micro-channel plates and scraped off the plates after calcination at 450 °C (Experiment 12). The performance of resulting catalyst material, pelletized and evaluated in a packed bed reactor, is essentially unchanged compared to the fresh catalyst in terms of both activity level and stability, suggesting that the coating method does not alter the catalyst properties. In this regard, the thickness of the catalyst layer precoated onto the metal substrates might have been considerably thicker than was the case for coatings in the actual micro-channels, such that interactions between catalyst and metal substrate may have been much less than in the micro-channels and this may have diluted any effects of negative metal-catalyst interactions.

The addition of alumina to the coating suspension and resulting catalyst layer did not improve catalyst XR stability in the micro-channel configuration (Experiment 13) and nor did the reduction in average catalyst particle size (Experiment 14). Since both these variables (alumina addition and catalyst particle size) were expected to improve catalyst layer adhesion, it may be reasonable to deduct that catalyst loss from the micro-channels during reaction is not the cause of the observed time-on-stream deactivation for all catalysts coated according to the method of Section 4.2.2. Indeed, this deduction is supported by visual inspection (images not included in this dissertation) which showed no obvious loss of catalyst (e.g. layer spalling) in opened micro-channel reactors post reaction (and deactivation).

In summary, it has been shown that stable steam methane reforming performance can be obtained over platinum group metal catalysts coated into micro-channel reactor configurations, and that such performances readily meet the requirements of a downstream low temperature PEM fuel cell in the envisaged standalone fuel cell based power generator. Moreover, high catalyst activity has been demonstrated, such that the required performance can be achieved at the low temperature of 700 °C yet still at high specific space velocity above 100 000 ml/(g_{cat}h) at typical fuel cell conditions of 1 bar, 70 – 100 °C and relative humidities of 50 – 80%, without the need for water condensation prior to the fuel cell. This stable micro-channel performance has, however, only been shown for commercially coated micro-channel plates.

Whereas both commercial catalysts, YR and XR, as well as the self-prepared Rh/Al_2O_3 catalyst exhibit stable performance at 700 °C in packed bed testing, in-house coating based on the method of Zapf et al., (2006), and as detailed in Section 4.2.2, has not yielded stable SMR performance in a micro-channel reactor configuration. Instead, such coated catalysts exhibit an immediate and continues decline in activity with time-on-stream. The reason for this observed deactivation in the case of in-house coated catalysts is not clear, but the following possible causes have been discounted as a consequence of a series of experiments, viz.

- Hydro-thermal degradation, i.e. high temperature or steam induced sintering
- Carbon deposition or coking

- Direct influences of the catalyst coating processing, chemistry or catalyst-metal (substrate) adhesion

Furthermore, it was shown that neither the addition of fine alumina particles nor further catalyst particle size reduction (via micronizing) effected any improvement in conversion stability of the coated catalyst layers.

Despite the failures in this study to achieve stable SMR performance for the catalyst layers coated according to the method of Section 4.2.2, it is clear from the stable performance of the commercially coated catalyst YR that such stability can be achieved. It is thus recommended that further studies to develop the coating procedure consider the use of alternative binders such as Tylose and water-based tape casting binders (Germani et al., 2007) as well as methods which involve an initial substrate (e.g. Al_2O_3, CeO_2, etc.) coating step followed by subsequent metallization of the coated substrate ((Venkataraman et al., 2003; Zhai et al.,2011).

7 References

Agrafiotis, C., Tsetsekou, A., 2000a. The effect of powder characteristics on washcoat quality. Part I: Alumina washcoats. J. Eur. Ceram. Soc. 20, 815–824.

Agrafiotis, C., Tsetsekou, A., 2000b. The effect of processing parameters on the properties of γ-alumina washcoats deposited on ceramic honeycombs. 35, 951–960.

Anttila, T., Anttonen, M., Fontell, E., Heiskanen, J., Kauppinen, H., 2006. Fuel cell technology development and commercialisation in Finland.

Cao, C., Wang, Y., Rozmiarek, R.T., 2005. Heterogeneous reactor model for steam reforming of methane in a microchannel reactor with microstructured catalysts. Catal. Today 110, 92–97.

Carrette, L., Friedrich, K. A., Stimming, U., 2001. Fuel cells - fundamentals and applications. Fuel Cells 1, 5–39.

Christensen, T.S., 1996. Adiabatic prereforming of hydrocarbons—an important step in syngas production. Appl. Catal. A Gen. 138, 285–309.

De Miguel, N., Manzanedo, J., Thormann, J., Pfeifer, P., Arias, P.L., 2010. Ni catalyst coating on Fecralloy microchanneled foils and testing for methane steam reforming. Chem. Eng. Technol. 33, 155–166.

Ehrfeld, W., Hessel, V., Haverkamp, V., 1999. Microreactors. In: Ullman's Encyclopedia of Industrial Chemistry. Wiley-VCH.

Ehwald, H., Hessel, V., Löwe, H., 2000. Micro-reactors: New technology for modern chemistry, Micro-reactors: New Technology for Modern Chemistry. Wiley-VCH.

Eleta, A., Navarro, P., Costa, L., Montes, M., 2009. Deposition of zeolitic coatings onto FeCralloy microchannels: Washcoating vs. in situ growing. Microporous Mesoporous Mater., 113–122.

Farrauto, R., Hwang, S., Shore, L., Ruettinger, W., Lampert, J., Giroux, T., Liu, Y., Ilinich, O., 2003. New material needs for hydrocarbon fuel processing: Generating hydrogen for the PEM fuel cell. Annu. Rev. Mater. Res. 33, 1–27.

Germani, G., Stefanescu, A., Schuurman, Y., van Veen, A.C., 2007. Preparation and characterization of porous alumina-based catalyst coatings in microchannels. Chem. Eng. Sci. 62, 5084–5091.

Giroux, T., Hwang, S., Liu, Y., Ruettinger, W., Shore, L., 2005. Monolithic structures as alternatives to particulate catalysts for the reforming of hydrocarbons for hydrogen generation. Appl. Catal. B Environ. 56, 95–110.

Hessel, V., Löwe, H., Müller, A., Kolb, G., 2005. Chemical micro process engineering: processing and plants. Wiley-VCH.

Holladay, J.D., Hu, J., King, D.L., Wang, Y., 2009. An overview of hydrogen production technologies. Catal. Today 139, 244–260.

Hwang, S., Kwon, O., Kim, J., 2007. Method of catalyst coating in micro-reactors for methanol steam reforming. Appl. Catal. A Gen., 83–89.

Joensen, F., Rostrup-Nielsen, J.R., 2002. Conversion of hydrocarbons and alcohols for fuel cells. J. Power Sources 105, 195–201.

Johnson, B.R., Canfield, N.L., Tran, D.N., Dagle, R. A., Li, X.S., Holladay, J.D., Wang, Y., 2007. Engineered SMR catalysts based on hydrothermally stable, porous, ceramic supports for microchannel reactors. Catal. Today 120, 54–62.

Kasture, M., Niphadkar, P., Bokade, V., Joshi, P., 2007. On the catalytic performance in isopropylation of benzene over H/β zeolite catalysts: Influence of binder. Catal. Commun. 8, 1003–1008.

Kim, T., Kwon, S., 2006. Design, fabrication and testing of a catalytic microreactor for hydrogen production, J. Micromech. Microeng 16, 1760–1768.

Kiwi-Minsker, L., Renken, A., 2005. Microstructured reactors for catalytic reactions. Catal. Today 110, 2–14.

Kolb, G., 2008. Fuel Processing for Fuel Cells. Wiley-VCH.

Kolb, G., Hessel, V., 2004. Micro-structured reactors for gas phase reactions. Chem. Eng. J. 98, 1–38.

Kolb, G., Zapf, R., Hessel, V., Löwe, H., 2004. Propane steam reforming in micro-channels results from catalyst screening and optimisation. Appl. Catal. A Gen. 277, 155–166.

Mathiak, J., Heinzel, A., Roes, J., Kalk, T., Kraus, H., Brandt, H., 2004. Coupling of a 2.5 kW steam reformer with a 1 kWel PEM fuel cell. J. Power Sources 131, 112–119.

Matsumura, Y., Nakamori, T., 2004. Steam reforming of methane over nickel catalysts at low reaction temperature. Appl. Catal. A Gen. 258, 107–114.

Meille, V., 2006. Review on methods to deposit catalysts on structured surfaces. Appl. Catal. A Gen. 315, 1–17.

Mitra, B., Kunzra, D., 2008. Washcoating of different zeolites on cordierite monoliths. J. Am. Ceram. Soc., 64–70.

Narusawa, K., Hayashida, M., Kamiya, Y., Roppongi, H., Kurashima, D., Wakabayashi, K., 2003. Deterioration in fuel cell performance resulting from hydrogen fuel containing

impurities: poisoning effects by CO, CH4, HCHO, and HCOOH. J. Soc. Automot. Eng. Japan, 41–46.

Navascuès, N., Escuin, M., Irusta, S., Mallada, R., Santamaria, J., 2010. Combustion of volatile organic compounds at trace concentration levels in zeolite- coated microchannel reactors. Ind. Eng. Chem. Res. 49, 6941–6947.

Neef, H.-J., 2009. International overview of hydrogen and fuel cell research. Energy 34, 327–333.

Nijhuis, T.A., Beers, A.E.W., Vergunst, T., Hoek, I., Moulijn, J.A., 2001. Preparation of monolithic catalysts. Catal. Rev. Sci. Eng. 43, 345–380.

O'Connell, M., Kolb, G., Schelhaas, K.P., Schuerer, J., Tiemann, D., Ziogas, A., Hessel, V., 2009. Development and evaluation of a microreactor for the reforming of diesel fuel in the kW range. Int. J. Hydrogen Energy 34, 6290–6303.

Peters, T., 2003. Plant design and economics for chemical engineers, 5th Edition. McGraw-Hill.

Quiram, D.J., Jensen, K.F., Schmidt, M. A., Mills, P.L., Ryley, J.F., Wetzel, M.D., Kraus, D.J., 2007. Integrated microreactor system for gas-phase catalytic reactions. 1. Scale-up microreactor design and fabrication. Ind. Eng. Chem. Res. 46, 8292–8305.

Reuse, P., Renken, A., Haas-Santo, K., Görke, O., Schubert, K., 2004. Hydrogen production for fuel cell application in an autothermal micro-channel reactor. Chem. Eng. J. 101, 133–141.

Rostrup-Nielsen, J.R., 1993. Production of synthesis gas. Catal. Today 18, 305–324.

Rostrup-Nielsen, J.R., Sehested, J., Norskov, J.K., 2002. Hydrogen and synthesis gas by steam-and CO2 reforming. Adv. Catal. 47, 65–139.

Sandler, S.I., 1999. Chemical and Engineering Thermodynamics, 3rd Edition. Wiley & Sons.

Schmidt, V.M., BrÖckerhoff, P., HÖhlein, B., Menzer, R., Stimming, U., 1994. Utilization of methanol for polymer electrolyte fuel cells in mobile systems. J. Power Sources 49, 299–312.

Sebastian, V., Mallande, R., Casado, L., 2009. Preparation of zeolite films as catalytic coatings on microchannels. Microporous Mesoporous Mater. 115, 147–155.

Seris, E.L.C., Abramowitz, G., Johnston, A.M., Haynes, B.S., 2005. Demonstration plant for distribution production of hydrogen from steam reforming of methane. Chem. Eng. Res. Des. 83, 619–625.

Trimm, D.L., Önsan, Z.I., 2011. Onboard fuel conversion for hydrogen-fuel-cell-driven vehicles. Catal. Rev. Sci. Eng. 43, 31–84.

Truter, L., 2011. Development of a zeolite washcoating technique for microchannel reactors. University of Cape Town.

Twigg, M. V., 1989. Catalyst handbook, 2nd Edition. Wolfe Publishing Ltd.

USGS, 2011. Fact sheet: Platinum group metals. Polinares working paper n. 35.

Venkataraman, K., Wanat, E.C., Schmidt, L.D., 2003. Steam reforming of methane and water-gas shift in catalytic wall reactors. AIChE J. 49, 1277–1284.

Veser, G., Ziauddin, M., Schmidt, L.D., 1999. Ignition in alkane oxidation on noble-metal catalysts. Catal. Today 47, 219–228.

Walter, S., Malmberg, S., Schmidt, B., Liauw, M. A., 2005. Mass transfer limitations in microchannel reactors. Catal. Today 110, 15–25.

Wang, S., Lu, G.Q., 1998a. Reforming of methane with carbon dioxide over Ni/Al2O3 catalysts: Effect of nickel precursor. Appl. Catal. A Gen., 271–280.

Wang, S., Lu, G.Q., 1998b. Catalytic activities and coking characteristics of oxides supported Ni catalysts for CH 4 reforming with carbon dioxide. Energy & Fuels, 248–256.

Wang, Y., Chin, Y.H., Rozmiarek, R.T., Johnson, B.R., Gao, Y., Watson, J., Tonkovich, A. Y.L., Vander Wiel, D.P., 2004. Highly active and stable Rh/MgOAl2O3 catalysts for methane steam reforming. Catal. Today 98, 575–581.

Wei, J., Iglesia, E., 2004. Structural requirements and reaction pathways in methane activation and chemical conversion catalyzed by rhodium. J. Catal. 225, 116–127.

Wikipedia.org, 2013. Fuel cell [WWW Document]. URL http://en.wikipedia.org/wiki/Fuel_cell (accessed 4.25.13).

Wörz, O., Jäckel, K.-P., Richter, T., Wolf, A., 2001. Microreactors – a new efficient tool for reactor development. Chem. Eng. Technol. 24, 138-142.

Xu, J., Froment, G.F., 1989. Methane steam reforming, methanation and water-gas shift: I. Intrinsic kinetics. AIChE J. 35, 88–96.

Yasaki, S., Yoshino, Y., Ihara, K., Ohkubo, K., 1993. Method of manufacturing an exhaust gas purifying catalyst. United States Patent number: 5,208,206.

Yueng, K., Kwan, S., Lau, W., 2009. Zeolites in microsystems for chemical synthesis and energy generation. Top. Catal. 52, 101–110.

Zapf, R., Kolb, G., Pennemann, H., Hessel, V., 2006. Basic study of adhesion of several alumina-based washcoats deposited on stainless steel microchannels. Chem. Eng. Technol. 29, 1509–1512.

Zhai, X., Cheng, Y., Zhang, Z., Jin, Y., Cheng, Y., 2011. Steam reforming of methane over Ni catalyst in micro-channel reactor. Int. J. Hydrogen Energy 36, 7105–7113.

Zhao, S., Zhang, J., Weng, D., Wu, X., 2003. A method to form well-adhered γ-Al2O3 layers on FeCrAl metallic supports. Surf. Coatings Technol. 167, 97–105.

Appendices

Appendix A – Summary of experiments

Table A-1: Catalyst Properties

Catalyst	Type	Format	Active metal	Support
YR	commercial	wash-coated/ 2 mm egg shell sphere	-	-
XR	commercial	powder	Pt	ZrO_2-CeO_2
Rh/Al_2O_3	in-house synthesised	powder	Rh	Al_2O_3

Table A-2: Summary of experiments

Experiment	Reactor type	Catalyst	Temperature	S/C	Notes
1	micro-channel	blank	700 °C	3	Blank run
2	packed bed	YR	700 °C	3	
3	micro-channel	YR	700 °C	2 - 5	
4	micro-channel	YR	700 °C	2 - 5	
5	micro-channel	YR	700 °C	3	In-house coated
6	packed bed	XR	700 °C	3	
7	micro-channel	XR	700 °C	3	
8	micro-channel	XR	800 °C	3	
9	micro-channel	XR	900 °C	3	
10	micro-channel	XR	700 °C	3	Thermal pretreatment
11	micro-channel	XR	700 °C	3	Hydro-thermal pretreatment
12	micro-channel	XR	700 °C	3	Wash-coating process effect
13	micro-channel	XR	700 °C	3	Alumina addition
14	micro-channel	XR	700 °C	3	Reduced catalyst particle size
15	packed bed	Rh/Al_2O_3	700 °C	3	
16	micro-channel	Rh/Al_2O_3	700 °C	3	

Table A-3: Experiment 2 data

Time-on-stream (hours)	X_{CH4} (%)	C balance (%)	F_{H2} (sccm)	F_{CH4} (sccm)	F_{CO} (sccm)	F_{CO2} (sccm)
1.94	68.1	98.7	115.92	14.17	14.53	16.02
2.96	70.8	99.9	121.58	13.09	15.29	16.86
4.01	73.0	100.0	127.91	11.57	16.87	17.17
6.03	75.2	100.0	129.38	11.06	16.94	17.44
10.30	78.64	100.0	132.68	9.67	18.37	17.45
20.20	80.51	100.0	134.94	8.81	19.34	17.37
30.1	83.41	101.0	141.03	7.17	21.02	17.55
40.0	84.42	100.0	141.19	6.85	21.11	17.58
50.1	84.54	100.0	141.34	6.67	22.78	16.44
60.3	84.94	100.0	139.19	7.06	22.24	16.40
71.7	85.62	100.0	141.28	6.60	22.36	16.89
80.1	85.63	100.1	141.28	6.60	22.36	16.89
91.1	85.63	100.0	141.28	6.60	22.37	16.89

Table A-4: Experiment 3 data

Time-on-stream (hours)	X_{CH4} (%)	C balance (%)	F_{H2} (sccm)	F_{CH4} (sccm)	F_{CO} (sccm)	F_{CO2} (sccm)
10.56	80.06	101.0	351.72	23.57	47.24	48.24
12.03	80.62	100.0	353.65	22.89	47.70	48.63
13.13	80.79	101.0	354.82	22.69	48.64	48.28
14.23	81.44	100.0	355.79	21.92	48.20	48.78
15.25	81.68	100.0	357.48	21.65	48.91	48.78
16.26	81.87	100.0	357.65	21.41	49.06	48.66
138.9	80.95	100.9	352.56	22.50	47.79	48.86
140.8	81.55	100.4	352.35	21.79	48.42	48.41
141.5	81.66	100.0	353.17	21.67	48.56	48.54

Table A-5: Experiment 3 and 4 *space velocity* data at S/C of 2

Space velocity ($ml/g_{cat}h$)	X_{CH4} (%)	C balance (%)	F_{H2} (sccm)	F_{CH4} (sccm)	F_{CO} (sccm)	F_{CO2} (sccm)
50 000	84.5	100.0	87.98	4.65	15.78	9.117
60 000	84.0	99.9	105.01	5.45	19.01	10.87
100 000	79.88	100.0	167.91	11.69	29.21	18.13
200 000	71.69	100.0	302.51	33.24	47.65	36.18
300 000	59.64	100.0	382.93	71.06	54.79	49.39
400 000	52.15	100.0	443.57	112.34	66.15	55.03
500 000	46.19	100.1	484.79	157.92	75.05	57.95

Table A-6: Experiment 3 and 4 *space velocity* data at S/C of 3

Space velocity ($ml/g_{cat}h$)	X_{CH4} (%)	C balance (%)	F_{H2} (sccm)	F_{CH4} (sccm)	F_{CO} (sccm)	F_{CO2} (sccm)
50 000	91.72	99.9	96.43	2.54	14.13	12.98
60 000	91.70	100.0	113.62	3.26	17.48	14.74
100 000	88.34	100.0	186.84	6.77	28.27	24.53
200 000	81.73	99.9	337.46	21.43	47.48	46.98
300 000	73.41	100.0	457.97	46.82	59.14	67.75
400 000	64.75	100.0	532.41	82.76	64.07	82.82
500 000	57.66	99.9	583.60	124.27	68	91.35

Table A-7: Experiment 3 and 4 *space velocity* data at S/C of 5

Space velocity ($sml/g_{cat}h$)	**X_{CH4}** (%)	**C balance** (%)	**F_{H2}** (sccm)	**F_{CH4}** (sccm)	**F_{CO}** (sccm)	**F_{CO2}** (sccm)
50 000	96.85	100.0	108.07	0.92	11.52	17.28
100 000	94.72	100.0	210.28	3.12	22.09	33.85
200 000	85.79	101.0	385.8	16.78	36.82	64.6
400 000	62.7	99.0	544.05	88.1	50.5	91.83
500 000	56.46	97.8	587.95	128.56	62.7	93.3

Table A-8: Experiment 5 data

Time-on-stream (hours)	**X_{CH4}** (%)	**C balance** (%)	**F_{H2}** (sccm)	**F_{CH4}** (sccm)	**F_{CO}** (sccm)	**F_{CO2}** (sccm)
0.311	45.29	94.7	24.43	8.42	2.04	3.97
2.189	57.55	99.9	31.97	6.53	3.61	5.21
5.078	65.16	100.0	35.64	5.37	4.53	5.75
10.01	66.80	99.9	35.47	5.11	4.60	5.58
20.14	58.96	99.9	31.87	6.32	3.75	5.30
30.06	50.64	100.0	28.33	7.60	3.17	4.80
41.31	37.16	101.0	23.37	9.69	2.13	4.27
50.84	30.43	102.2	19.82	10.72	1.64	3.73
61.34	25.44	101.0	17.11	11.48	1.29	3.28

Table A-9: Experiment 6 data

Time-on-stream (hours)	X_{CH4} (%)	C balance (%)	F_{H2} (sccm)	F_{CH4} (sccm)	F_{CO} (sccm)	F_{CO2} (sccm)
37.34	78.0	100.5	102.20	8.07	15.09	13.69
38.07	77.5	100.6	101.36	8.22	15.28	13.33
39.08	77.6	100.0	101.21	8.19	15.11	13.42
40.09	77.6	100.4	101.38	8.20	15.13	13.46
91.80	73.2	98.9	94.21	9.81	13.08	13.27
92.81	74.2	99.9	96.50	9.44	12.96	13.92
93.97	73.8	100.0	96.20	9.60	13.24	13.63

Table A-10: Experiment 7 data

Time-on-stream (hours)	X_{CH4} (%)	C balance (%)	F_{H2} (sccm)	F_{CH4} (sccm)	F_{CO} (sccm)	F_{CO2} (sccm)
0.67	79.4	96.3	35.24	2.20	1.82	6.27
1.03	80.0	99.8	35.79	2.13	2.07	6.35
2.13	69.6	100.2	29.09	3.25	3.90	3.76
4.33	60.6	99.9	24.40	4.21	2.88	3.44
6.16	53.9	99.3	22.23	4.92	2.33	3.36
8.00	46.7	98.9	19.42	5.69	1.71	3.16
10.2	37.4	99.9	15.53	6.69	1.10	2.70
14.23	25.6	100.0	10.13	8.06	0.48	1.92
20.47	12.56	99.8	5.02	9.34	0.13	1.03
25.97	8.17	99.9	3.05	9.82	0.04	0.68

Table A-11: Experiment 8 data

Time-on-stream (hours)	X_{CH4} (%)	C balance (%)	F_{H2} (sccm)	F_{CH4} (sccm)	F_{CO} (sccm)	F_{CO2} (sccm)
0.10	92.9	98.9	53.14	1.11	6.99	7.71
0.55	93.3	99.9	51.32	1.04	8.57	6.03
1.00	89.6	99.3	50.81	1.66	8.60	5.81
1.60	80.6	99.7	45.58	3.07	7.04	5.68
2.05	68.1	99.6	39.32	5.05	5.51	5.24
2.50	44.6	100.5	26.67	8.77	2.85	4.11
3.10	16.5	99.8	9.60	13.23	0.67	1.68

Table A-12: Experiment 9 data

Time-on-stream (hours)	X_{CH4} (%)	C balance (%)	F_{H2} (sccm)	F_{CH4} (sccm)	F_{CO} (sccm)	F_{CO2} (sccm)
0.17	72.3	96.5	13.45	2.86	1.96	1.68
0.31	59.0	99.5	10.92	4.23	1.35	1.48
1.07	25.6	99.9	4.76	7.68	0.25	0.79
2.71	9.28	99.9	1.27	9.37	0.04	0.28
5.56	5.57	100.1	0.79	9.76	0.03	0.22

Table A-13: Experiment 10 data

Time-on-stream (hours)	X_{CH4} (%)	C balance (%)	F_{H2} (sccm)	F_{CH4} (sccm)	F_{CO} (sccm)	F_{CO2} (sccm)
14.70	80.2	101.7	50.83	2.17	6.21	7.71
14.85	81.7	100.9	50.35	1.95	7.07	6.97
15.00	81.8	99.9	50.10	1.93	7.35	6.68
15.15	82.1	100.0	50.32	1.88	7.55	6.56

Table A-14: Experiment 11 data

Time-on-stream (hours)	X_{CH4} (%)	C balance (%)	F_{H2} (sccm)	F_{CH4} (sccm)	F_{CO} (sccm)	F_{CO2} (sccm)
14.15	81.9	100.2	47.44	2.86	6.24	6.81
14.25	80.9	100.0	46.89	2.78	6.75	6.56
14.80	74.3	100.2	42.20	4.07	5.95	5.86
15.97	63.2	99.8	39.63	4.11	3.98	6.06
19.11	58.6	99.9	36.81	4.82	3.79	5.31
20.91	54.7	99.9	34.58	5.45	3.29	5.36

Table A-15: Experiment 12 data

Time-on-stream (hours)	X_{CH4} (%)	C balance (%)	F_{H2} (sccm)	F_{CH4} (sccm)	F_{CO} (sccm)	F_{CO2} (sccm)
0.02	72.5	101.0	99.94	9.62	13.15	12.63
1.02	80.6	102.1	104.59	6.79	15.73	13.14
2.84	80.7	100.2	105.86	6.74	15.32	13.82
6.50	80.2	100.0	103.88	6.93	15.74	13.11
10.17	80.5	101.2	104.71	6.80	15.08	13.81
13.84	79.95	100.0	102.63	7.14	15.13	13.33

Table A-16: Experiment 13 data

Time-on-stream (hours)	X_{CH4} (%)	C balance (%)	F_{H2} (sccm)	F_{CH4} (sccm)	F_{CO} (sccm)	F_{CO2} (sccm)
0.37	35.81	100.1	30.59	10.49	3.62	2.51
1.09	52.72	101.6	34.34	7.73	3.44	5.45
2.10	45.26	100.1	29.84	8.95	2.70	4.93
4.41	30.47	99.9	20.46	11.37	1.37	3.69
8.81	13.90	99.9	9.55	14.08	0.43	1.83

Table A-17: Experiment 14 data

Time-on-stream (hours)	X_{CH4} (%)	C balance (%)	F_{H2} (sccm)	F_{CH4} (sccm)	F_{CO} (sccm)	F_{CO2} (sccm)
0.51	19.13	101.1	19.65	14.72	0.83	2.96
0.80	29.54	99.8	22.71	12.82	1.23	3.92
1.23	24.15	99.9	18.84	13.80	0.87	3.34
2.10	15.00	99.9	12.22	15.46	0.41	2.20
3.11	7.20	99.9	6.00	16.88	0.14	1.05

Table A-18: Experiment 15 data

Time-on-stream (hours)	X_{CH4} (%)	C balance (%)	F_{H2} (sccm)	F_{CH4} (sccm)	F_{CO} (sccm)	F_{CO2} (sccm)
7.37	53.24	100.3	386.24	90.54	52.09	51.60
17.27	76.90	100.2	555.37	44.73	88.43	65.93
37.80	83.23	99.7	571.21	32.47	94.78	65.93
47.70	84.87	99.9	578.28	29.29	97.30	66.43
57.97	85.62	101.1	602.47	27.85	101.19	68.02
71.70	85.59	99.9	600.61	27.89	100.75	68.23
90.23	85.78	101.1	601.41	27.53	101.72	67.92
110.80	86.24	101.2	603.31	26.65	102.41	67.53

Table A-19: Experiment 16 data

Time-on-stream (hours)	X_{CH4} (%)	C balance (%)	F_{H2} (sccm)	F_{CH4} (sccm)	F_{CO} (sccm)	F_{CO2} (sccm)
0.50	9.97	98.4	8.99	23.90	0.63	1.49
4.07	13.66	99.9	12.54	22.92	0.89	2.21
9.57	16.52	98.9	15.30	22.17	1.09	2.70
54.30	12.18	99.7	10.96	23.31	0.59	2.06

Appendix B – Catalyst particle size distributions

Catalyst XR and Rh/Al_2O_3 particle size distributions after micronizing are shown in the table below. In addition, fresh catalyst XR particle size distribution is also included for comparison.

Table B-1: Catalyst particle size distributions

Catalyst	Particle size distribution (vol%)			
	0.36 – 1 (µm)	**1 – 5 (µm)**	**5 – 10 (µm)**	**10 – 200 (µm)**
Fresh XR	0.7	3.2	2.5	93.7
XR after micronizing	11.5	42.3	10.5	33.9
Rh/Al_2O_3 after micronizing	3.2	45.7	20.2	30.9

Appendix C – Calculation on the S/C ratio and minimum CH_4 conversion requirement

The feed S/C ratio was calculated based on the moisture content desired in a downstream fuel cell feed. For calculation purposes, PEM fuel cell operating temperatures of 70 °C, 85 °C and 100 °C with a relative humidity of between 50 % to 80 % were considered for fuel cell operating pressure of 1 bar_g. The moisture contents at different relative humidity with the corresponding PEM fuel cell operating temperature are presented in Table C-1.

Table C-1: PEM fuel cell feed moisture contents at different relative humidity

Relative humidity	Moisture content at different PEMFC temperature		
	70 °C	**85 °C**	**100 °C**
50%	7.66 vol%	14.25 vol%	25.07 vol%
60%	9.20 vol%	17.10 vol%	30.09 vol%
70%	10.73 vol%	19.95 vol%	35.10 vol%
80%	12.26 vol%	22.80 vol%	40.11 vol%

A series of calculations based on the different reaction stages in the fuel processor were performed. The feed to the reformer was set on dry basis to 98 vol% CH_4 and 2 vol% Ar, with the S/C ratio of the SMR feed as a variable. CH_4 conversion in SMR was assumed to be at 95 % and the CO/CO_2 ratio in the product stream of SMR was taken as 1:1. The products of SMR were used as the feed for the WGS reaction. A CO conversion of 90 % was assumed in the WGS reaction and the product was used as the feed for the PrOx or methanation process. The CO conversions in these two latter processes were assumed to be close to complete. The final product from the PrOx or methanation process was used as the feed for the PEM fuel cell.

Various S/C can be determined by moisture content from Table C-1 by means of a spreadsheet and solver function. The results of the S/C ratio required in SMR feed is presented in Table C-2 and, consequently, the S/C ratios chosen for this study were 2, 3 and 5.

Table C-2: The reformer feed S/C required at different relative humidity with the corresponding PEM fuel cell operating temperatures

Relative humidity	Reformer feed S/C at different PEMFC temperature		
	70 °C	**85 °C**	**100 °C**
50%	2.10	2.57	3.34
60%	2.27	2.75	3.78
70%	2.36	2.95	4.29
80%	2.45	3.16	4.89

The poisoning effect of methane is very small for conventional PEM fuel cells and concentrations up to 5 vol% are known to have no detrimental effect on the performance. Therefore, minimum CH_4 conversions at different S/C in the SMR reaction were calculated to achieve less than 5 vol% CH_4 in fuel cell feed. The calculations were similar to these for the S/C calculations. However, in this case, the S/C is known and the CH_4 conversion in the SMR reaction is the variable and the final concentration of CH_4 in the PrOx or methanation products stream was calculated by means of a spreadsheet and solver function. The results of the minimum CH_4 conversion with corresponding S/C are presented in Table C-3.

Table C-3: Minimum CH4 conversion with corresponding S/C

S/C	Minimum CH_4 conversion
2	80 %
3	77 %
5	70 %

Appendix D – Determination of equilibrium CH_4 conversion in SMR

Table D-1: The molar heat capacities of gases in the ideal gas state (Sandler, 1999)

Compound	a	b × 10^2	c × 10^5	d × 10^9	Temperature range, K
H_2	29.088	-0.192	0.400	-0.870	273 – 1800
CO	28.142	0.176	0.537	-2.221	273 – 1800
CH_4	19.875	5.021	1.268	-11.004	273 – 1500
H_2O(vapour)	32.218	0.192	1.055	-3.593	273 – 1800

Constants are the equation $C_p = a + bT + cT^2 + dT^3$, where T is in degrees Kelvin and C_p is in $J(mol.K)^{-1}$

Table D-2: Heats and Gibbs free energies of formation of gases (Sandler, 1999)

Compound	State	$\Delta H^f_{25\,°C}$ (kJ/mol)	$\Delta G^f_{25\,°C}$ (kJ/mol)
H_2	gas	0	0
CO	gas	-110.5	-137.2
CH_4	gas	-74.5	-50.5
H_2O	gas	-241.8	-228.6

For the SMR reaction, the equilibrium CH_4 conversion calculation is based on a dry feed composition of 98 vol% CH_4 and 2 vol% Ar. The S/C ratio is represented by "S" and the total pressure is 1 bar_g.

Table D-3: Mass balance compound conversion table for SMR

	CH_4	+	H_2O	↔	CO	+	$3H_2$
$P_{gases,in}$	$\frac{0.98}{0.98S+1}P_{total}$		$\frac{0.98S}{0.98S+1}P_{total}$		0		0
$P_{Gases,change}$	$-\frac{0.98}{0.98S+1}P_{total}X_{CH_4}$		$-\frac{0.98}{0.98S+1}P_{total}X_{CH_4}$		$+\frac{0.98}{0.98S+1}P_{total}X_{CH_4}$		$+\frac{3\times 0.98}{0.98S+1}P_{total}X_{CH_4}$
$P_{gases,out}$	$\left(\frac{0.98P_{total}}{0.98S+1}\right)(1 - X_{CH_4})$		$\frac{0.98S}{0.98S+1}P_{total} - \frac{0.98}{0.98S+1}P_{total}X_{CH_4}$		$\frac{0.98}{0.98S+1}P_{total}X_{CH_4}$		$\frac{3\times 0.98}{0.98S+1}P_{total}X_{CH_4}$

For SMR reaction, equilibrium constant for the reaction is defined by the relationship below

$$K_P = \frac{P_{CO}.P_{H_2}^3}{P_{CH_4}.P_{H_2O}}$$

The equilibrium constant for the reaction is also defined by the relationship below:

$$K = K_P = e^{\left(\frac{-\Delta G_{rxn}}{RT}\right)} \quad \textbf{eqn A-1}$$

The Gibbs free energy of reaction at the particular reaction condition is a function of temperature only.

The Gibbs free energy of reaction and the standard heat of reaction can be determined from the standard Gibbs free energies of formation and standard heats of formation respectively, via the expressions below:

$$\Delta G_{298K}^{rxn} = \Delta G_{H_2}^f + \Delta G_{CO}^f - \Delta G_{CH_4}^f - \Delta G_{H_2O}^f \quad \textbf{eqn A-2}$$

$$\Delta H_{298K}^{rxn} = \Delta H_{H_2}^f + \Delta H_{CO}^f - \Delta H_{CH_4}^f - \Delta H_{H_2O}^f \quad \textbf{eqn A-3}$$

In order to calculate the equilibrium constant K_P using the Gibbs free energies of formation, it can be seen that

$$\frac{\partial}{\partial T}\left(\frac{\overline{G_i}}{T}\right)_P = \frac{1}{T}\left(\frac{\partial \overline{G_i}}{\partial T}\right)_P - \frac{\overline{G_i}}{T^2} = -\frac{\overline{S_i}}{T} - \frac{\overline{H_i}}{T^2} + \frac{\overline{S_i}}{T} = -\frac{\overline{H_i}}{T^2} \quad \textbf{eqn A-4}$$

Using the fact that $\ln K_P = \frac{\sum v_i \Delta G_{f,i}}{RT}$, we obtain the van't Hoff eqn:

$$\left(\frac{\partial ln\, K_P}{\partial T}\right)_P = -\frac{1}{R}\frac{\partial}{\partial T}\left[\frac{\sum v_i \Delta G_{f,i}^0}{T}\right] = \frac{1}{RT^2}\sum v_i \Delta G_{f,i}^0 = \frac{\Delta H_{rxn}^0(T)}{RT^2} \quad \textbf{eqn A-5}$$

Therefore, $ln(K_P)_T - ln(K_P)_{298K} = \int_{298}^{T} \frac{\Delta H^{rxn}}{RT^2} dT$ **eqn A-6**

But since, $\Delta H^{rxn}(T) = \Delta H_{298K}^{rxn} + \int_{298}^{T} \Delta C_P\, dT$ **eqn A-7**

And knowing that

$$\begin{aligned}\Delta H_{298K}^{rxn} &= \Delta H_{H_2}^{f} + \Delta H_{CO}^{f} - \Delta H_{CH_4}^{f} - \Delta H_{H_2O}^{f} \\ &= (0) + (-110.5) - (-74.5) - (-241.8) \\ &= 205.8 \frac{kJ}{mol} at\ 298\ K\end{aligned}$$

$$\begin{aligned}\Delta G_{298K}^{rxn} &= \Delta G_{H_2}^{f} + \Delta G_{CO}^{f} - \Delta G_{CH_4}^{f} - \Delta G_{H_2O}^{f} \\ &= (0) + (-137.2) - (-50.5) - (-228.6) \\ &= 141.9 \frac{kJ}{mol} at\ 298\ K\end{aligned}$$

$$\begin{aligned}\Delta C_P &= C_{P,H_2} + C_{P,CO} - C_{P,CH_4} - C_{P,H_2O} \\ &= (29.088 - 0.192 \times 10^{-2}.T + 0.400 \times 10^{-5}.T^2 - 0.870 \times 10^{-9}.T^3) \\ &\quad +(28.142 + 0.167 \times 10^{-2}.T + 0.537 \times 10^{-5}.T^2 - 2.221 \times 10^{-9}.T^3) \\ &\quad -(19.875 + 5.021 \times 10^{-2}.T + 1.268 \times 10^{-5}.T^2 - 11.004 \times 10^{-9}.T^3) \\ &\quad -(32.218 + 0.192 \times 10^{-2}.T + 1.055 \times 10^{-5}.T^2 - 3.593 \times 10^{-9}.T^3) \\ &= 5.137 - 5.238 \times 10^{-2}.T - 1.386 \times 10^{-5}.T^2 - 11.506 \times 10^{-9}.T^3\end{aligned}$$

And

$$K_{P,298K} = e^{\frac{-\Delta G_{298}^{rxn}}{RT}} = e^{\frac{-141900}{8.314 \times 298}} = 1.3775 \times 10^{-25}$$

With eqn A-7 be expanded to

$$\begin{aligned}\Delta H^{rxn}(T) &= \Delta H_{298K}^{rxn} \\ &\quad + \int_{298}^{T} 5.137 - 5.238 \times 10^{-2}.T - 1.386 \times 10^{-5}.T^2 - 11.506 \times 10^{-9}.T^3\, dT\end{aligned}$$

Therefore,

$$\begin{aligned}\Delta H^{rxn}(T) &= \Delta H_{298K}^{rxn} + 5.137(T - 298) - \frac{5.238 \times 10^{-2}}{2}(T^2 - 298^2) - \frac{1.386 \times 10^{-5}}{3}(T^3 \\ &\quad - 298^3) - \frac{11.506 \times 10^{-9}}{4}(T^4 - 298^4)\end{aligned}$$

K_P can be algebraically determined at various temperatures from eqn A-6 by means of a spreadsheet package, and thus the conversion of CH_4 can be calculated from the compound

table expression for K_P in terms of conversion at different S/C ratios. Figure D-1 presents the equilibrium curves for CH_4 conversion at different temperatures with S/C ratios between 2 and 5.

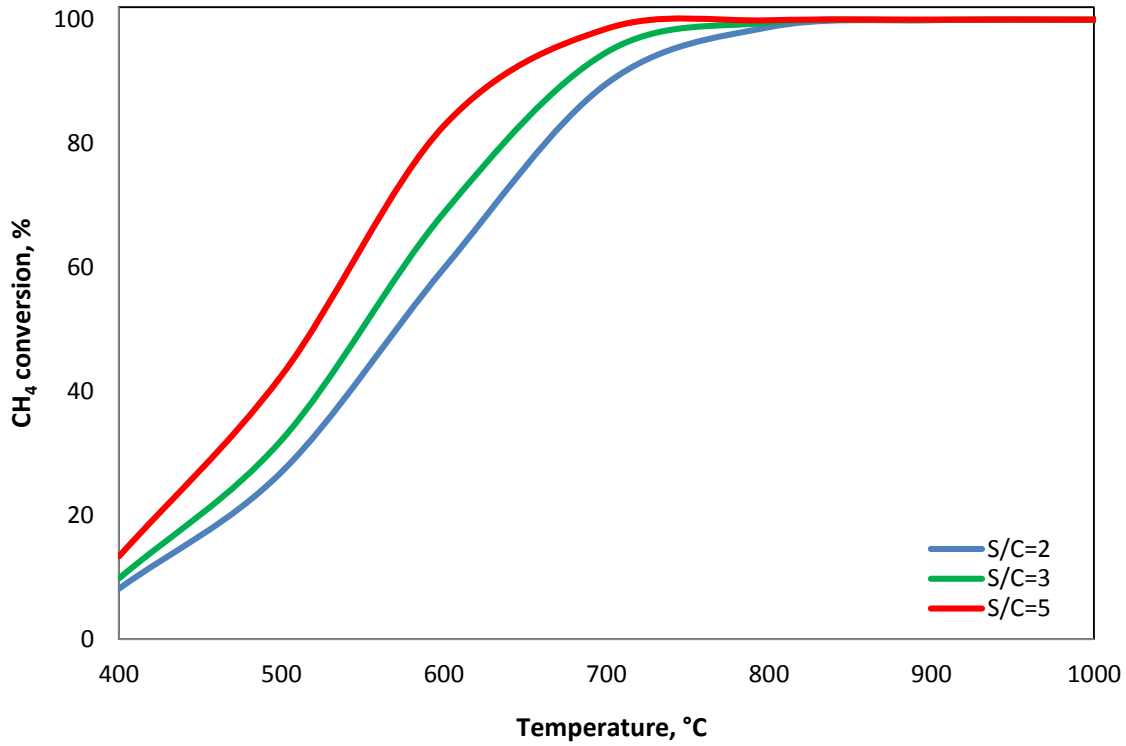

Figure D-1: Equilibrium curves for CH4 conversion using the experimentally applied feed conditions

Appendix E – Determination of equilibrium CO conversion in WGS

A similar approach to that used in Appendix D for SMR is applied for calculating equilibrium CO conversion in WGS reaction. Since the WGS reaction is subsequent to SMR, the inlet feed compositions for WGS depend on the product compositions of SMR at the given reaction conditions and can be found from Appendix A.

Table E-1: Mass balance compound conversion table for WGS

	CO	**+**	**H_2O**	**↔**	**CO_2**	**+**	**H_2**
$F_{gases,in}$	$F_{CO} + F_{CO_2}$		$F_{CH_{4,feed}}.S$ $- F_{CH_{4,feed}}.X_{CH_4}$		0		$F_{H_2} - F_{CO_2}$
$F_{Gases,change}$	$-(F_{CO} + F_{CO_2})X_{CO}$		$-(F_{CO} + F_{CO_2})X_{CO}$		$+(F_{CO} + F_{CO_2})X_{CO}$		$+(F_{CO} + F_{CO_2})X_{CO}$
$F_{gases,out}$	$(F_{CO} + F_{CO_2})(1$ $- X_{CO})$		$(S - X_{CH_4})F_{CH_{4,feed}}$ $-(F_{CO} + F_{CO_2})X_{CO}$		$(F_{CO} + F_{CO_2})X_{CO}$		$(F_{H_2} - F_{CO_2})$ $+(F_{CO} + F_{CO_2})X_{CO}$

For WGS reaction, equilibrium constant for the reaction is defined by the relationship below

$$K_P = \frac{F_{CO_2}.F_{H_2}}{F_{CO}.F_{H_2O}}$$

Following the similar calculation as conducted in Appendix D, it can be seen that

$$ln(K_P)_T - ln(K_P)_{298K} = \int_{298}^{T} \frac{\Delta H^{rxn}}{RT^2} dT \qquad \textbf{eqn A-6}$$

But since, $\Delta H^{rxn}(T) = \Delta H^{rxn}_{298K} + \int_{298}^{T} \Delta C_P \, dT$ **eqn A-7**

And knowing that

$$\begin{aligned}\Delta H^{rxn}_{298K} &= \Delta H^{f}_{CO_2} + \Delta H^{f}_{H_2} - \Delta H^{f}_{CO} - \Delta H^{f}_{H_2O} \\ &= (-393.5) + (0) - (-110.5) - (-241.8) \\ &= -41.16 \frac{kJ}{mol} at\ 298\ K\end{aligned}$$

$$\Delta G^{rxn}_{298K} = \Delta \ {}^{f}_{H_2} + \Delta G^{f}_{CO_2} - \Delta G^{f}_{CO} - \Delta G^{f}_{H_2O}$$
$$= (0) + (-394.4) - (-137.3) - (-228.6)$$
$$= -28.52 \frac{kJ}{mol} at\ 298\ K$$

$$\Delta C_P = C_{P,CO_2} + C_{P,H_2} - C_{P,CO} - C_{P,H_2O}$$
$$= (22.242 + 5.977 \times 10^{-2}.T - 3.499 \times 10^{-5}.T^2 + 7.464 \times 10^{-9}.T^3)$$
$$+(29.087 - 0.192 \times 10^{-2}.T + 0.400 \times 10^{-5}.T^2 - 0.870 \times 10^{-9}.T^3)$$
$$-(28.142 + 0.167 \times 10^{-2}.T + 0.537 \times 10^{-5}.T^2 - 2.221 \times 10^{-9}.T^3)$$
$$-(32.218 + 0.192 \times 10^{-2}.T + 1.055 \times 10^{-5}.T^2 - 3.593 \times 10^{-9}.T^3)$$
$$= 9.031 + 5.426 \times 10^{-2}.T - 4.691 \times 10^{-5}.T^2 - 1.241 \times 10^{-8}.T^3$$

And

$$K_{P,298K} = e^{\frac{-\Delta G^{rxn}_{298}}{RT}} = e^{\frac{-28520}{8.314 \times 298}} = 99834.58$$

With eqn A-7 be expanded to

$$\Delta H^{rxn}(T) = \Delta H^{rxn}_{298K} + \int_{298}^{T} 9.031 + 5.426 \times 10^{-2}.T - 4.691 \times 10^{-5}.T^2 - 1.241 \times 10^{-8}.T^3\, dT$$

Therefore,

$$\Delta H^{rxn}(T) = \Delta H^{rxn}_{298K} + 9.031(T - 298) + \frac{5.426 \times 10^{-2}}{2}(T^2 - 298^2) - \frac{4.691 \times 10^{-5}}{3}(T^3 - 298^3) - \frac{1.214 \times 10^{-8}}{4}(T^4 - 298^4)$$

K_P can be algebraically determined at various temperatures from eqn A-6 by means of a spreadsheet package, and thus the conversion of CO can be calculated from the compound table expression for K_P in terms of conversion at different feed compositions. The equilibrium CO conversions can be found in Figure 5-7.

Appendix F – TGA results for coating suspension

PVA was used as binder in the catalyst coating suspension. Thermogravimetric analysis (TGA) was utilised to confirm the complete removal of PVA from the coated layer after calcination. 47.83 mg of coating suspension with 20 wt% catalyst loading (9.56 mg catalyst) was placed into the instrument in an air environment, and the temperature program used is described below:

- Heat to 120 ˚C at 1 ˚C/min and hold for 1 hour
- Heat to 900 ˚C at 1 ˚C/min
- Cool to room temperature

The results of the TGA test are showing in Figure F-1. The weight reading at 400 °C was 9.52 mg and no change was observed up to the temperature of 900 °C. The final weight corresponds to the initial catalyst weight in the coating suspension, in other words, the PVA in the coating suspension was removed completed at a temperature above 400 °C.

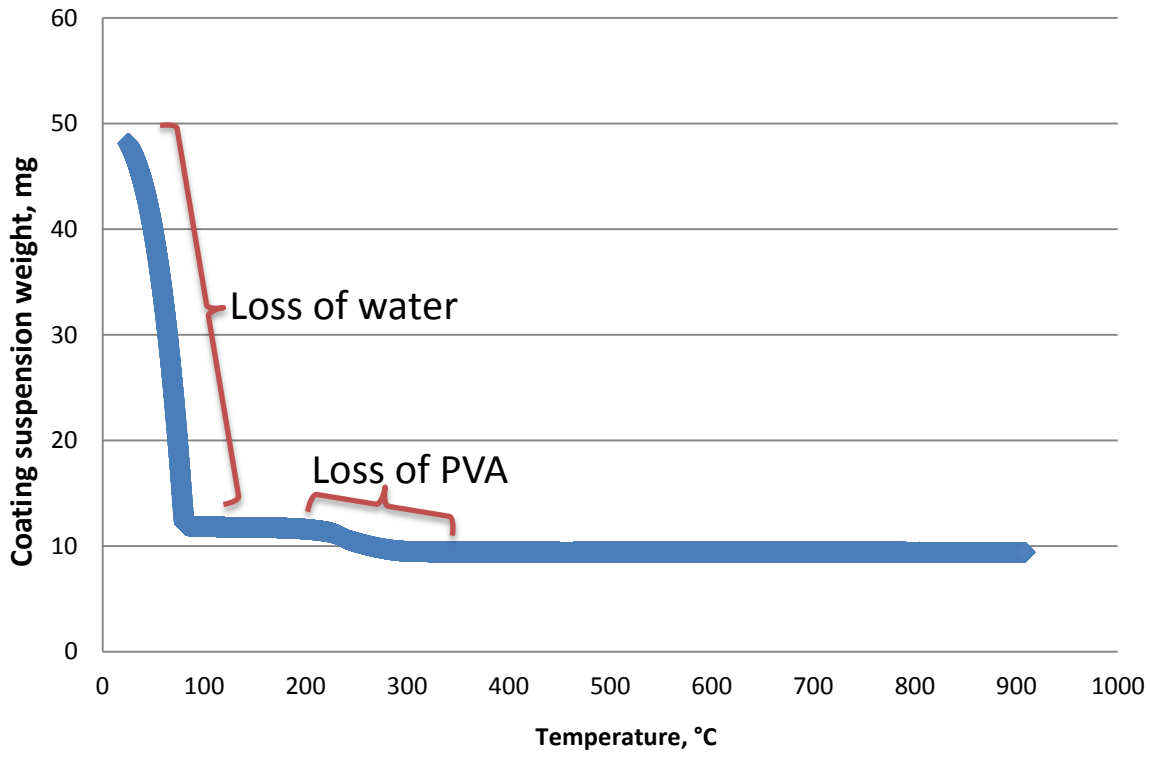

Figure F-1: TGA results for coating suspension

Appendix G – Calculation of GC response factors

Ar was used as an internal standard to quantify the amount of each species present in a given gas sample. The response factor of a species, relative to Ar, is defined as:

$$RRF_{species} = \frac{(\frac{Moles_{species}}{Moles_{Ar}})}{(\frac{Area_{species}}{Area_{Ar}})} \qquad \textbf{eqn A-8}$$

The relative response factor for a given species was determined by passing a mixture with known composition through the GC sample loop. The area response of the compound relative to the area response of Ar was determined by integrating the area under the species peak and the Ar peak respectively. This procedure was repeated several times for a variety of gas compositions. The relationship of the molar ratios and the area ratios was then plotted and a straight line passing through the origin was fitted to the data. As indicated on the graphs below, the relative response factors were valid over quite a wide range of concentrations which covered all those applicable to the experiments of this study.

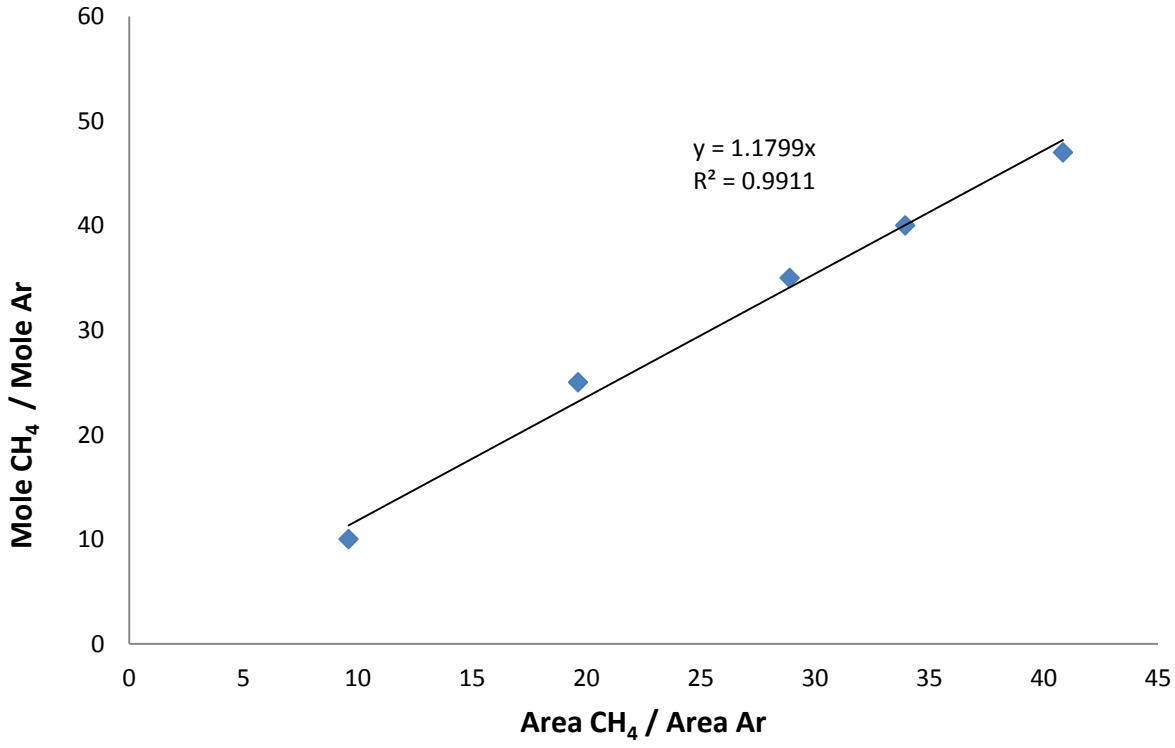

Figure G-1: Methane relative response factor

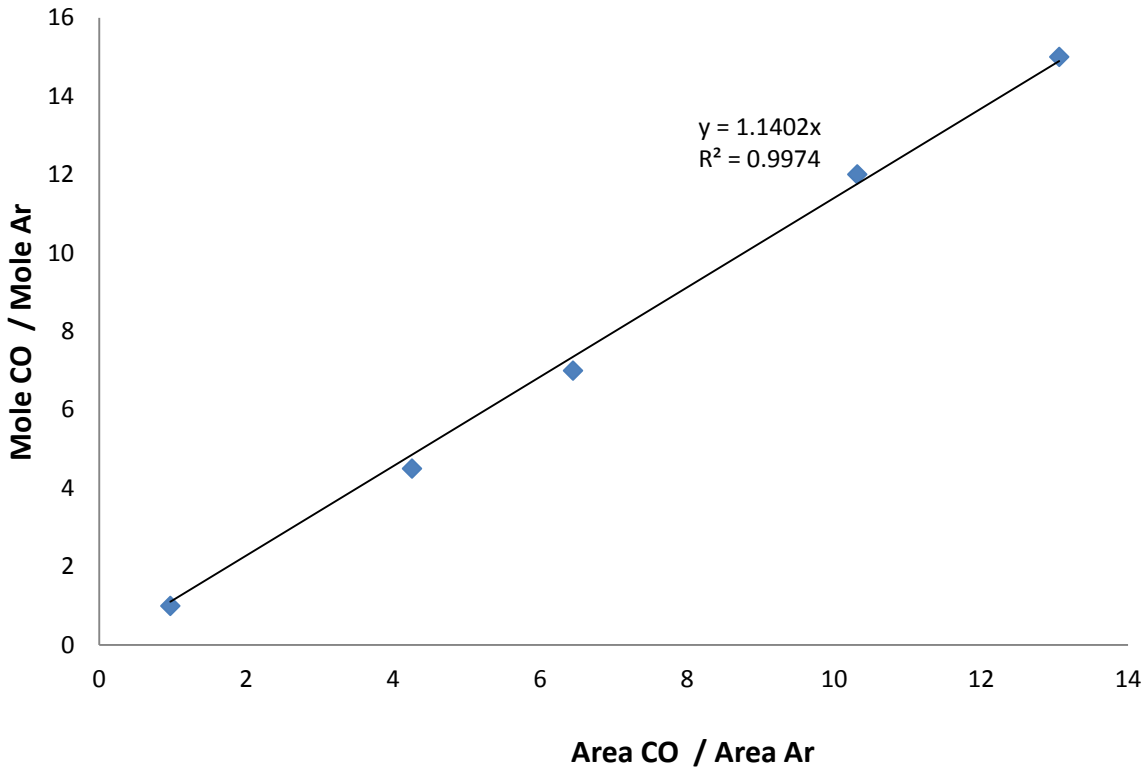

Figure G-2: Carbon monoxide relative response factor

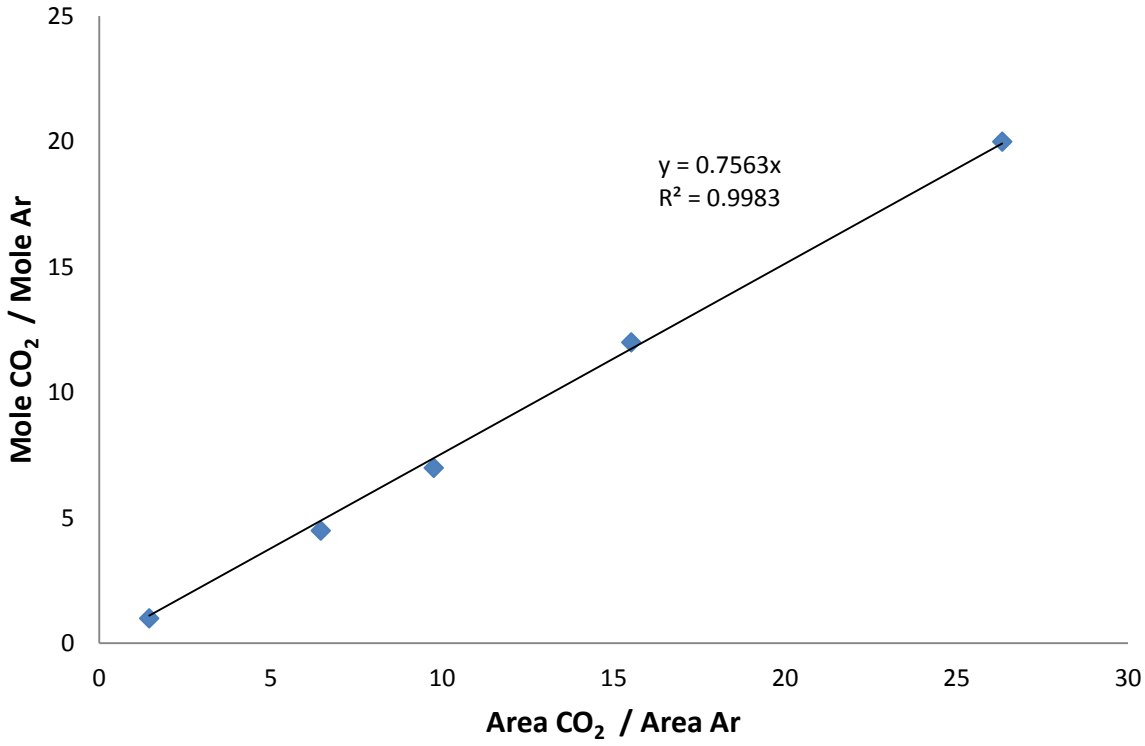

Figure G-3: Carbon dioxide relative response factor

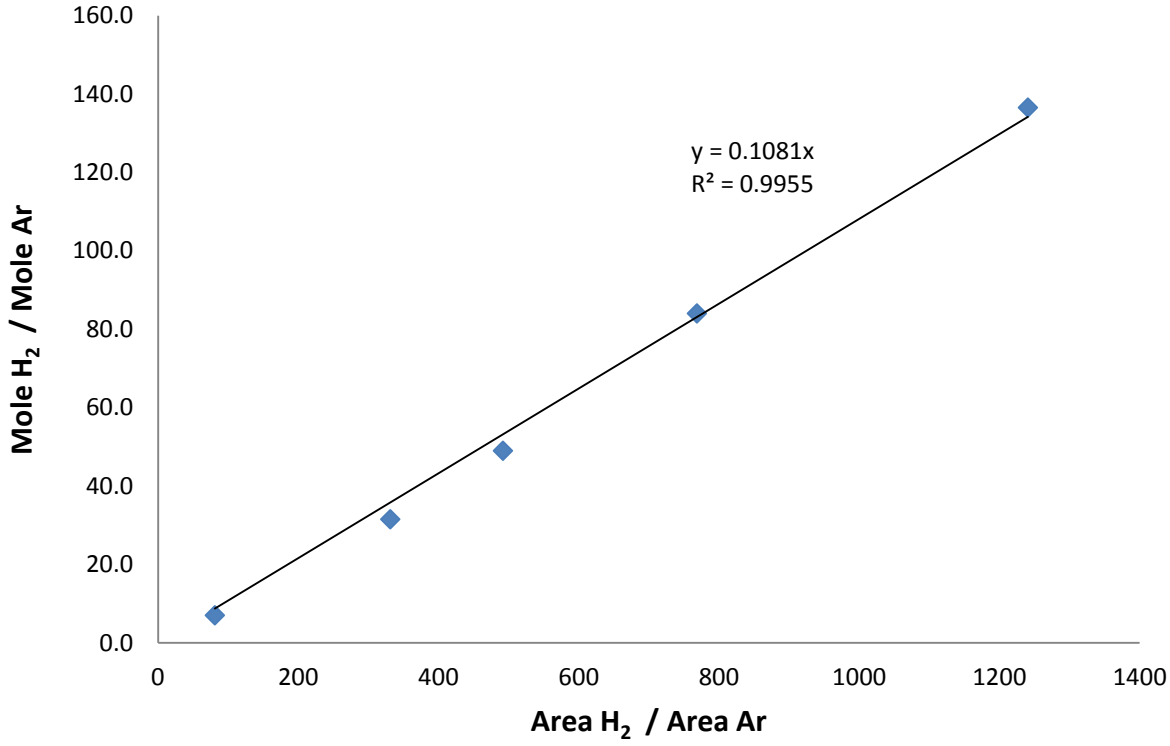

Figure G-4: Hydrogen relative response factor